Investigating the role of the microtubule-severing enzyme spastin in axonal endoplasmic reticulum morphology and stress

Dissertation

submitted with the aim of achieving a doctoral degree at the

Faculty of Mathematics, Informatics and Natural Sciences

Department of Biology of University of Hamburg

Submitted by

Rebecca Jark

Hamburg 2025

Thesis evaluators

Prof. Dr. Matthias Kneussel

Prof. Dr. Christian Lohr

Examiners

Prof. Dr. Baris Tursun

Prof. Dr. Thomas Oertner

Prof. Dr. Matthias Kneussel

Prof. Dr. Christian Lohr

Disputation date

21st of November 2025

Table of contents

Table of contents ... 3

Eidesstattliche Erklärung ... 6

Summary ... 7

Zusammenfassung ... 9

List of abbreviations ... 11

List of units ... 14

List of prefixes ... 14

1. Introduction ... 15

1.1 The Central Nervous System ... 15

1.2 Hereditary spastic paraplegias ... 18

1.3 The microtubule network ... 20

1.4 The endoplasmic reticulum: functions and neuronal distribution ... 23

1.5 ER, protein synthesis and folding ... 25

1.6 ER and Lipid Metabolism ... 25

1.7 ER and Calcium Dynamics ... 26

1.8 ER-MT interactions ... 26

1.9 Spastin ... 28

1.10 ER-shaping proteins ... 34

1.11 ER stress and its role in neurodegeneration ... 36

1.12 Tubulin post-translational modifications: polyglutamylation and spastin ... 39

1.13 Aims of this study ... 41

2. Materials and methods ... 43

2.1 Instrumentation ... 43

2.2 Chemicals ... 43

2.3 Cell lines 45
2.4 Solutions 45
2.5 Restriction enzymes 47
2.6 Plasmid DNA 47
2.7 Antibody list 50
2.8 Bacterial Transformation following Site-Directed mutagenesis 51
2.9 Bacterial Transformation and Retransformation 51
2.10 Plasmid DNA isolation (Midiprep) 52
2.11 Animals 53
2.12 Primary neuronal culture of cortical neurons 53
2.13 Isolation of genomic DNA and genotyping 54
2.14 Agarose gel electrophoresis 56
2.15 Transfection 56
2.16 Immunocytochemistry 58
2.17 Electron microscopy 58
2.18 Time-lapse imaging 59
2.19 Total brain lysates and Western blot analysis 59
2.20 Data analysis 60
2.21 Statistics 61

3. Results 63

3.1 Spastin depletion does not influence total axon length 63
3.2 Spastin depletion leads to enlarged distal axon areas 63
3.3 Spastin depletion leads to a decrease in axonal ER area and density in mouse corticospinal axons 65
3.4 Spastin depletion leads to an increase in axonal ER aggregates in primary cortical neurons 68

3.5 Axonal ER aggregates induced by spastin depletion show higher levels of ER stress 71

3.6 Distal axonal ER aggregates induced by spastin depletion are in close proximity to MT alterations 72

3.7 Spastin-mediated MT severing is necessary for distal axonal ER distribution and homeostasis 75

3.8 Tubulin polyglutamylation is necessary for proper distal axon ER distribution and homeostasis 77

3.9 Spastin co-expression with mCherrySec61β in primary cortical neurons leads to extensive cell death, even in the background of spastin depletion 80

3.10 Compound N- and C-terminal M1 spastin mutations lead to proximal axonal ER distribution defects 83

4. Discussion 91

4.1 Spastin loss affects distal axon morphology 91

4.2 Spastin affects axonal ER distribution and stress 92

4.3 Spastin-mediated MT severing is necessary for distal axonal ER distribution and stress 96

4.4 Tubulin polyglutamylation regulates distal axonal ER distribution and stress .. 97

4.5 Spastin overexpression leads to extensive cortical neuron death 99

4.6 M1 spastin is involved in axonal ER distribution and homeostasis both through its N- and C-terminal domains 100

References 105

Acknowledgements 125

Eidesstattliche Erklärung

Declaration on Oath

Hiermit erkläre ich an Eides statt, dass ich die vorliegende Dissertationsschrift selbst verfasst und keine anderen als die angegebenen Quellen und Hilfsmittel benutzt habe.

I hereby declare upon oath that I have written the present dissertation independently and have not used further resources and aids than those stated in the dissertation.

Hamburg, 15.10.2025

Unterschrift | Signature

Summary

Hereditary spastic paraplegias (HSPs) are disorders primarily characterized by the degeneration of corticospinal axons. Patients affected by HSPs present lower limb motor impairments, distal sensory loss, and in some cases, cognitive impairments and epilepsy.

HSPs can be caused by X-linked recessive, autosomal recessive, or autosomal dominant mutations, or can even be sporadic. The majority of autosomal dominant HSPs are caused by mutations in the *SPAST* gene, encoding the microtubule-severing protein spastin. In humans, the spastin protein is mainly expressed in two isoforms, M1 and M87 spastin. Both isoforms share a microtubule (MT) interacting and endosome trafficking domain, an MT binding domain, and an AAA ATPase domain required for MT severing. The M1 isoform also contains an N-terminal hydrophobic region, required for endoplasmic reticulum (ER) morphogenesis and interaction with ER-shaping proteins such as atlastin-1, REEP1, and reticulon-1 and -2. Interestingly, mutations in these proteins have also been shown to cause HSPs, indicating that disruptions in ER morphogenesis and shaping might be involved in the development of HSPs.

The ER interacts with MTs, and this interaction is crucial for proper axonal ER dynamics and morphology. The involvement of spastin in both MT severing and ER morphogenesis suggests a role for spastin in mediating the crosstalk between these two organelles.

In this study, alterations in ER size and density were found in corticospinal axons of spastin-depleted mice prior to the development of motor symptoms. Furthermore, abnormalities in axonal ER distribution and ER stress were found in primary mouse cortical neurons upon (i) spastin depletion, (ii) MT severing disruption, and (iii) tubulin polyglutamylation reduction, which has been previously shown to regulate spastin-mediated MT severing. In addition, M1 spastin was found to orchestrate axonal ER distribution and homeostasis through the combined action of its N-terminal hydrophobic region and its MT-severing domain.

In conclusion, spastin is required not only for proper MT severing but also for axonal ER homeostasis, and disruptions in this process are likely causative for the development of HSPs.

Zusammenfassung

Hereditäre spastische Paraplegien (HSP) sind Erkrankungen, die in erster Linie durch eine Degeneration der kortikospinalen Axone gekennzeichnet sind. Patienten, die von HSP betroffen sind, weisen motorische Beeinträchtigungen der unteren Extremitäten, einen distalen Sensibilitätsverlust und in einigen Fällen kognitive Beeinträchtigungen und Epilepsie auf.

HSP können durch X-chromosomal-rezessive, autosomal-rezessive oder autosomal-dominante Mutationen verursacht werden oder auch sporadisch auftreten. Die meisten autosomal-dominanten HSPs werden durch Mutationen im *SPAST*-Gen verursacht, das für das Mikrotubuli-spaltende Protein Spastin kodiert. Beim Menschen wird das Spastin-Protein hauptsächlich in zwei Isoformen exprimiert, M1- und M87-Spastin. Beide Isoformen haben eine Mikrotubuli (MT)-rekrutierende Domäne, eine MT-Bindungsdomäne und eine AAA-ATPase-Domäne gemeinsam, die für die MT-Spaltung erforderlich ist. Die M1-Isoform enthält außerdem eine N-terminale hydrophobe Region, die für die Morphogenese des endoplasmatischen Retikulums (ER) und die Interaktion mit ER-formenden Proteinen wie atlastin-1, REEP1 und reticulon-1 und -2 erforderlich ist. Interessanterweise wurde gezeigt, dass Mutationen in diesen Proteinen ebenfalls HSPs verursachen, was darauf hindeutet, dass Störungen der ER-Morphogenese und -Formung an der Entstehung von HSPs beteiligt sein könnten.

Das ER interagiert mit MTs, und diese Interaktion ist entscheidend für die richtige Dynamik und Morphologie des axonalen ER. Die Beteiligung von Spastin sowohl an der MT-Spaltung als auch an der ER-Morphogenese deutet auf eine Rolle von Spastin bei der Vermittlung der Wechselwirkung zwischen diesen beiden Organellen hin.

In dieser Studie wurden Veränderungen der Größe und Dichte des ER in kortikospinalen Axonen von Mäusen mit Spastin-Mangel vor dem Auftreten motorischer Symptome festgestellt. Darüber hinaus wurden Anomalien in der Verteilung des axonalen ER und ER-Stress in primären kortikalen Neuronen von Mäusen nach (i) Spastin-Mangel, nach (ii) Unterbrechung der MT-Spaltung und nach

(iii) Verringerung der Tubulin-Polyglutamylierung festgestellt, von der bereits zuvor gezeigt wurde, dass sie die Spastin-vermittelte MT-Spaltung reguliert. Darüber hinaus wurde festgestellt, dass M1-Spastin die axonale ER-Verteilung und Homöostase durch die kombinierte Wirkung seines N-terminalen hydrophoben Bereichs und seiner MT-Spaltungsdomäne koordiniert.

Zusammenfassend lässt sich sagen, dass Spastin nicht nur für die korrekte MT-Spaltung, sondern auch für die axonale ER-Homöostase erforderlich ist und dass Störungen in diesem Prozess wahrscheinlich für die Entwicklung von HSPs mitverantwortlich sind.

List of abbreviations

AD	Autosomal Dominant
ANOVA	Analysis of Variance
APS	Ammonium Persulfate
ATP	Adenosine triphosphate
BSA	Bovine Serum Albumin
Ca^{2+}	Calcium
CCP	Cytoplasmic carboxypeptidase deglutamylase
CNS	Central Nervous System
CO_2	Carbon dioxide
C-terminal	Carboxyl-terminal
Cy5	Cyanine 5
ddH_2O	Double-distilled water
DIV	Days *in vitro*
DNA	Deoxyribonucleic acid
dNTP	Deoxynucleotide triphosphate
DTT	Dithiothreitol
EDTA	Ethylenediaminetetraacetic Acid
EF	Endotoxin-free
EGFP	Enhanced green fluorescent protein
EM	Electron microscope
ER	Endoplasmic reticulum
ERAD	ER-associated degradation
FIB-SEM	Focused Ion Beam Scanning Electron Microscopy
GAPDH	Glyceraldehyde 3-phosphate dehydrogenase
GRP78	Glucose regulated-protein 78
GTP	Guanosine triphosphate
HBS	HEPES-Buffered Saline
HBSS	Hanks' Balanced Salt Solution

HEPES	4-(2-hydroxyethyl)-1-piperazineethanesulfonic acid
HSP	Hereditary Spastic Paraplegia
ICC	Immunocytochemistry
IgG	Immunoglobulin G
iPSC	Induced pluripotent stem cell
K388	Lysine 388
KCl	Potassium chloride
KH_2PO_4	Potassium dihydrogen phosphate
$MgCl_2$	Magnesium chloride
$MgSO_4$	Magnesium sulfate
MT	Microtubule
MTBD	Microtubule binding domain
NaCl	Sodium chloride
Na_2HPO_4	Disodium hydrogen phosphate
N-terminal	Amino-terminal
O_2	Oxygen
P97	Proline 97
P361	Proline 361
PBS	Phosphate Buffered Saline
PCR	Polymerase Chain Reaction
PMSF	Phenylmethylsulfonyl fluoride
PNGM	Primary Neuron Growth Medium
PNS	Peripheral Nervous System
PVDF	Polyvinylidene fluoride
R431	Arginine 431
REEP	Receptor Expression Enhancing Protein
rpm	Revolutions per minute
RT	Room temperature
S44	Serine 44
SDS	Sodium Dodecyl Sulfate

SDS-PAGE	Sodium Dodecyl Sulfate-Polyacrylamide gel electrophoresis
SEM	Standard error of the mean
SOC	Super Optimal broth with Catabolite repression
SPAST	Spastin
SPG	Spastic Paraplegia type
TAE	Tris-Acetate-EDTA
TBS	Tris-Buffered Saline
TBS-T	Tris-Buffered Saline with Tween-20
TEM	Transmission electron microscope
TEMED	Tetramethylethylenediamine
TTLL	Tyrosine ligase-like glutamylase
UPR	Unfolded Protein Response
WB	Western blot
ZMNH	Zentrum für Molekulare Neurobiologie Hamburg

List of units

A	Ampere
b	base
°C	degree Celsius
Da	Dalton
g	gram
l	litre
M	molar
m	meter
s	second
V	Volt

List of prefixes

n	nano (10^{-9})
µ	micro (10^{-6})
m	milli (10^{-3})
k	kilo (10^{3})

1. Introduction

1.1 The Central Nervous System

In mammals, the nervous system is divided into the central nervous system (CNS) and the peripheral nervous system (PNS). The CNS includes the brain and spinal cord, while the PNS is composed of nerves and ganglia.

The main function of the CNS consists in receiving, processing, and storing information. The CNS exerts its functions via neurons and non-neuronal cells. Neurons are polarized cells that connect to one another to ensure the proper delivery of information from the brain to the periphery and vice versa. They typically are composed of three main components: numerous dendrites, the cell body, and an axon. Dendrites are processes that extend from the cell body and receive information from other neurons, while the axon is a long process responsible for the delivery of information to other neurons (Figure 1). Each neuron is part of a larger neuronal network, and dendrites connect to axons of different neurons through structures known as synapses. The specific connectivity between neurons within a specific region or among different brain regions is crucial for proper brain function.

The brain is divided into distinct regions, each performing specific functions. The largest portion of the brain is known as the cerebrum, and it can be divided into substructures, namely the cerebral cortex, the hypothalamus, the amygdala, and the hippocampus. The cerebral cortex is the outer layer of the cerebrum and can be further divided into 4 lobes: frontal, parietal, occipital, and temporal. Its main functions include sensory processing, integration of sensory information, and control of voluntary movements (Bear et al., 2016).

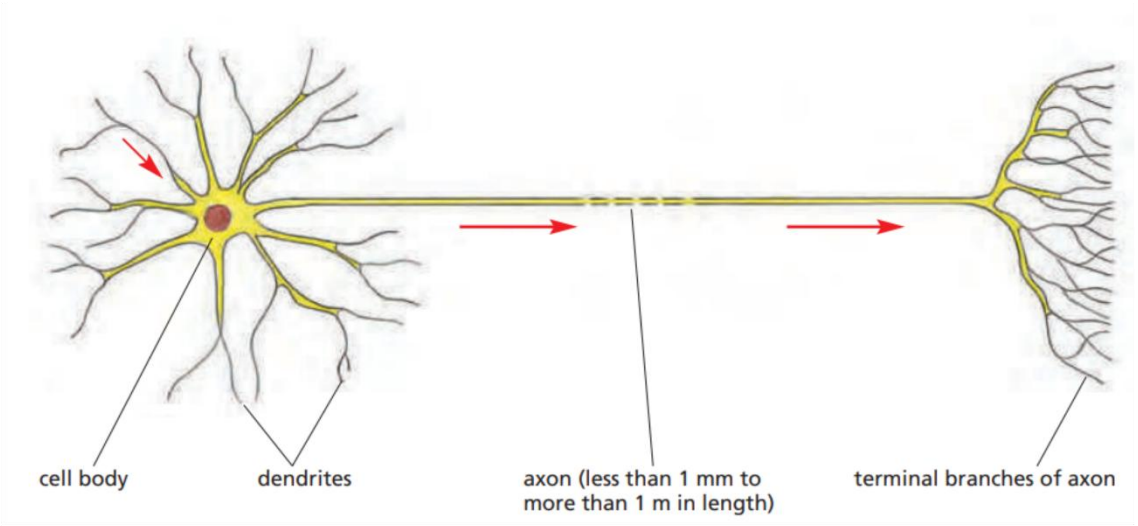

Figure 1. A typical mammalian neuron.

Neurons are polarized cells made up of three main components: cell body, dendrites, and axon. Typically, dendrites are responsible for receiving signals from other neurons, while the axon conducts signals away from the cell body. Red arrows indicate the direction of signal propagation. Axon terminals form synapses to contact dendrites of other neurons or, e.g., muscle cells for innervation. (Alberts et al., 2002)

The spinal cord departs from the brain stem and is enclosed within the vertebral column. Its main functions are connecting the brain to the rest of the body by delivering sensory information from the body to the brain, sending motor commands from the brain to the body, and coordinating motor reflexes (Bican et al., 2013). Voluntary movement control is dependent on the human pyramidal motor system. Upper motor neurons from the motor cerebral cortex and brain stem extend their axons into the spinal cord along the corticospinal tract. Most of these axons form synapses with spinal interneurons, which are in turn connected to lower motor neurons. Some corticospinal axons form synapses directly with lower motor neurons, which innervate skeletal muscles through neuromuscular junctions and are responsible for muscle contraction and voluntary movement (Figure 2) (Bear et al., 2016).

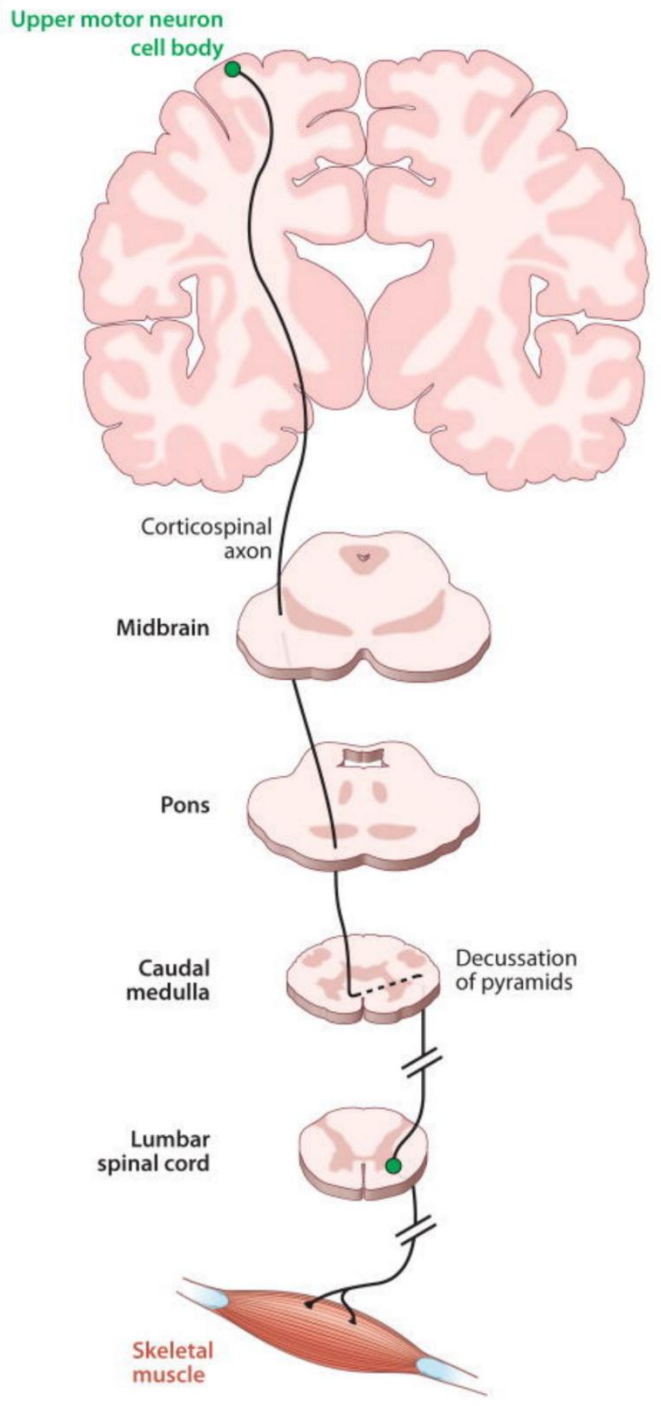

Figure 2. The human pyramidal motor system.

Upper motor neurons originating from the cerebral motor cortex extend their axons within the spinal cord. The majority of axons decussate within the caudal medulla and descend as lateral corticospinal tracts. Corticospinal axons establish connections with spinal interneurons, which then establish synapses with lower motor neurons. Lower motor neurons form specialized synapses known as neuromuscular junctions with the skeletal muscles and regulate their contraction (Blackstone, 2012).

Corticospinal axons can be up to 1 m long and can even constitute more than 99% of the cell volume (Blackstone, 2012). This is crucial for rapid relay of action potentials and timely control of voluntary movement, but also represents a source of high vulnerability for these neurons. Neurons with long axonal projections are typically more prone to neurodegeneration, and length-dependent axonal degeneration is a hallmark of many neurodegenerative disorders, including Charcot/Marie/Tooth disease (Sleigh et al., 2020), hereditary spastic paraplegias (Blackstone, 2012) and amyotrophic lateral sclerosis (Ovsepian et al., 2023). Studies have shown that the removal of synapses, typically preceding axonal degeneration, happens with a higher probability in neurons with long axons than in same-type neurons with short axons (Tenedini et al., 2024).

The high vulnerability of long axons is due to different factors. Firstly, given their extensive length, axons are highly susceptible to mechanical damage. Also, the long-distance transport of materials from and back to the cell body and the metabolic supply needed to fuel this transport process are highly demanding. Furthermore, misfolded proteins, aggregates, and organelles tend to accumulate in axons with aging, leading to substantial neuronal stress and subsequent degeneration (Hetz & Saxena, 2017). These factors can be a trigger to a phenomenon known as dying-back axonopathy, where distal axons form axonal swellings and gradually degenerate, starting from the synaptic terminals and continuing towards the cell body (Saxena & Caroni, 2007).

1.2 Hereditary spastic paraplegias

Hereditary spastic paraplegias (HSPs) are a large heterogeneous group of neurological disorders with main symptoms being lower body spasticity and gait impairment, with a large majority of patients also affected by distal sensory loss and urinary urgency (A. E. Harding, 1983). From a cellular point of view, they are mainly characterized by the length-dependent dying-back degeneration of longer axons, particularly those of corticospinal neurons, but also ascending long sensory fibres

(Blackstone, 2012). In 1876, neurologist Adolph Seeligmüller first described four siblings in a consanguineous family presenting progressive spasticity and weakness of the lower limbs (Seeligmüller, 1876). Between 1893 and 1898, neurologists Adolph Strümpell and Maurice Lorrain were the first to suggest that this disease might be hereditary (Lorrain, 1898; Strümpell, 1893).

HSPs can be pure, with patients mainly presenting motor defects, urinary urgency, and mild cognitive impairments, or complex, with patients showing other symptoms as well, including ataxia, seizures, optic atrophy, epilepsy, and/or severe cognitive defects (Blackstone, 2012). HSPs affect between 0.1 and 9.6 people per 100,000, and they can be caused by X-linked recessive, autosomal recessive, or autosomal dominant mutations; up to 40% of cases are sporadic, present in patients with no HSP family history. The onset of the disease is also extremely variable, ranging from the first decade of life to 60-70 years of age, and patients with HSPs, especially when pure, typically have a normal lifespan (Shribman et al., 2019).

To date, over 80 spastic gait genetic loci have been identified, and the corresponding spastic paraplegia genes have been identified. The autosomal dominant (AD) form of the disease accounts for roughly 75-80% of registered cases of pure HSP, and the most prevalent form of AD-HSP is caused by mutations in the *SPAST* gene (this form of the disease is known as SPG4). The second and third most common AD-HSPs are caused by mutations in the *ATL1* gene (encoding the protein atlastin-1) and mutations in the *REEP1* gene (encoding the protein REEP1) (Shribman et al., 2019).

Proteins involved in the development of the disease orchestrate numerous cellular processes which are disrupted in HSP, including mitochondrial homeostasis, axonal transport, endocytosis, lipid metabolism, myelination, microtubule dynamics and morphology, and endoplasmic reticulum morphogenesis (Figure 3) (Denton et al., 2016).

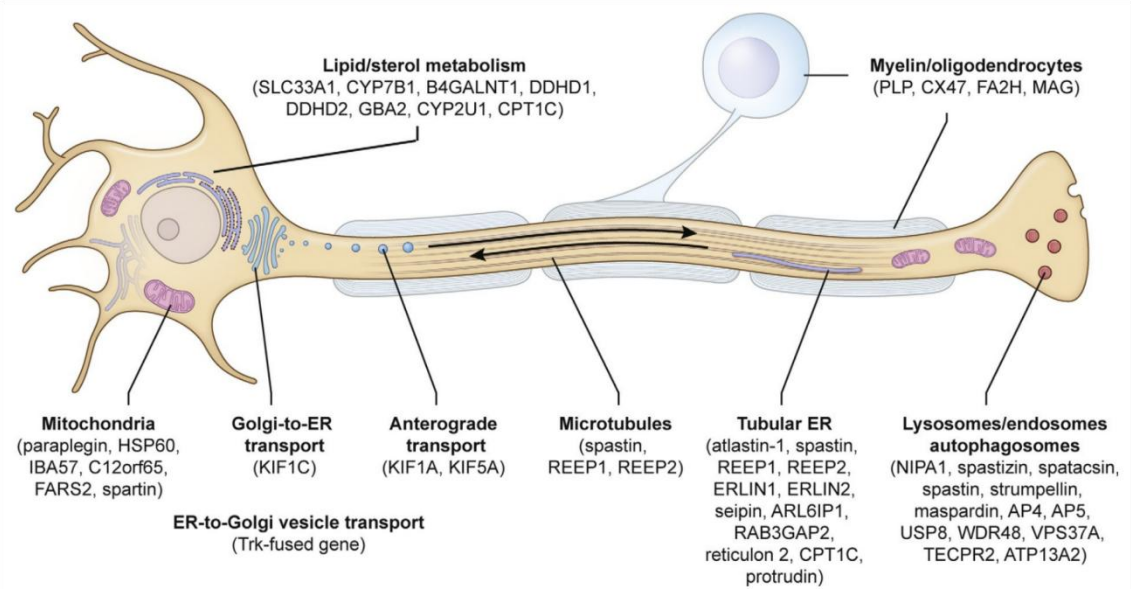

Figure 3. Pathways involved in HSP.

Schematic representation of neuronal processes involved in the pathogenesis of HSP. Between parentheses, proteins related to HSP involved in these processes. (Blackstone, 2018).

1.3 The microtubule network

The cytoskeleton is an organelle present in all eukaryotic and prokaryotic cells. It is crucial for numerous processes, such as the spatial organization of cell contents, maintaining the connection of the cell with the external environment, allowing for cell movement, cell division, and intracellular transport (Alberts et al., 2002). Rather than being a static structure, the cytoskeleton is extremely dynamic due to the constant rearrangement of its components. There are three different types of cytoskeletal networks: actin filaments, intermediate filaments, and microtubules. Actin filaments are mainly responsible for the maintenance of cell shape and movement. Intermediate filaments are mainly involved in mechanical resistance. Microtubules (MTs) are, in turn, crucial for intracellular organization, transport, and cell division (Hohmann & Dehghani, 2019).

MTs are straight, hollow cylinders formed via the polymerization of α- and β-tubulin monomers. These monomers bind to each other in a head-to-tail manner, and new αβ-tubulin dimers are added on the growing tip of MTs. The growing end, where the β-tubulin subunits are exposed, is known as the plus end, while the other end, where the α-tubulin subunits are exposed, is known as the minus end (Figure 4A). MTs are extremely dynamic and undergo constant polymerization and depolymerization (Alberts et al., 2002). The integration of αβ-tubulin dimers into growing MTs is dependent on GTP binding and hydrolysis, which occurs within the β-tubulin subunit. The addition of GTP-bound tubulin subunits to growing MTs creates a GTP cap at the plus end of MTs, which stabilizes MTs and protects them from depolymerization. Based on the needs of the cell, MTs can rapidly switch from growing to shrinking, where GTP hydrolyzation causes GDP-bound tubulin to be exposed and leads to rapid MT depolymerization (Figure 4B) (Alberts et al., 2002).

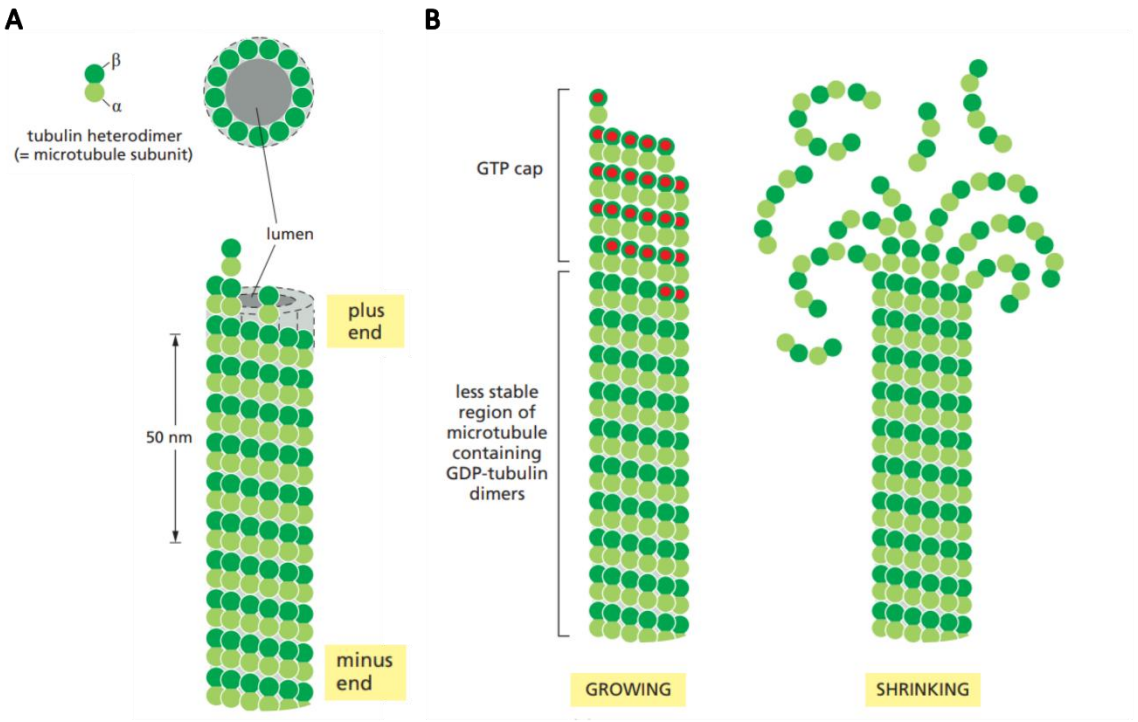

Figure 4. MT structure and dynamics.

(A) MTs are made up of heterodimers of α- and β-tubulin, which are added following a specific orientation. The growing end, where β-tubulin subunits are exposed, is known as the plus end, while α-tubulin subunits are exposed at the minus end. (B) MTs are extremely dynamic structures and often switch from a growing to a shrinking state based on cell needs. The plus end is characterized by the presence of a GTP cap, which is responsible for MT stabilization and protection from

depolymerization. Over time, GTP is hydrolysed to fuel the addition of further αβ-tubulin heterodimers. When GTP is hydrolysed more rapidly than the addition of αβ subunits, the plus end loses the GTP cap and MT depolymerization is favoured. Adapted from (Alberts et al., 2002).

The maintenance of proper MT dynamics is crucial for proper cell function. In neurons, MTs are crucial for the maintenance of cell polarity. While in dendrites, MTs present a mixed orientation, in axons, MTs are uniformly distributed, and the plus ends face distal axons (Baas et al., 1988). MT polarity also plays an important part in intracellular transport. Motor proteins move along MT tracks to deliver components throughout the cell; different protein families are responsible for anterograde (towards the plus end) and retrograde (towards the minus end) transport of cell components. Anterograde transport is typically orchestrated by kinesin proteins, while retrograde transport is performed by dynein proteins (Hirokawa & Takemura, 2005). Neuronal MT polarity is crucial for the selective transport of components in axons, for example, in transporting components to growth cones during axonal development and to presynaptic terminals in adult neurons (Alberts et al., 2002). The highly dynamic nature of the MT network is orchestrated by numerous factors, including MT-severing proteins. In mammals, MT severing is orchestrated by proteins of the AAA ATPase family of enzymes known as spastin, katanin, and fidgetin. These proteins form hexamers with a central pore and orchestrate MT severing into smaller fragments via the hydrolysis of ATP (steps of MT severing are shown in Figure 5) (Sharp & Ross, 2012).

Tubulin post-translational modifications were shown to play a direct role in the regulation of MT severing (Lacroix et al., 2010; Sudo & Baas, 2010).

Spastin depletion causes alterations in MT dynamics, morphology, and an increase in MT length in primary mouse neurons, *Drosophila melanogaster* motor neurons, and zebrafish embryos (Butler et al., 2010; Fassier et al., 2012; Lopes et al., 2020; Sherwood et al., 2004). MT alterations are also seen in SPG4-HSP mouse models and HSP patient-derived neurons (Denton et al., 2014; Qiang et al., 2019). Interestingly, spastin loss also leads to an accumulation of disorganized MTs in axonal swellings and a decrease in MT plus ends in primary mouse cortical neurons.

Axonal swellings were dramatically reduced upon treatment with MT-targeting drugs (Fassier et al., 2012).

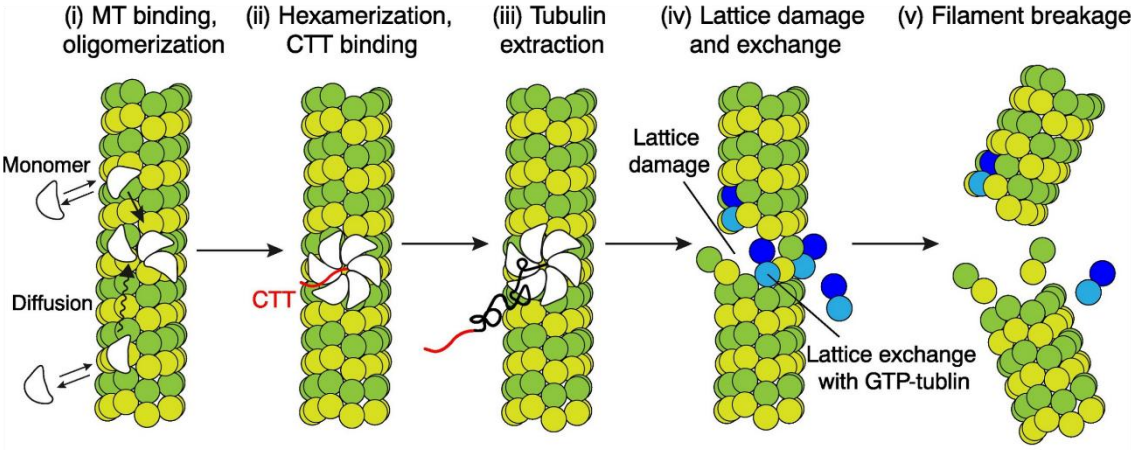

Figure 5. Molecular mechanisms of MT severing.

MT severing by enzymes follows different steps: (i-ii) first, MT severing enzymes form hexamers and bind to the C-terminal tail of tubulin (CTT); (iii-v) then, the tubulin polypeptide is pulled through the central pore of the hexamer and cleaved, forming lattice damage and subsequent breakage of the MT filament (Kuo & Howard, 2021).

1.4 The endoplasmic reticulum: functions and neuronal distribution

The endoplasmic reticulum (ER) is a membrane-bound organelle present throughout the cytoplasm of all eukaryotic cells. It is composed of different membrane compartments, and can be divided into two domains: rough and smooth ER. Rough ER is mainly perinuclear and characterized by wide sheets and many ribosomes attached to its surface. Its main functions are protein synthesis, folding, and export (Schwarz & Blower, 2016). Smooth ER is usually more peripheral, has few ribosomes, and is composed of narrow interconnected tubules and irregularly spaced cisternae. Tubules are the key sites for lipid synthesis and ER contacts with other organelles, while cisternae have a large lumen and function as storage sites for intracellular calcium (Shibata et al., 2006). In neurons, because of their peculiar morphology and polarization, rough ER is mainly found in the somatodendritic region, while axonal ER is primarily smooth, with occasional small sheets (Figure 6) (Öztürk et al., 2020).

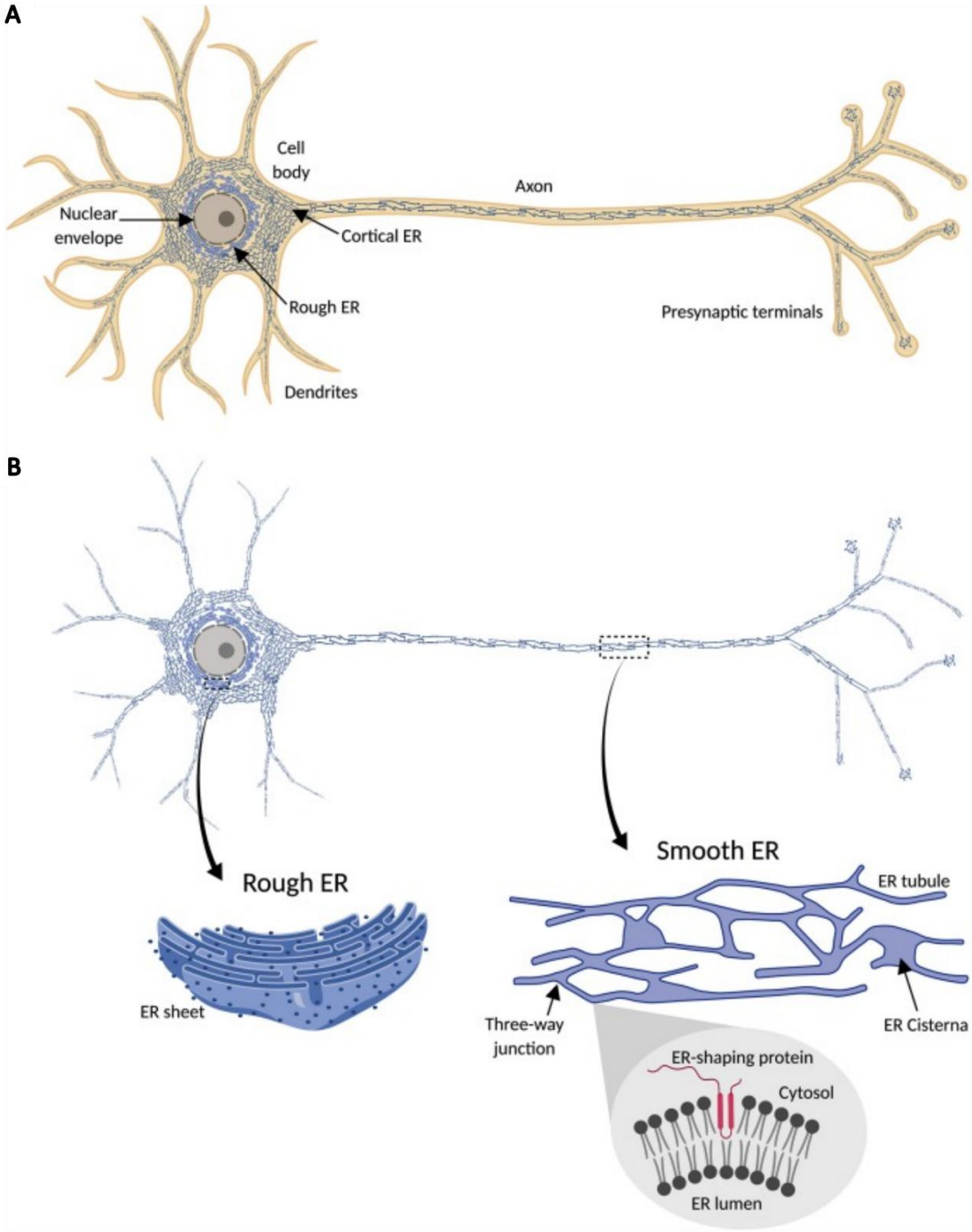

Figure 6. The neuronal ER.

(A) The ER network is distributed continuously throughout the neuron. (B) In the somatodendritic region, the ER is mainly rough, characterized by flat and large ER sheets and surface ribosomes. Axonal ER is instead largely smooth, characterized by ER tubules and cisternae. The membrane curvature and the three-way junctions necessary for proper tubular morphology are orchestrated by ER-shaping proteins, which, through hydrophobic hairpin loops present in their sequence, perform hydrophobic wedging and insert themselves into the ER bilayer. (Öztürk et al., 2020)

1.5 ER, protein synthesis and folding

The rough ER is crucial for protein synthesis of transmembrane, secreted, and a subpopulation of cytosolic proteins (Schwarz & Blower, 2016). Protein synthesis requires the docking of an mRNA-ribosome complex on the ER membrane. Transmembrane proteins contain one or more hydrophobic regions that span across the phospholipid bilayer and allow for their anchorage to the membrane. These proteins typically start to be translated in the cytosol by mRNA-ribosome-polypeptide complexes and are subsequently trafficked to and docked on the ER, where translation continues. The emerging polypeptide will then enter the ER through a complex known as the translocon, a channel composed of several Sec proteins, through which it will be inserted within the membrane. Proper protein folding and membrane insertion typically occur during translation (Rapoport, 2007). If a protein is to be secreted, translation also initiates in the cytosol and continues in the ER, but following translation and translocation to the ER lumen, it will undergo folding and modifications, which are orchestrated by chaperones and folding enzymes. The protein will then be released and trafficked through the Golgi to its final destination (Seiser & Nicchitta, 2000). When proteins are not folded correctly, they need to be cleared in order not to negatively affect cellular function. Misfolded proteins are recognized in the ER by protein folding sensors, which target them for the ER-associated degradation pathway mediated by the proteasome (Ruggiano et al., 2014). Several disorders are associated with protein misfolding, such as diabetes, inflammatory bowel disease, various cancers, and neurodegenerative disorders (Schwarz & Blower, 2016).

1.6 ER and Lipid Metabolism

The smooth ER is responsible for bulk synthesis and distribution of lipids in the cell, processes which are crucial for cellular membrane maintenance. Lipids can be trafficked via vesicular transport or through contact sites present between the ER

and other organelles. Following their synthesis, lipids are transferred to a region known as the ER-Golgi intermediate compartment, which distributes them in the cell through contacts with organelles or secretory vesicles (Appenzeller-Herzog & Hauri, 2006).

Moreover, the biogenesis of lipid droplets, the main fat storage sites, and peroxisomes, involved in lipid decomposition, starts in the ER (Öztürk et al., 2020).

1.7 ER and Calcium Dynamics

The ER is a major intracellular calcium (Ca^{2+}) storage site and mediates the release and reuptake of Ca^{2+} to and from the cytosol. The ER contains numerous Ca^{2+} channels, necessary for Ca^{2+} release into the cytosol. This process is critical and needs to be tightly regulated, as intracellular Ca^{2+} concentrations need to be kept constant. Ca^{2+} is crucial for numerous cellular functions, including synaptic signalling, protein localization, function and association, metabolism, and cell survival (La Rovere et al., 2016). The disruption of intracellular Ca^{2+} homeostasis can lead to defects in mitochondrial function, impaired synaptic transmission, and ultimately, cell death (McDaid et al., 2020). Alterations in intracellular Ca^{2+} levels have been linked to neuronal dysfunction in various neurodegenerative diseases, including HSPs. SPG4 iPSC-derived neurons were found to present a decrease in store-operated Ca^{2+} entry and disruptions in Ca^{2+} homeostasis (Rizo et al., 2022). In iPSC-derived neurons derived from patients affected by HSP caused by missense mutations in ER Lipid Raft Associated 2 (ERLIN2), intracellular free Ca^{2+} levels were found to be decreased, triggering ER stress-mediated apoptosis (X. Zhu et al., 2023).

1.8 ER-MT interactions

The cytoskeleton has a central role in the regulation of the tubular ER network, as MTs and the ER have been shown to interact, leading to tubular ER formation and support of ER dynamics (Terasaki et al., 1986). Depolymerization of MTs has been

found to lead to ER tubule loss, increasing the ratio of ER sheets to tubules (Joensuu et al., 2014). The interaction between MTs and ER is necessary for axonal ER maintenance, as alterations in ER morphology in a MT-severing deficient spastin mutant *Drosophila melanogaster* model were rescued by the administration of vinblastine, a MT-destabilizing drug (Vajente et al., 2019). Vinblastine treatment was also found to rescue axonal defects in SPG4 and neurite outgrowth defects in SPG3A iPSC-derived neurons (Denton et al., 2016).

Although the MT cytoskeleton was found not to be required for ER network formation, MT-based ER motility is crucial for tubular ER morphology, distribution, and organization within the cell (Hu et al., 2009). MT-based ER motility can be orchestrated via two main mechanisms: ER sliding, orchestrated by kinesin and dynein motor proteins (Waterman-Storer & Salmon, 1998) and the Tip attachment complex (TAC), where the tip of an ER tubule attaches to an extending MT (Grigoriev et al., 2008). The two mechanisms are independent of each other, and data suggest that the TAC mechanism might not be essential for axonal ER transport, while ER sliding seems to be the main mechanism that orchestrates anterograde and retrograde axonal ER transport (Figure 7) (Farías et al., 2019). In neurons, which are highly polarized cells, coordinated dynamics between MTs and the ER are tightly controlled to ensure proper ER distribution.

Furthermore, ER movement can also happen when ER-associated organelles are transported along MTs. For example, ER tubules were found to maintain their contact sites with mitochondria during their trafficking, in order to regulate numerous mitochondrial processes such as their fission, lipid composition, and Ca^{2+} levels (H. Wu et al., 2018). These processes are crucial for proper mitochondrial function, as for example, mitochondrial ATP production was found to

be dependent on proper Ca^{2+} uptake at ER-mitochondrial contact sites (Paillard et al., 2013).

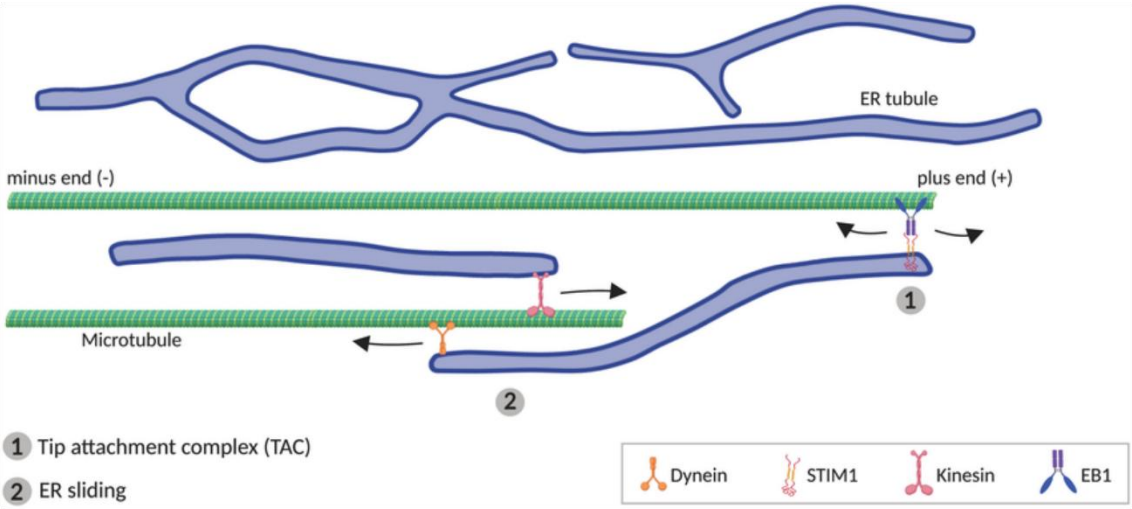

Figure 7. Mechanisms of MT-based ER movement.

MTs can mediate ER transport with two distinct mechanisms: (1) The tip attachment complex (TAC) is characterized by the interaction between an ER tubule and an MT plus end tip, orchestrated through the interaction between ER protein STIM1 and EB1, a protein present on growing MT tips. (2) ER sliding is dependent on the association between ER tubules and MTs and is orchestrated by kinesin and dynein proteins, which mediate anterograde and retrograde ER movement. (Öztürk et al., 2020)

1.9 Spastin

Roughly 40% of all AD-HSP cases are due to mutations in the *SPAST* gene, which encodes for a MT-severing enzyme known as spastin. It spans around 90 kb in genomic length, consists of 17 exons, and is located on the short arm of chromosome 2 (Hentati et al., 1994). This form of the disease is known as SPG4, and it is typically a pure form of HSP, with gait impairment and weakness of the lower limbs. The age of onset and the severity of SPG4 are variable. On average, SPG4-HSP manifests in patients between 31and 32 years of age (Meyyazhagan & Orlacchio, 2022; Solowska & Baas, 2015). There are some cases of patients with SPG4 also presenting some complex symptoms, such as cognitive impairment

(Orlacchio et al., 2004), cerebellar ataxia (Nielsen et al., 2004) and thin corpus callosum (Orlacchio et al., 2004), but these represent a minority of cases.

Spastin is a ubiquitous MT-severing protein of the AAA ATPase superfamily (together with katanin and fidgetin) with a predicted molecular weight of 68 kDa. Spastin is involved in numerous cellular processes, but its role in the regulation of MT severing is crucial for the formation, elongation, and maintenance of axons (Brill et al., 2016; Riano et al., 2009; Yu et al., 2008). Through the use of alternative translational initiation sites and splicing of exon 4, spastin can exist in four different isoforms. Among these, two isoforms are the most abundant protein products, and these are the full-length form of the protein, known as M1 (68 kDa, 616 amino acids), and a shorter isoform lacking 86 amino acids on its N terminus, known as M87 (60 kDa, 530 amino acids) (Claudiani et al., 2005; Mancuso & Rugarli, 2008). M87 spastin is ubiquitously expressed, while M1 spastin is more abundant in the brain and spinal cord (Claudiani et al., 2005; Solowska et al., 2008). M1 spastin is mainly perinuclear, found in the ER and to a lesser extent on endosomes, while M87 is localized throughout the cytoplasm and is recruited to midbodies and endosomes (Connell et al., 2009; Reid et al., 2005). M1 and M87 share an MT interacting and endosomal trafficking (MIT) domain, required for recruitment to midbodies and endosomes, a MT binding domain (MTBD), and an AAA ATPase domain, which is necessary for spastin-mediated severing of MTs. M1 also contains an N-terminal hydrophobic region, which forms an intramembrane hairpin loop, predicted to insert itself in a lipid bilayer via hydrophobic wedging (Figure 8) (Solowska & Baas, 2015).

Hydrophobic wedging is also displayed by reticulons, atlastins, and REEPs, which use this mechanism to insert themselves in ER membranes to generate tubular ER membrane curvature. Reticulon-1 and -2, atlastin-1, and REEP1 have been found to interact with M1 spastin, which was found to localize to the endoplasmic reticulum (Park et al., 2010). Reticulons, atlastin-1, and REEPs are also involved in HSP, suggesting that M1 spastin might have similar roles in ER shaping and morphology.

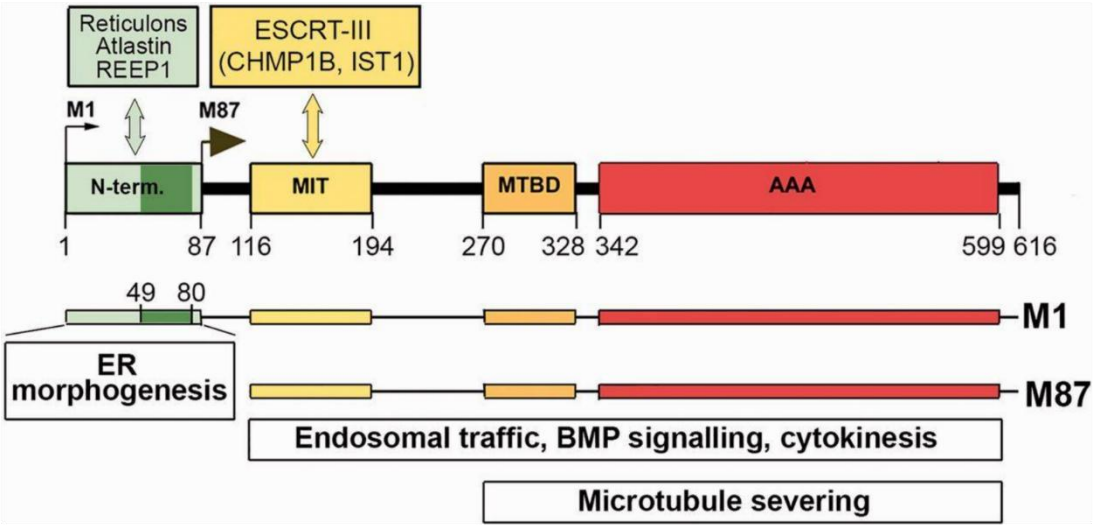

Figure 8. M1 and M87 spastin isoforms: structure and functions.

M1 and M87 spastin share three domains: the MT interacting and endosome trafficking domain (MIT), needed for interaction with ESCRT-III complex proteins for endosomal trafficking and cytokinesis, the MT binding domain (MTBD), and the AAA domain, required for MT binding and severing but which also play a role in endosomal trafficking and cytokinesis. M1 presents an N-terminal hydrophobic region necessary for ER morphogenesis and interaction with reticulons, atlastin-1, and REEP1. (Solowska & Baas, 2015)

The localization to the ER of four major HSP proteins has led to the hypothesis that defects in an ER morphogen complex formed by spastin, atlastin-1, REEP1, and reticulons, are the cause underlying HSPs in over 60% of cases. The function of the complex would be to regulate ER formation and localization. In this complex, atlastin-1 is crucial for tubular ER fusion, ER shaping is orchestrated by reticulons and REEP1, the latter responsible also for the tethering of the ER to MTs, and spastin regulates MT dynamics and connects the ER to MTs (Figure 9) (Denton et al., 2016). Although there are studies linking spastin to ER defects (Raby et al., 2024; Vajente et al., 2019), further investigation is needed to shed light on the precise role of spastin in mediating the ER-MT crosstalk and its role in ER morphology regulation.

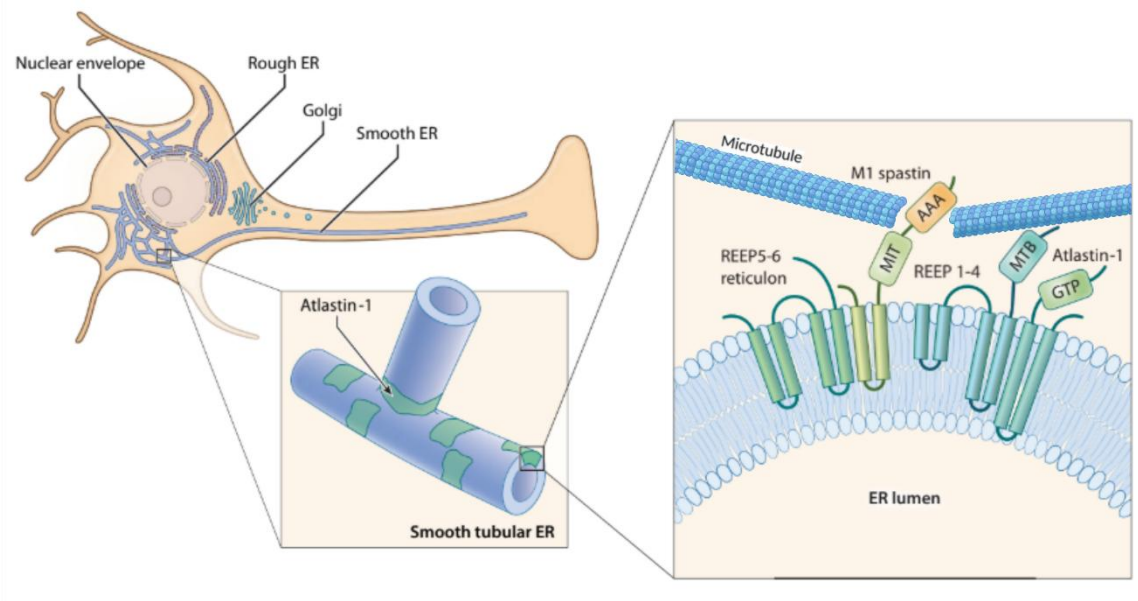

Figure 9. The ER morphogen complex.

Left: schematic of neuronal ER distribution. Center: depiction of a three-way junction of tubular ER. Atlastin-1 is the main protein responsible for the formation of these junctions. Right: schematic representation of the proposed role of spastin in ER regulation: M1 spastin inserts itself in the ER bilayer and interacts with reticulons, atlastin-1, and REEP proteins. This interaction is hypothesized to mediate ER-MT crosstalk and regulate the tubular ER network. Modified from (Blackstone, 2012).

Although the exact roles of the two isoforms are yet to be elucidated, evidence suggests that the M1 isoform might be less crucial within MT severing and more important for interaction with organelles and lipid droplets (Papadopoulos et al., 2015; Park et al., 2010). Conversely, M87 spastin is more involved in MT severing (Yu et al., 2008).

Furthermore, studies suggest M1 spastin may be more involved than M87 in the development of HSP. Firstly, it is mainly enriched within the spinal cord, the site of corticospinal axon degeneration. Secondly, M1 spastin can interact through its N terminus with atlastin-1, reticulons, and REEP1, responsible for endoplasmic reticulum morphogenesis. Also, dysfunctional M1 protein expression led to higher protein accumulation and was more detrimental to neurite outgrowth than dysfunctional M87 (Solowska et al., 2017).

However, data also indicate that both M1 and M87 are crucial for axonal outgrowth, as the overexpression of either isoform rescues neurite outgrowth defects in SPG4

iPSC-derived neurons, and to date, it is unclear how much each isoform contributes to axonal maintenance *in vivo* (Denton et al., 2016).

SPG4 mutations can be missense (28%), nonsense (15%), splice-site (26.5%), deletions (23%), and insertions (7.5%) (Fonknechten, 2000). Most of the mutations lead to a reduction in the expression of spastin or disrupt spastin-mediated MT severing, indicating that the disease might be caused by a haploinsufficiency mechanism (Lumb et al., 2012) or also a dominant negative mechanism (Pantakani et al., 2008). However, data suggest that the disease could also be caused by toxic gain-of-function mechanisms (Qiang et al., 2019). Axonal defects in SPG4 patients have been linked to the perturbation of numerous cellular pathways, including axonal transport, mitochondrial function, MT organization, ER shaping, and membrane trafficking (Blackstone, 2018).

Many studies have used spastin level reduction, the overexpression of WT or mutant spastin isoforms, and SPG4-HSP-derived neurons or animal models to gain insight into cellular defects underlying the pathogenesis of HSP.

Spastin reduction via knockdown was found to lead to impairments in axon outgrowth (Wood et al., 2006), a reduction in synaptic area and strength, and accumulation of stabilized MTs (Trotta et al., 2004).

In 22-month-old mice, reduced levels of spastin led to minor gait alterations. Furthermore, they presented axonal defects and swellings in both the ascending and descending tracts of the spinal cord, accompanied by cytoskeletal disorganization. When cultured, cortical neurons derived from these mice presented disruptions in retrograde axonal transport of organelles from axonal swellings (Tarrade et al., 2006). In cortical neurons of another mouse model of spastin reduction, anterograde rather than retrograde axonal transport was shown to be affected (Kasher et al., 2009).

Studies using global knock-out spastin mice have shown that spastin loss causes impairments in motor coordination and balance, memory deficits, synaptic loss, and MT alterations (Lopes et al., 2020).

Drosophila melanogaster, zebrafish, and mouse models of SPG4 show mobility impairments, axonal swellings, axonal outgrowth defects, and alterations in the MT cytoskeleton in motor neurons (Butler et al., 2010; Qiang et al., 2019; Sherwood et al., 2004; Wood et al., 2006). MT-binding agents can rescue axonal defects in *Drosophila melanogaster* mutant neurons, knock-out mouse-derived neurons, and SPG4 iPSC-derived neurons (Denton et al., 2014; Fassier et al., 2012; Orso, 2005). SPG4 iPSC-derived neurons present an increase in axonal swellings and axonal transport deficits, together with a reduction in neurite complexity. Overexpression of both spastin isoforms in these neurons rescued the axonal swellings and restored neurite complexity. These data suggest that both isoforms, and not only M1, are involved in the development of HSP (Denton et al., 2016).

In the context of ER morphology regulation, the overexpression of an MT severing-deficient M1 spastin mutant leads to an increase in ER tubulation and atlastin-1 redistribution (Sanderson et al., 2006). In more recent studies, the loss of spastin has been found to induce ER enlargement and a reduction in store-operated Ca^{2+} entry in induced pluripotent stem cell-derived neurons from HSP patients (Rizo et al., 2022). Furthermore, the expression of a dominant-negative spastin mutant was found to lead to an increase in ER sheet to tubule ratio in *Drosophila melanogaster,* while also leading to ER Ca^{2+} content reduction (Vajente et al., 2019).

Moreover, spastin was found to be involved in the formation of ER-mitochondria contacts, as spastin downregulation was found to lead to ER-mitochondrial contact number enhancement, and alterations in ER, mitochondrial morphology, and Ca^{2+} homeostasis (Raby et al., 2024). Also, spastin has been linked to lipid droplet metabolism, as in *Drosophila melanogaster,* M1 spastin overexpression leads to a decrease in lipid droplet numbers but an increase in size. Also, the expression of an MT binding and severing-deficient mutant induces lipid droplet clustering (Papadopoulos et al., 2015).

1.10 ER-shaping proteins

Both rough and smooth ER structures are extremely dynamic and are constantly rearranging to maintain the physiological density and continuity of the ER (Schwarz & Blower, 2016). ER tubular structure levels need to be maintained in order to ensure ER continuity, while also avoiding an excess of ER tubules. ER tubules are constantly undergoing fusion and branching events, resulting in novel three-way junctions. Dynamic ER tubules were found to drive the ER network into axonal growth cones, a process necessary for axon growth (Farías et al., 2019). Tubular ER morphology is crucial for homeostasis, and its disruption has been linked to numerous neurodegenerative disorders, including Alzheimer's disease, where an accumulation of abnormal tubular ER was also found in areas surrounding amyloid plaques (Sharoar et al., 2016).

This constant rearrangement is orchestrated by multiple factors, including ER-associated proteins. The formation and maintenance of ER sheets and tubules require factors acting in opposite directions, as sheets need to have a stable flat membrane and constant thickness, while tubule structure is dependent on the maintenance of a necessary curvature. Such curvature is orchestrated by curvature-inducing proteins, which are exclusively localized on ER tubules and the curved edges of ER sheets, through hydrophobic wedges (McMahon & Boucrot, 2015). To date, several integral membrane proteins have been found to be involved in ER bending, and interestingly, they are involved in HSP and interact with M1 spastin. Reticulons (reticulon-1, -2, -3, and -4 are known in mammals) are ubiquitously expressed, and the overexpression of some isoforms is sufficient to induce the formation of ER tubules. Conversely, reticulon depletion leads to the disruption of peripheral ER tubules and the formation of large ER sheets (O'Sullivan et al., 2012; Voeltz et al., 2006). Reticulons have also been shown to constrict ER tubules, resulting in their fragmentation, an important process for ER autophagy (Espadas et al., 2019). Importantly, both reticulon-1 and -2 are known to interact with M1 spastin (Mannan et al., 2006; Montenegro et al., 2012).

REEPs (REEP1-6 in mammals) are a family of membrane-bound proteins that work with reticulons to induce and maintain tubule curvature. REEP1 and REEP2 are only expressed in neuronal tissue, and REEP1, also known as HSP31 (SPG31) protein, can interact with spastin and atlastin-1 to shape ER tubules and mediate the interaction between ER and MTs (Park et al., 2010). Some members (REEP1-4) can also bind to MTs via an extended C-terminal domain. The depletion of REEP proteins has been shown to induce ER sheet expansion, ER discontinuity, and partial ER loss in distal motor axon regions in *Drosophila melanogaster* (Yalçın et al., 2017). Moreover, REEP1 loss in SPG31 mouse models leads to a decrease in neuronal axon length and branching, peripheral ER abnormalities in the primary motor cortex, and motor dysfunction (Beetz et al., 2013; Renvoisé et al., 2016). The deletion of one of the MT-interacting domains of REEP1 leads to a decrease in peripheral ER three-way junctions (Park et al., 2010).

Atlastins are a family of GTPases that mediate homotypic ER fusion and are therefore crucial for the formation of ER three-way junctions and maintenance of ER dynamics (Orso et al., 2009). Among the three atlastin paralogs known in mammals, atlastin-1, also known as the HSP 3A (SPG3A) protein, is abundantly expressed in the cerebral cortex and is a primary binding partner of M1 spastin (Park et al., 2010). SPG3A is the most common early-onset form of HSP. Atlastin-1 mutations and deletion lead to axonal growth and transport defects in human iPSC-derived neurons (Denton et al., 2016; P.-P. Zhu et al., 2014), while the overexpression of a dominant negative mutant leads to an increase in ER sheet formation in HeLa cells (P.-P. Zhu et al., 2003). A knockdown of the atlastin-1 homolog in zebrafish leads to disorganized spinal motor axons and reduced larval movement (Fassier et al., 2010). Furthermore, in a double mutant mouse model of REEP1 and atlastin-1, a dramatic transverse and periodic expansion of the ER was observed in corticospinal axons (P.-P. Zhu et al., 2022). Atlastin-1 is also involved in lipid droplet formation, a process that involves close interaction with the ER and which is crucial for proper fat storage (Klemm et al., 2013).

1.11 ER stress and its role in neurodegeneration

The ER is tightly linked to cellular stress and neurodegeneration. Cells can be subject to various types of stress, such as misfolded protein accumulation, oxidative stress, disruption in Ca^{2+} homeostasis, high energetic and secretory demands that cannot be fulfilled, and ultimately aging (Hetz & Saxena, 2017).

The ER is an organelle involved in a vast array of processes, and must therefore be extremely tightly regulated to correctly perform its functions. The unfolded protein response (UPR) is typically activated to restore homeostasis when misfolded or unfolded proteins accumulate within the lumen of the ER. If homeostasis is not reached, the neuron will undergo degeneration and ultimately cell death (Hetz & Saxena, 2017). Numerous other causes of ER stress can trigger the UPR, such as imbalances in lipid biosynthesis and degradation, disruptions in Ca^{2+} homeostasis, defects in organelles in contact with the ER, and viral infection (Hetz & Saxena, 2017; M. Wang et al., 2009).

Molecular chaperones are proteins that are usually expressed in response to cellular stress and assist with processes such as proper protein folding and translocation, but also regulation of Ca^{2+} homeostasis and quality control decisions, such as sorting misfolded proteins for ER-associated degradation (ERAD) (M. Wang et al., 2009).

A well-characterized ER chaperone is the 78-kDa glucose-regulated protein (GRP78), also known as BiP or HSPA5. In non-stressed cells, GRP78 binds to ER-transmembrane signalling molecules and ER-associated caspases and maintains them in an inactive state. Whenever the ER undergoes stress, such as protein misfolding, GRP78 is released from the signalling molecules and leads to the activation of the UPR (M. Wang et al., 2009). Consequently to the release of GRP78 from ER-signalling molecules, general protein synthesis is transiently attenuated (H. P. Harding et al., 1999) and ER chaperones, including GRP78, protein folding enzymes, and proteins involved in ERAD are upregulated (M. Li et al., 2000). If the stress is not resolved, GRP78 signalling can switch from being pro-survival to pro-

apoptotic. Whenever ER stress is too severe or prolonged, the UPR activates pathways that lead to apoptotic cell death, involving a crosstalk between the ER and mitochondria (J. Wu & Kaufman, 2006).

GRP78 is also involved in ER stress-induced autophagy, a process in which defective or long-lived proteins and organelles are degraded to promote cell survival. Upon GRP78 knockdown, ER integrity was found to be disrupted, and autophagy was suppressed (J. Li et al., 2008). GRP78 function is also crucial during embryonic development, as GRP78 knock-out mice exhibit lethality on embryonic day 3.5 (Luo et al., 2006).

Accumulation of misfolded proteins or mutated gene products and subsequent UPR activation have been linked to numerous neurodegenerative disorders, including Alzheimer's and Parkinson's diseases, where GRP78 localization and levels were found to be altered (Ghribi et al., 2003; Hoozemans et al., 2012).

Disruptions in ER interactions and contacts with other organelles have also been linked to axonal dysfunction and neurodegeneration (Figure 10).

For example, ER-mitochondrial contact sites are crucial for mitochondrial Ca^{2+} regulation, necessary for ATP production, and required for energy homeostasis (H. Wu et al., 2018). Another process dependent on ER-mitochondrial contact sites is mitophagy, the autophagy-dependent degradation of damaged mitochondria (Puri et al., 2019). The disruption of either process has been linked to oxidative stress and neurodegenerative disorders (Nunnari & Suomalainen, 2012; Raby et al., 2024). ER contact sites with mitochondria are also important for proper lipid exchange between the two organelles, which is crucial for mitochondrial lipid composition and the maintenance of the balance between mitochondrial fusion and fission (Steenbergen et al., 2005). Both spastin and REEP1 have been found at ER-mitochondrial contact sites, and spastin downregulation leads to an increase in ER-mitochondrial contact site numbers, accompanied by alterations in mitochondrial morphology and impaired mitochondrial Ca^{2+} homeostasis (Lim et al., 2015; Raby et al., 2024).

Moreover, lipid droplet biogenesis is crucial for cell survival as it regulates lipid storage and energy metabolism. Lipid droplets are dependent on close interaction with the ER. Spastin, atlastin-1, and reticulons have been found to affect lipid droplet metabolism (Chen et al., 2021; Klemm et al., 2013; Papadopoulos et al., 2015).

Furthermore, the ER contacts the plasma membrane mainly through its cisternae. These structures are necessary not only for the proper delivery of lipids and proteins, but also for the regulation of Ca^{2+} dynamics, and defects in this interaction have been linked to impairments in cell function (Saheki & De Camilli, 2017; Smith et al., 2024).

In addition, ER-MT interactions are crucial for processes including MT organization, ER movement, and tubular ER formation. Both spastin and REEP1-4 proteins can interact with MTs, and have been suggested to mediate the crosstalk between ER and MTs to orchestrate MT tethering and severing, but also ER morphology regulation (Park et al., 2010).

Finally, disruptions in ER-endosome contact sites have also been suggested to lead to axonal dysfunction and neurodegeneration. ER-endosome contacts are required for proper endosomal fission and protein trafficking. Both spastin and atlastin-1 have been found at these contact sites, and their loss has been linked to alterations in lysosomal morphology and function, endosomal fission, and receptor trafficking (Zlamalova et al., 2024).

Mutations in genes encoding both ER tubule-shaping proteins and proteins involved in the formation or maintenance of ER contacts with other organelles are found in patients with different disorders characterized by the degeneration of axons, including HSPs, Alzheimer's, and Parkinson's Disease (Raby et al., 2024; Sharoar et al., 2016; Vajente et al., 2019; Valadas et al., 2018). This indicates that axonal ER homeostasis is crucial for axonal maintenance and neuronal function.

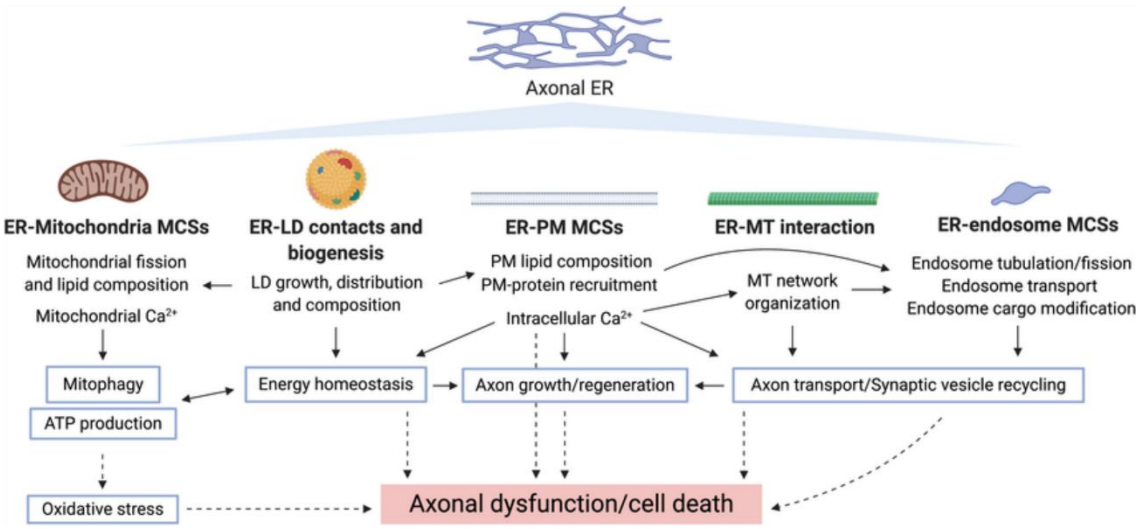

Figure 10. ER contacts and interactions with organelles and their role in axonal homeostasis.
The ER interacts with numerous organelles to ensure proper cell function. In neurons, disruptions of these interactions have been frequently linked to axonal dysfunction and neurodegeneration. The functions of ER interactions and contacts with organelles are shown, with a focus on their function and interdependency. (Öztürk et al., 2020)

1.12 Tubulin post-translational modifications: polyglutamylation and spastin

MTs can undergo post-translational modifications, such as phosphorylation, acetylation, tyrosination, detyrosination, or polyglutamylation (Figure 11) (Janke & Bulinski, 2011; Janke & Kneussel, 2010; Peris et al., 2009; Reed et al., 2006). These modifications function as MT modulators, as they can directly influence the activity of motor proteins and severing enzymes, and processes such as MT disassembly (Janke & Bulinski, 2011). Polyglutamylation is the addition of glutamates to the C-terminal tails of tubulin (Eddé et al., 1990). These are also the sites involved in the interaction of MTs with the MTBD of spastin (White et al., 2007).

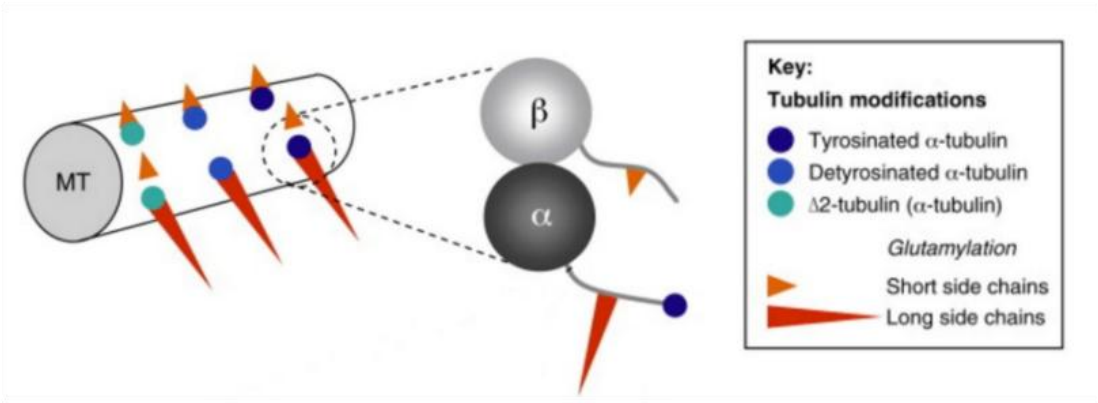

Figure 11. Schematic representation of C-terminal tubulin post-translational modifications. C-terminal α-tubulin tails can undergo numerous post-translational modifications, such as tyrosination, detyrosination, Δ2-tubulin generation, and glutamylation, which is orchestrated through the addition of short or long glutamate side chains to C-terminal tubulin tails. Adapted from (Janke & Kneussel, 2010).

The MT binding affinity of spastin was shown to linearly increase with the increasing number of glutamates on tubulin tails, while its severing activity non-linearly decreases (Valenstein & Roll-Mecak, 2016). High levels of polyglutamylation would therefore shift the activity of spastin from MT severing to MT stabilization. Previous data have shown that polyglutamylation levels are significantly increased in spastin-depleted neurons, and the reduction of these levels rescues some dysfunctional processes observed in these neurons, such as transport deficits and reduction of synapse numbers (Lopes et al., 2020). Altered levels of polyglutamylation are a possible cause of degeneration, as higher levels of polyglutamylated tubulin were observed in brain regions undergoing degeneration in mice with a mutation in the deglutamylating enzyme CCP1 (known as Purkinje cell degeneration mice) (Rogowski et al., 2010). Furthermore, data have shown that the degeneration of neurons in the cerebral cortex of these CCP1 mice could be rescued by the simultaneous knock-out of TTLL1, the major brain polyglutamylase (Magiera et al., 2018).

1.13 Aims of this study

Since the main cellular hallmark of HSP is the length-dependent degeneration of motor neuron axons within the corticospinal tract, research on the molecular mechanisms underlying HSP is not only important to be able to gain insight into the pathogenesis of the disease but also to shed light on the numerous pathways important for axon formation and maintenance. These results would be crucial not only for the development of therapies for HSP but also for other diseases characterized by axonopathy, such as many neurodegenerative diseases and spinal cord injury.

This research study aims to address the following research questions:

1) Do spastin reduction and loss affect axonal morphology, ER distribution and stress?
2) Does spastin-mediated MT severing affect axonal ER?
3) Does tubulin polyglutamylation reduction have a similar effect on axonal ER to spastin reduction or loss?
4) Which spastin domains are involved in axonal ER morphology regulation?

2. Materials and methods

2.1 Instrumentation

Microscopes:

Zeiss LSM900 equipped with a 20x air and 40x oil objective (for fixed sample imaging), Zeiss

Nikon spinning disc microscope equipped with a 100x oil objective (for live cell imaging), Visitron

Zeiss EM 900N TEM equipped with a 20,000x objective (for transmission electron microscopy), Zeiss

Cell culture incubator: HeraCell 150/150i, Thermo Fisher Scientific

Microtiter plate reader: Infinite 200 PRO NanoQuant, Tecan

Spectrophotometer: NanoDrop 2000/2000c, Thermo Fisher Scientific

PCR: PTC-200 Thermal Cycler, MJ Research, Marshall Scientific

DNA gel Imager: Intas Gel Imager, Intas

Semi Dry Blotter: V20-Semi Dry Blotter, SCIE-PLAS

Western blot detection system: Li-Cor Odyssey CLx Imaging System, Li-Cor

2.2 Chemicals

Table 1 - List of chemicals

Reagent	Manufacturer	Cat. No.
Acrylamide/Bis-acrylamide ROTIPHORESE® 40%	Carl Roth GmbH and Co. KG	T802.1
Molecular Biology Grade Agarose	Eurogentec	EP-0010-05
Ammonium peroxydisulfate (APS)	Carl Roth GmbH and Co. KG	9592
Aqua-Poly/Mount	Polysciences	18606
Bovine Serum Albumin (BSA)	Sigma-Aldrich	A3156

Bromophenol Blue	Carl Roth GmbH and Co. KG	T116
cOmplete™, EDTA-free Protease Inhibitor Cocktail	Sigma-Aldrich	04693132001
1,4-Dithiothreitol (DTT)	Carl Roth GmbH and Co. KG	6908
Ethanol	Carl Roth GmbH and Co. KG	9065
Ethidium bromide solution	Carl Roth GmbH and Co. KG	2218
Ethylenediaminetetraacetic acid disodium salt dihydrate (EDTA)	Carl Roth GmbH and Co. KG	8043
FastGene 1 kb DNA Marker Plus	Nippon Genetics	MWD1P
Fetal Bovine Serum (FBS)	Capricorn Scientific	FBS-12A
Acetic acid	Carl Roth GmbH and Co. KG	6755
Glycerol	Carl Roth GmbH and Co. KG	3783.1
Glycine	Sigma-Aldrich	G8898
Glucose solution	Gibco	A2494001
Hanks‘ Balanced Salt Solution (HBSS)	Gibco	14170088
HEPES	Carl Roth GmbH and Co. KG	9105
Hibernate™-E Medium	Gibco	1247601
2-Propanol	Carl Roth GmbH and Co. KG	6752
Kanamycin	Carl Roth GmbH and Co. KG	T832
Methanol	Carl Roth GmbH and Co. KG	P717
Milk powder	Carl Roth GmbH and Co. KG	T145
dNTPs	Promega	U1240
OptiMEM™ Reduced Serum Medium	Gibco	31985070
Paraformaldehyde	Carl Roth GmbH and Co. KG	0335
Penicillin-Streptomycin	ThermoFisher	15140122
Phenylmethylsulfonyl fluoride (PMSF)	Carl Roth GmbH and Co. KG	6367
Pierce™ BCA Protein Assay Kit	Thermo Fisher Scientific	23227
PNGM™ Primary Neuron Growth Medium BulletKit® (PNGM)	Lonza	CC-4461
Poly-L-lysine-hydrobromide	Sigma-Aldrich	P2636

Precision Plus Protein™ Kaleidoscope™ Prestained Protein Standards	BioRad	1610375
QuickExtract DNA Extraction Solution	Biozym	101098
Sodium dodecyl sulfate (SDS)	Sigma-Aldrich	L4509
N,N,N',N'-Tetramethylethylenediamine (TEMED)	Sigma -Aldrich	T9821
TRIS	Carl Roth GmbH and Co. KG	5429
Triton® X 100	Carl Roth GmbH and Co. KG	3051
Trypsin-EDTA (0.05%), phenol red	Invitrogen	25300054
Tween® 20	Carl Roth GmbH and Co. KG	9127

2.3 Cell lines

Table 2 - List of bacterial cell lines used for plasmid transformation

Cell line	Manufacturer	Cat. No.
NEB 5-alpha competent *E. coli* cells	New England BioLabs	C2987H
DH5-alpha chemically competent cells	New England BioLabs	C2989K

2.4 Solutions

10X PBS

1.37 M NaCl

27 mM KCl

100 mM Na_2HPO_4

18 mM KH_2PO_4

Total brain lysis buffer

1X PBS

1% (v/v) Triton X 100

1X cOmplete protease inhibitor

1 mM PMSF

10X SDS-Running Buffer	250 mM Tris-Base 2.5 M Glycine 1% (w/v) SDS pH=8.3
6X Laemmli Buffer	12% (w/v) SDS 60% (w/v) Glycerol 0.6 M DTT 0.06% (w/v) Bromophenol Blue
SOC medium	0.5% (w/v) yeast extract 2% (w/v) tryptone 10 mM NaCl 2.5 mM KCl 10 mM $MgCl_2$ 10 mM $MgSO_4$ 20 mM Glucose
10X TBS	0.2 M Tris 1.5 M NaCl
10X TBS-T	1X TBS 1% (v/v) Tween® 20
SDS-Transfer Buffer	25 mM Tris 192 mM Glycine 20% (v/v) Methanol

50X TAE	242 g Tris 57.1 mL glacial acetic acid 0.5 M EDTA pH=8
2X HBS	280 mM NaCl 10 mM KCl 1.5 mM Na_2HPO_4 12 mM dextrose pH=7.4
HEPES buffer for live cell imaging	10 mM HEPES 135 mM NaCl 5 mM KCl 2 mM $CaCl_2$ 2 mM $MgCl_2$ 15 mM Glucose pH=7.4

2.5 Restriction enzymes

Table 3 - List of restriction enzymes

Restriction enzyme	Manufacturer	Cat. No.
FastDigest Eco91I	ThermoScientific	FD0394
FastDigest EcoRI	ThermoScientific	FD0275

2.6 Plasmid DNA

Table 4 - List of constructs used for cloning and transfection

Name	Source
pEGFP-C1	Clontech (#6084-1)
mCherrySec61β	Addgene (#49155)

pEGFP-M85-K388R	Dr. André Lopes, ZMNH
pEGFP-M1	Prof. Dr. Peter Baas, Drexel University
pEGFP-M85	Prof. Dr. Peter Baas, Drexel University
pEGFP-M1 P97T	This study
pEGFP-M1 P361L	This study
pEGFP-M1 P97T P361L	This study
pEGFP-M85 P97T	This study
pEGFP-M85 P361L	This study
pEGFP-M85 P97T P361L	This study

pEGFP-M1 P97T was generated by site-directed mutagenesis based on the pEGFP-M1 backbone, making use of the Q5 Site-Directed Mutagenesis Kit (New England Biolabs, Ipswich, Massachusetts, USA). The nucleotide exchange of P97T was introduced using the following primers:

P542T_FW, CGGGACCGCGACCGCGCCCGCCT;

P542T_M1_RV, GAGCTCCTCTTGGCGGCCATGAGGG.

The PCR was performed using the following cycling conditions:

Step 1: 98°C for 30 seconds

Step 2: 98°C for 10 seconds

Step 3: 72°C for 30 seconds

Step 4: 72°C for 160 seconds (again steps 2 to 4 for other 24 cycles)

Step 5: 72°C for 120 seconds

Step 6: 4°C ∞

pEGFP-M85 P97T was generated by site-directed mutagenesis based on the pEGFP-M85 backbone, making use of the Q5 Site-Directed Mutagenesis Kit (New England Biolabs, cat. No. E0554S). The nucleotide exchange of P97T was introduced using the following primers:

P542T_FW, CGGGACCGCGACCGCGCCCGCCT;

P458T_M85_RV, GAGCTCCTCTTGGCGGCGGATCTGAGTC.

The PCR was performed using the following cycling conditions:

Step 1: 98°C for 30 seconds

Step 2: 98°C for 10 seconds

Step 3: 72°C for 30 seconds

Step 4: 72°C for 160 seconds (again steps 2 to 4 for other 24 cycles)

Step 5: 72°C for 120 seconds

Step 6: 4°C ∞

pEGFP-M85 P361L was generated by site-directed mutagenesis based on the pEGFP-M85 backbone, making use of the Q5 Site-Directed Mutagenesis Kit (New England Biolabs, Ipswich, Massachusetts, USA). The nucleotide exchange of P361L was introduced using the following primers:

P805L_FW, TGTCATCCTTCTGTCTCTGCGGC;

P805L_RV, ATCTCCTGCAGCGCT.

The PCR was performed using the following cycling conditions:

Step 1: 98°C for 30 seconds

Step 2: 98°C for 10 seconds

Step 3: 65°C for 30 seconds

Step 4: 72°C for 160 seconds (again steps 2 to 4 for other 24 cycles)

Step 5: 72°C for 120 seconds

Step 6: 4°C ∞

pEGFP-M1 P361L was generated by using FastDigest Eco91I (ThermoScientific, FD0394) and EcoRI (ThermoScientific, FD0275) restriction enzymes on the pEGFP-M85 P361L backbone; the resulting fragment was ligated with the complementary pEGFP-M1 fragment obtained via digestion with the same restriction enzymes.

pEGFP-M1 P97T P361L was generated by using FastDigest Eco91I and EcoRI restriction enzymes on the pEGFP-M85 P361L backbone; the resulting fragment was ligated with the complementary pEGFP-M1 P97T fragment obtained via digestion with the same restriction enzymes.

pEGFP-M85 P97T P361L was generated by using FastDigest Eco91I and EcoRI restriction enzymes on the pEGFP-M85 P361L backbone; the resulting fragment was ligated with the complementary pEGFP-M85 P97T fragment obtained via digestion with the same restriction enzymes.

2.7 Antibody list

Table 5 - List of primary antibodies

Target	Species	Manufacturer	Cat. No.	Clone	Dilution
Ankyrin G	Guinea pig	Synaptic Systems	386 005	polyclonal	ICC 1:2,000
Calreticulin	Rabbit	Invitrogen	PA3-900	polyclonal	WB 1:1,000
GAPDH	Mouse	GeneTex	GTX28245	6C5	WB 1:1,000
GRP78	Rabbit	Abcam	ab21685	polyclonal	ICC 1:400 WB 1:1,000
Alpha-tubulin	Mouse	Abcam	ab7291	DM1A	ICC 1:1,000

Table 6 - List of secondary antibodies

Name	Manufacturer	Cat. No.	Dilution
Alexa Fluor® 488 AffiniPure® $F(ab')_2$ Fragment Donkey Anti-Mouse IgG (H+L)	Jackson ImmunoResearch	715-546-150	ICC 1:500
Cy5™ AffiniPure® Donkey Anti-Mouse IgG (H+L)	Jackson ImmunoResearch	715-175-151	ICC 1:500
Cy5™ AffiniPure® Donkey Anti-Rabbit IgG (H+L)	Jackson ImmunoResearch	711-175-152	ICC 1:500
Goat anti-Guinea Pig IgG (H+L) Highly Cross-Adsorbed Secondary Antibody Alexa Fluor™ 647	Invitrogen	A-21450	ICC 1:1,000

IRDye® 680RD Goat Anti-Rabbit IgG Secondary Antibody	LICORbio	926-68071	WB 1:15,000
IRDye® 800CW Goat Anti-Mouse IgG Secondary Antibody	LICORbio	926-32210	WB 1:15,000

2.8 Bacterial Transformation following Site-Directed mutagenesis

When using the Q5 Site-Directed mutagenesis kit, transformation was performed following the instructions provided by the manufacturer. Briefly, NEB 5-alpha competent *E. coli* were thawed on ice. 5 µl of the DNA mix obtained by using the kit was added to the cells and gently mixed, followed by 30 minutes of incubation on ice. Then, heat shock was performed by placing the mix at 42°C for 30 seconds, followed by incubation for 5 minutes on ice. 950 µl of SOC medium (provided by the manufacturer) was added, and the mixture was incubated at 37°C for 60 minutes with constant shaking at 250 rpm. The cell suspension was then centrifuged at 20,000xg for a few seconds, and the supernatant was discarded so that only 50-100 µl was left in the tube. The pellet was gently resuspended and the cells were plated onto Agarplates (0.5% yeast extract, 1% tryptone, 1% NaCl, 1.5% bactoagar in ddH_2O) with the appropriate antibiotic and incubated at 37°C overnight. All of the following steps were performed as described in the Plasmid DNA isolation section below.

2.9 Bacterial Transformation and Retransformation

In order to perform DNA amplification, 100 µl (for transformation) or 50 µl (for retransformation) of DH5-alpha competent cells were thawed on ice. After 20 minutes, 3 µg (for transformation) or 1 µg (for retransformation) of DNA was added to the competent cells and the mixture was incubated for 20 minutes on ice. Then the mixture was placed at 42°C for 45 seconds and subsequently placed on ice for

2 minutes. 500 µl (for transformation) or 250 µl (for retransformation) of SOC medium were added to the tube and the cells were allowed to grow for 1 hour at 37°C. The cells were then centrifuged at 20,000xg for a few seconds and then the supernatant was discarded so that only 50-100 µl was left in the tube. After resuspending gently, the remaining mixture was plated onto Agarplates containing the appropriate antibiotic. The plates were then kept at 37°C overnight to allow the cells containing the plasmid of interest to grow.

2.10 Plasmid DNA isolation (Midiprep)

The following day, a single colony was inoculated into 150 ml of LB medium supplemented with the appropriate antibiotic (1:1,000 concentration) and the mixture was placed overnight at 37°C while shaking (180 rpm). Then, the tubes were centrifuged at 5,000xg for 10 minutes at 4°C. DNA was then purified using the Nucleobond Xtra Midi EF Kit (Macherey-Nagel, cat. No. 740410) following the instructions provided by the manufacturer. To precipitate the DNA, 3.5 ml of 2-propanol was added and mixed with the eluted DNA. Then, the mixture was centrifuged at 15,000xg for 30 minutes at 4°C using a Fixed-Angle JA-25.50 Rotor in an Avanti J-26 XP centrifuge (Beckman Coulter). The supernatant was discarded, and then 2 ml of 70% ethanol was added, followed by centrifugation at 15,000xg for 5 minutes at room temperature. The supernatant was discarded and the pellet was left to dry for 30 minutes at room temperature. The pellet was then resuspended in endotoxin-free water and DNA concentration and purity were measured using a microtiter plate reader (Infinite 200 PRO NanoQuant) equipped with a NanoQuant Plate for DNA measurements or using a NanoDrop 2000/2000c spectrophotometer. Sample absorbance at 260 and 280 nm was measured and the ratio of A260/A280 was used to assess DNA purity. DNA was only kept when this ratio was between 1.8 and 2.0.

2.11 Animals

In this study, we used mice constitutively depleted of spastin, as previously described (Brill et al., 2016; Lopes et al., 2020).+/+, spastin +/-, and -/- mice were generated from heterozygous matings and bred in a specific-pathogen-free animal facility.

We also made use of tuba4aΔpolyGlu mice, which are knock-in mice carrying C-terminal tubulin-alpha4a point mutations that disrupt the polyglutamylation of this isoform (Hausrat et al., 2022). +/+ and tuba4aΔpolyGlu p/p mice were generated from heterozygous matings and bred in a specific-pathogen-free animal facility.

2.12 Primary neuronal culture of cortical neurons

12 mm (for fixed neurons) and 18 mm (for live cell imaging) glass coverslips were coated with Poly-L-Lysine overnight at 37 ºC, 5% CO_2. Pregnant mice were euthanized by CO_2/O_2 inhalation and subsequent cervical dislocation. The embryos were removed from the uterus by opening the embryonic sacs and they were decapitated. Whole brains were removed from the embryos in ice-cold autoclaved Glucose-PBS buffer and then placed in Hibernate-E Medium and kept on ice. Small sections of tails were cut from the embryos to be used for genotyping (see below). After genotyping, brains from embryos with the correct genotypes were used to derive cortical neurons. The meninges were removed and the cortices were isolated, cut into small sections and placed in 0.05 % trypsin/EDTA for 5 minutes at 37°C. Trypsin/EDTA was removed and the tissue was washed once with PBS+10% FBS and then twice with HBSS. The tissue was triturated by pipetting up and down with 2 glass pipets, gradually decreasing in diameter. 10 µL of the cell suspension was then placed on a Neubauer counting chamber and cells were counted, then plated at a density of 70,000 per 12 mm coverslip and 40,000 per 18-mm coverslip in cell culture dishes pre-filled with PNGM medium (supplemented with P/S, L-Glutamine, and NSF-1) and kept at 37 ºC and 5% CO_2.

2.13 Isolation of genomic DNA and genotyping

Spastin knock-out mouse line

Genomic DNA of the experimental mice was extracted by incubating the tail sections with Quick Extract Buffer for 15 minutes at 65 ºC and then for 3 minutes at 95 ºC. Then 2 µl per DNA extract was added to the reaction mix and the PCR was performed.

Table 7 – Genotyping mix components for the spastin knock-out line

Reagent Stocks	Reaction mix
ddH_2O	32.8 µl
10X Loading Buffer	5 µl
dNTPs 2 mM	5 µl
Primer PLR41 10 µM	2 µl
Primer PLR89 10 µM	2 µl
Primer PLR169 10 µM	2 µl
Taq Polymerase 5 U/l	0.2 µl
Genomic DNA	2 µl

Spastin knock-out mouse line genotyping PCR primer list

PLR41: AAGTCATGGCAGTCTTTCTGGCT

PLR89: CACATGGTGGCTCATAACCATTTA

PLR169: ATTTGCAAAAACTACTTGCTATTAAATCC

+/+ primers: PLR169 + PLR89

-/- primers: PLR41 + PLR89

PCR product sizes: 223 base pairs for the +/+ allele and 432 base pairs for the spastin -/- allele.

The PCR was performed using the following touchdown protocol:

Step 1: 95°C for 2 minutes

Step 2: 95°C for 25 seconds

Step 3: 65°C for 45 seconds

Step 4: 72°C for 1 minute and 15 seconds (again steps 2 to 4 for other 39 cycles)

Step 5: 72°C for 10 minutes

Step 6: 4°C ∞

Following the PCR reaction, the amplification product was loaded on 2% agarose gels and separated through electrophoresis to analyse the DNA size.

Tuba4aΔpolyglu knock-in mouse line

Genomic DNA of the experimental mice was extracted by incubating the tail sections with Quick Extract Buffer for 15 minutes at 65 ºC and then for 3 minutes at 95 ºC. Then 1 µl per DNA extract was added to the reaction mix and the PCR was performed.

Table 6 - Genotyping mix components for the tuba4aΔpolyglu knock-in line

Reagent Stocks	Reaction mix
ddH_2O	19.3 µl
10X Loading Buffer	2.5 µl
dNTPs 2 mM	1 µl
Primer 1 10 µM	0.5 µl
Primer 2 10 µM	0.5 µl
Taq Polymerase 5 U/l	0.2 µl
Genomic DNA	1 µl

TubA4AΔpolyglu knock-in mouse line genotyping PCR primer list

70252hom: GAGGAGGGAGCTTTGGACTCTGTGC

70253hom: AGCAGAAAGGGGGACAAGCAGAGG

PCR product sizes: 1302 base pairs for the wild-type allele

1440 base pairs for the knock-in allele.

The PCR was performed using the following touchdown protocol:

Step 1: 95°C for 2 minutes

Step 2: 95°C for 25 seconds

Step 3: 65°C for 45 seconds

Step 4: 72°C for 1 minute and 15 seconds (again steps 2 to 4 for other 39 cycles)

Step 5: 72°C for 10 minutes

Step 6: 4°C ∞

Following the PCR reaction, the amplification product was loaded on 2% agarose gels and separated through electrophoresis to analyse the DNA size.

2.14 Agarose gel electrophoresis

Agarose was dissolved in 1X TAE (to a final concentration of 2% agarose) by heating in the microwave. When dissolved, ethidium bromide (0.5 mg/ml) was added. When solidified, the gel was placed in a DNA Gel Electrophoresis chamber in 1X TAE, DNA samples were loaded, and the gel was subjected to a constant voltage of 120 V for 30 minutes to separate DNA fragments.

2.15 Transfection

DIV4-11 cortical neurons were transfected with 0.4-3 µg of plasmid DNA with Lipofectamine 2000 or Calcium Phosphate transfection methods.

With the Lipofectamine 2000 method, plasmid DNA was mixed with OptiMEM medium in one Eppendorf tube and Lipofectamine was mixed with other OptiMEM in a second Eppendorf tube (see Table below for volumes and DNA range). The solutions were incubated at RT for 5 minutes and then mixed and incubated at RT for 20 minutes. 500 µl-1ml of culture medium was left on top of each well and the transfection mix was added dropwise to the cells and incubated at 37°C, 5% CO_2 for 1 hour. Then, cells were washed twice with pre-warmed HEPES buffer, and the rest of the medium, which had been saved before, was added again to the cells.

Table 7 - Lipofectamine 2000 transfection mix components

Coverslip size and culture plate	Surface area/well	Medium volume left on cells	Transfection mix OptiMEM volume	DNA amount	Lipofectamine 2000 volume
12 mm – 24 well plate	1.9 cm^2	500 µl	2 x 50 µl	0.4-0.7 µg	2 µl
18 mm – 6 well plate	9.6 cm^2	1 ml	2 x 100 µl	0.8-1.4 µg	4 µl

With the Calcium Phosphate method, plasmid DNA was mixed with 1M $CaCl_2$ and ddH_2O (see Table below for volumes and DNA range). This mix was added dropwise to an equal volume of 2x HBS under vortex agitation and then incubated at RT for 10 minutes. 500 µl-1ml of culture medium was left on top of each well and the transfection mix was added dropwise to the cells and incubated at 37°C, 5% CO_2 for 60-90 minutes. Then, cells were washed twice with pre-warmed HEPES buffer, and the rest of the medium, which had been saved before, was added again to the cells.

Table 8 - Calcium phosphate transfection mix components

Coverslip size and culture plate	Surface area/well	Medium volume left on cells	1M $CaCl_2$ volume	DNA amount	Total volume (DNA + 1M $CaCl_2$ + ddH_2O)
12 mm – 24 well plate	1.9 cm^2	500 µl	6.25 µl	1-2 µg	30 µl
18 mm – 6 well plate	9.6 cm^2	1 ml	12.5 µl	1.5-3 µg	60 µl

Neurons were either used for live cell imaging or fixed in 4% paraformaldehyde/4% sucrose diluted in PBS for 15 minutes.

2.16 Immunocytochemistry

Cortical neurons were fixed in 4% paraformaldehyde/4% sucrose diluted in PBS for 15 minutes. Cells were then washed three times with PBS and permeabilized for 10 minutes at RT in PBS containing 0.1% Triton X 100 and blocked in PBS containing 1% (w/v) BSA for 1 hour at RT. Fixed neurons were then incubated with primary antibodies diluted in 1%BSA/PBS either overnight at 4°C or for 1 hour at RT. Coverslips were washed 3 times for 5 minutes each and then incubated with secondary antibodies diluted in 1%BSA/PBS for 45 minutes at RT. Coverslips were washed 3 times for 5 minutes each, quickly dipped in ddH_2O, and mounted on glass slides using Aqua-Poly/Mount mounting medium. Slides with mounted coverslips were left to dry in the dark overnight at RT. Coverslips were then imaged using a confocal microscope (Zeiss LSM900 equipped with a 20x and 40x objective), obtaining Z-stacks with a step size of 0.3 µm.
Quantifications were performed making use of the Metamorph 6.3 r7 software (Molecular Devices) or using the ImageJ software (Schindelin et al., 2012).

2.17 Electron microscopy

32-34-week-old mice were deeply anaesthetized by CO_2 inhalation and transcardially perfused with a mixture of 4% paraformaldehyde and 1% glutaraldehyde in 0.1 M PB buffer at pH 7.4. Spinal cords were dissected and after three washing steps, the sections were prepared as follows. Briefly, blocks were post-fixed in 0.1% (w/v) potassium ferrocyanide-reduced 2% (w/v) osmium tetroxide in cacodylate buffer for 1 hour. Thereafter, the blocks were rinsed in distilled water and treated with 0.1% aqueous thiocarbohydrazide, which stains carbohydrates, for 20 minutes. After further rinsing in distilled water, the tissue was

incubated with 2% (w/v) osmium tetroxide again for 30 minutes before staining with uranyl acetate and lead aspartate. The pieces were further dehydrated using ascending ethyl alcohol concentration steps, followed by two rinses in propylene oxide. Infiltration of the embedding medium was performed by immersing the samples in a 1:1 mixture of propylene oxide and Epon and finally in neat Epon and polymerized at 60°C. 100 µm cross-sections were obtained with a Vibratome (Leica VT 1000S). Images were acquired with a Zeiss EM 900N Transmission Electron Microscope equipped with a TRS 2K digital camera (A. Tröndle, Moorenweis, Germany). Images were acquired as tiled images of 5 x 5 tiles with a 20,000x magnification. Animal perfusion, sample preparation, and image acquisition were performed by Dr. Michaela Schweizer (Morphology and Electron Microscopy Core Facility, ZMNH, Hamburg, Germany). Quantifications were performed using the ImageJ software (Schindelin et al., 2012).

2.18 Time-lapse imaging

Neurons were transfected with pEGFP-C1 and mCherrySec61β constructs and imaged after 36-40 hours. Coverslips were placed in a prewarmed live cell imaging chamber in HBSS and kept at 37°C and 5% CO_2 while imaging.
Time-lapse imaging was performed with a Nikon spinning disc microscope (Visitron, Puchheim, Germany) with a 100x objective and 488 nm and 561 nm argon lasers.

2.19 Total brain lysates and Western blot analysis

Whole brains of 12-week-old mice were isolated and placed in ice-cold Homogenization Buffer (PBS supplemented with 0.1% Triton X 100, cOmplete Mini protease inhibitor cocktail, and PMSF protease inhibitor). Brains were lysed at 4°C by using a tissue triturator and placed on ice for 20 minutes. Then the tubes were spun down at 1000xg for 10 minutes and the supernatant was kept while the pellet was discarded. Protein equalization was performed with the Pierce BCA Protein

Assay. Samples were then diluted with 6X Laemmli Sample (with DTT) and boiled at 95°C for 5 minutes. Equal amounts of protein from brain lysates were then subjected to SDS-PAGE on 10% SDS-gels. The separated proteins present in the gel were then transferred to PVDF membranes pre-activated with 100% Methanol using the semidry transfer method (60 mA per membrane for 2 hours). Membranes were then blocked with 5% milk/TBS-T at RT for 1 hour and incubated with primary antibodies diluted in 5% milk/TBS-T overnight at 4°C. The following morning, membranes were washed 3 times for 10 minutes each with 1X TBS-T and then incubated with IRDye-conjugated secondary antibodies diluted in 5% milk/TBS-T for 1 hour at RT. Membranes were then washed 3 times for 10 minutes each with 1X TBS-T. Membranes were imaged and bands were visualized with the LI-COR Odyssey CLx detection system. The intensities of the individual bands were analysed with the ImageJ software(Schindelin et al., 2012).

2.20 Data analysis

All data analysis was performed with the MetaMorph 6.3 r7 software (Molecular Devices) or the Fiji software (Schindelin et al., 2012).

For axon length quantifications, whole neurons were reconstructed from acquired Z-stacks, whole axons were traced from the cell body to axon terminals and their length was measured with the Fiji software.

For axon width quantifications, axons were straightened from acquired Z-stacks and 50 µm regions were selected from distal axons. Axon area was measured with the Fiji software.

For electron microscopy quantifications, overview micrographs were reconstructed from tiled images. Regions of interest were traced around axons and axonal ER structures and average ER area, perimeter and density were measured using the Fiji software.

For Sec61β aggregate quantifications, measurements were performed with the MetaMorph 6.3 r7 software. Axons were straightened from acquired Z-stacks and

150 µm regions were selected from proximal and distal axons. ER aggregate signal was selected by signal thresholding and only aggregates formed by at least 2 pixels were selected, then aggregate number and area per axon were quantified. Measurements were performed on blinded images to avoid bias.

For GRP78 quantifications, analysis was performed with the Fiji software. ER-positive compartments were selected from acquired Z-stacks of distal axons by signal thresholding. GRP78 average signal intensity in the thresholded compartments was quantified.

Western blot quantifications were performed with the Fiji software. Regions of interest were traced around protein signal bands to obtain signal plots. The area under the curve in the plots was measured to quantify protein expression levels, which were normalized to loading control (GAPDH) protein levels.

2.21 Statistics

Statistical analysis of datasets was performed with the GraphPad software. Variance tests were performed according to data distribution and variance parameters.

When two datasets were compared, and the data were not normally distributed, the Mann-Whitney test was performed. When the data were normally distributed and presented equal variance, an unpaired t-test was performed. When the data were normally distributed but showed unequal variance, an unpaired t-test with Welch's correction was performed.

When three or more datasets were compared, and the data were not normally distributed, the Kruskal-Wallis test was performed. When the data was normally distributed and presented equal variance, an ordinary one-way ANOVA was performed. When the data was normally distributed but showed unequal variance, Brown-Forsythe and Welch ANOVA tests were performed.

3. Results

3.1 Spastin depletion does not influence total axon length

HSPs are a group of disorders mainly characterized by the length-dependent degeneration of corticospinal axons. Previous studies have found that spastin knockdown using siRNA in rat hippocampal neurons results in reduced axonal branching and decreased axon length (Ji et al., 2018; Yu et al., 2008). To determine whether axon length is also affected in a primary mouse cortical neuron culture system, neurons were derived from +/+, spastin +/- and -/- mice, and EGFP was expressed as a volume marker on DIV6. At DIV8, neurons were fixed, analysed by confocal microscopy, and total axon length was measured. When multiple axons or axon branches were present in one neuron, the longest axonal process was used for quantification. Quantifications revealed no significant difference in axon length between +/+, spastin +/-, and -/- primary mouse cortical neurons (Figure 12).

3.2 Spastin depletion leads to enlarged distal axon areas

When analysing total axon length in spastin +/- and -/- cortical neurons, numerous swellings could be observed along these axons, and studies have already shown how axonal swellings are often present in neurodegenerative disorders, including Alzheimer's Disease and HSPs (Ferreirinha et al., 2004; Stokin et al., 2005). These are sites where axonal transport is usually disrupted and organelles accumulate, eventually leading to axonal fragmentation and dying-back degeneration (Ferreirinha et al., 2004; Martinez & Friede, 1970; J. T. Wang et al., 2012). To investigate whether spastin depletion leads to an enlargement in distal axon areas, EGFP was expressed as a volume marker in +/+, spastin +/-, and -/- cortical neurons on DIV6. Neurons were fixed on DIV8 and analysed.

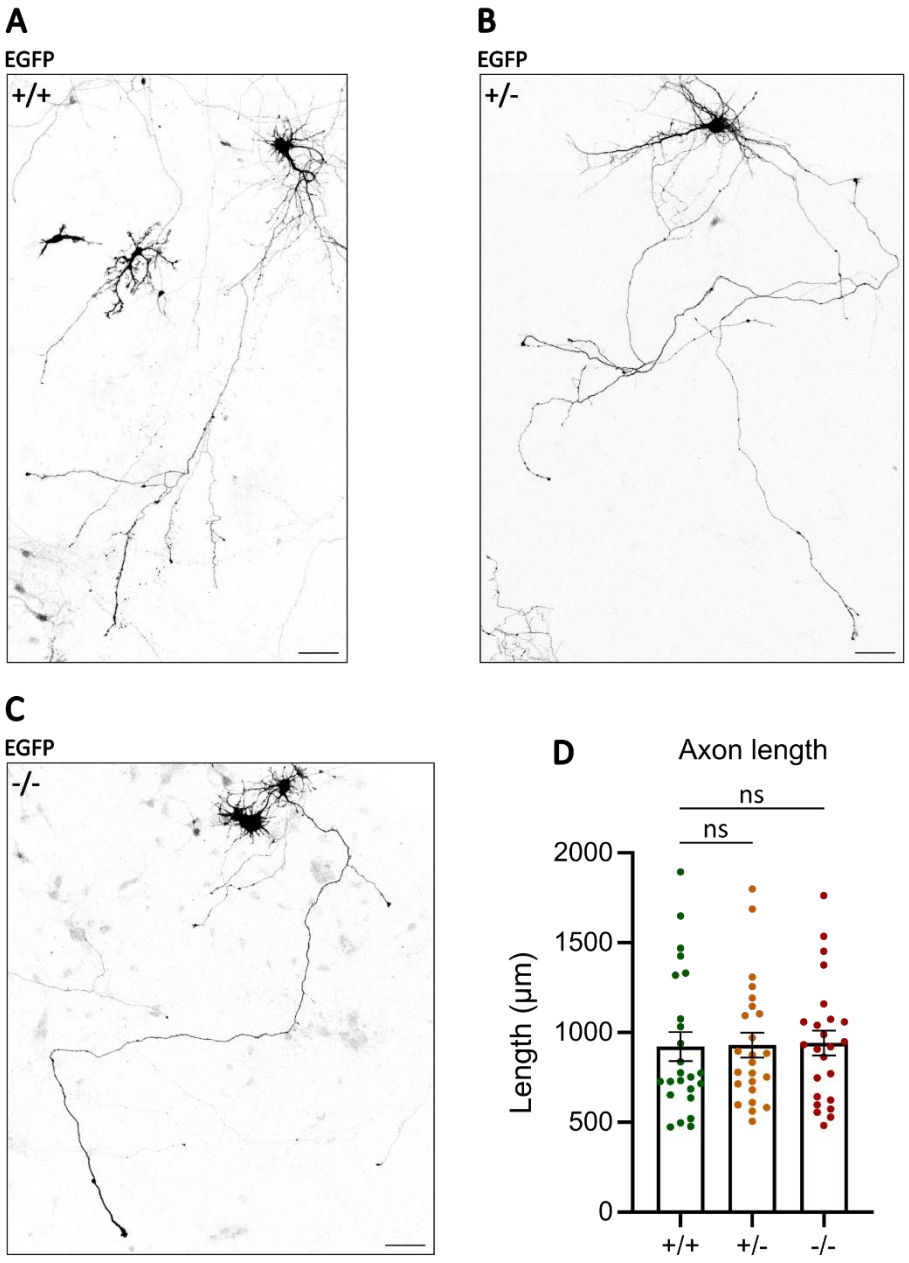

Figure 12. Analysis of axon length upon spastin depletion.
Representative images of whole DIV8 primary mouse cortical neurons derived from (A) +/+, (B) spastin +/-, and (C) spastin -/- mice. Neurons were transfected with EGFP as a volume marker on DIV6 and fixed on DIV8. Whole neurons were reconstructed from Z-stack images obtained with confocal laser scanning microscopy. Scale bar: 50 µm. (D) Quantification of axon length in +/+, spastin +/-, and -/-. n=24 neurons per condition. Kruskal-Wallis test p-values >0.999. Error bars represent mean ± standard error of the mean (SEM).

The total area of 50 µm-long distal axon regions was measured, and an increase in distal axon area in spastin +/- and -/- cortical axons was found (Figure 13). These results indicate that a reduction in spastin is sufficient to lead to the formation of axonal swellings already at early culture timepoints such as DIV8.

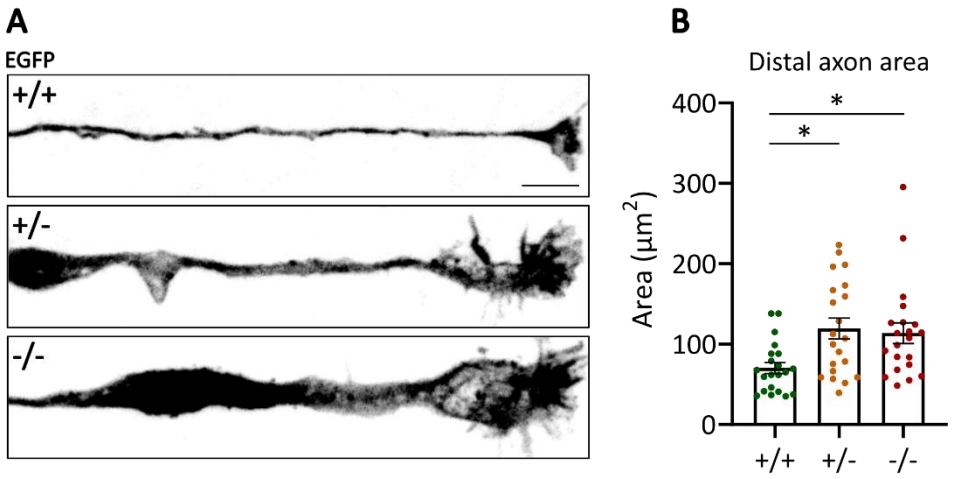

Figure 13. Analysis of distal axon area upon spastin depletion.
(A) Representative images of distal axon regions of DIV8 primary cortical neurons derived from +/+, spastin +/-, and -/- mice. Neurons were transfected with EGFP as a volume marker on DIV6 and fixed on DIV8. Straightened distal axons from reconstructed Z-stack images obtained with confocal laser scanning microscopy are shown. Axon terminals are seen on the right edge of the images. Scale bar: 5 µm. (B) Quantifications of distal axon area; n=21 neurons per condition. Kruskal-Wallis test p-value +/+ vs. +/- 0.0123; +/+ vs. -/- 0.0187; +/- vs. -/- > 0.9999. Error bars represent mean ± SEM.

These results, taken together with data from the literature, indicate that spastin loss affects distal axon morphology and induces axonal swelling formation. Disorganized MTs have been found to accumulate in swellings (Fassier et al., 2012), and M1 spastin has been proposed to mediate the crosstalk between ER and MTs in ER regulation (Blackstone, 2012), suggesting that distal axonal ER might be affected upon spastin loss.

3.3 Spastin depletion leads to a decrease in axonal ER area and density in mouse corticospinal axons

The ER is an extensive organelle composed of different membrane compartments, mainly responsible for protein and lipid synthesis and Ca^{2+} homeostasis. ER

dysfunction has already been linked to neurodegeneration and cell stress (Öztürk et al., 2020). In addition, studies have shown that the integrity of the axonal ER is disrupted in REEP1 and atlastin-1 animal models of HSP (Beetz et al., 2013; Yalçın et al., 2017; P.-P. Zhu et al., 2022). Since spastin can interact with both REEP1 and atlastin-1, we sought to investigate whether axonal ER morphology is affected by spastin depletion.

To examine endogenous ER morphology upon spastin depletion on the ultrastructural level, electron microscopy was employed. Studies have shown that at 6 months of age, there is a decrease in axon number and axon perimeter in spinal cord cross-sections derived from the lumbar region of SPG4 mouse models (Piermarini et al., 2022). Data also indicate that spastin -/- mice develop motor impairments between 8 and 14 months of age (Lopes et al., 2020). Taken together, these results indicate that already before the insurgence of the first HSP-related motor symptoms, axonal disruption and dying-back are present. To investigate whether there are also alterations in ER morphology in axons of the same region, cross-sections were derived from the lumbar region of the spinal cord of 32-34-week-old +/+, spastin +/-, and -/- mice and analysed with electron microscopy. Overview micrographs of these cross-sections were analysed to measure certain parameters such as average ER area per axon, average ER perimeter per axon, and ER density. We found that these parameters were drastically reduced in spastin +/- and -/- axons compared to +/+, indicating that fewer ER structures are present in lumbar regions of corticospinal axons upon spastin depletion (Figure 14). These samples were derived from animals months before the onset of HSP motor deficits, indicating that not only spastin levels have an effect on ER levels in corticospinal axons, but that such effects are already present before the development of motor deficits, suggesting ER defects are a cause and not a consequence of HSP.

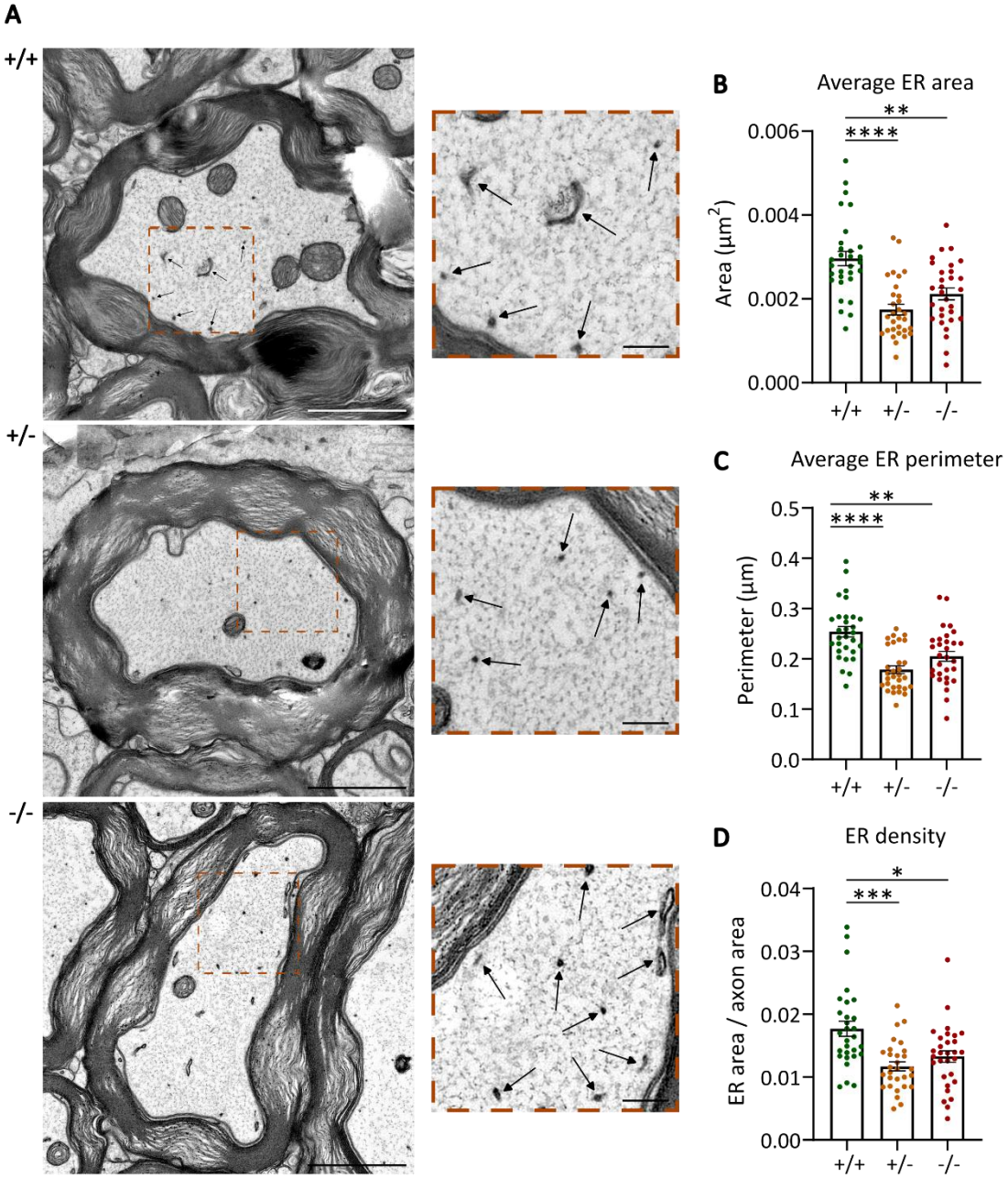

Figure 14. Analysis of axonal ER in spinal cord cross-sections upon spastin depletion.
(A) Representative overview images from cross-sections of axons from the spinal cord lumbar region of 32-34-week-old +/+, spastin +/-, and -/- mice are shown. Zoom-ins (orange-dashed boxes) are shown for each image; arrows indicate ER structures. Scale bar overview image: 1 µm. Scale bar zoom-in: 200 nm. (B) Quantification of average ER area per axon. n=30 axons per condition. Kruskal-Wallis test p-value +/+ vs. +/- <0.0001; +/+ vs. -/- 0.0042; +/- vs. -/- 0.1762. (C) Quantification of average ER perimeter per axon. n=30 axons per condition. Kruskal-Wallis test p-value +/+ vs. +/- <0.0001; +/+ vs. -/- 0.0098; +/- vs. -/- 0.1713. (D) Quantification of ER density per axon. n=30 axons per condition. Kruskal-Wallis test +/+ vs. +/- 0.0002; +/+ vs. -/- 0.0222; +/- vs. -/- 0.4836.
Error bars represent mean ± SEM.

3.4 Spastin depletion leads to an increase in axonal ER aggregates in primary cortical neurons

On an endogenous level, corticospinal axon ER area, perimeter, and density were found to be significantly reduced upon spastin reduction and loss. A limitation of the analysis of spinal cord cross-sections is the fact that it does not allow the visualization and analysis of ER morphology and integrity along the axon. A primary mouse cortical neuron culture system was therefore used to investigate whether there are any differences in ER morphology and distribution upon spastin depletion along the whole axon. It should be noted that to date, there is a scarcity of tools to visualize endogenous ER in neurons. The most commonly used system to visualize the ER using light microscopy is based on the overexpression of a plasmid encoding Sec61β, a component of the Sec61 complex, responsible for protein translocation within the ER membrane. To analyse axonal ER morphology in primary cortical neurons derived from +/+, spastin +/- and -/- mice, mCherrySec61β was expressed together with EGFP as a volume marker (for visualization of the complete axonal compartment). Both proximal and distal axon regions of these neurons were analysed. The data show that in both regions, the distribution of mCherrySec61beta in +/+ cortical neurons is quite homogeneous within the axonal compartment. In contrast, spastin +/- and -/- axons present numerous mCherrySec61β aggregates. The number and area of these aggregates were quantified in 150 µm-long axon sections. When measuring these parameters in proximal axon regions, quantification shows that the total number and average area of these aggregates are unchanged upon the depletion of spastin. However, the number of aggregates with an area larger than 0.2 μm^2 is significantly increased in spastin -/- cortical proximal axons, indicating that there is a higher number of large aggregates when spastin is absent (Figure 15A-D). Quantification of the same parameters in distal axon regions shows that both spastin +/- and-/- cortical axons present significant differences compared to +/+ distal axon regions. Spastin +/- distal axons present an increase in total aggregate number and average area of aggregates, and -/- distal

axons show an increase in aggregate area. Although total aggregate numbers are unvaried in spastin -/- distal axons, the number of large aggregates (with an area larger than 0.5 μm^2) is significantly increased (Figure 15E-H). These data suggest that the absence of spastin induces the formation of large aggregates in proximal axon regions, and that this situation progressively worsens moving towards the axon distal regions, where even a reduction in spastin levels is sufficient to induce an increase in both the number and area of ER aggregates. Although these results suggest there could be higher ER expression levels upon spastin reduction and depletion, the expression of calreticulin, an established ER marker, is actually slightly decreased in spastin +/- and -/- adult mouse brain lysates. However, this decrease did not reach statistical significance (Figure 15I, J). Live cell imaging of +/+, spastin +/-, and -/- primary mouse cortical neurons co-expressing Sec61β and EGFP was performed, and similar aggregates were observed in spastin +/- and -/- distal axons. Kymographs obtained from time-lapse imaging data indicate these aggregates are largely stationary rather than dynamic (Figure 15K).

Furthermore, the expression of mCherrySec61β along the axon in +/+ neurons appears to be largely continuous, but upon spastin reduction or depletion, the distribution of the ER changes. The expression of the ER marker in spastin-depleted axons appears largely discontinuous, with the formation of mCherrySec61β aggregates with high signal intensity, accompanied by regions between one aggregate and the next where the ER appears more discontinuous. It was not possible to quantify overall axonal ER levels due to the use of overexpression rather than endogenous ER labeling.

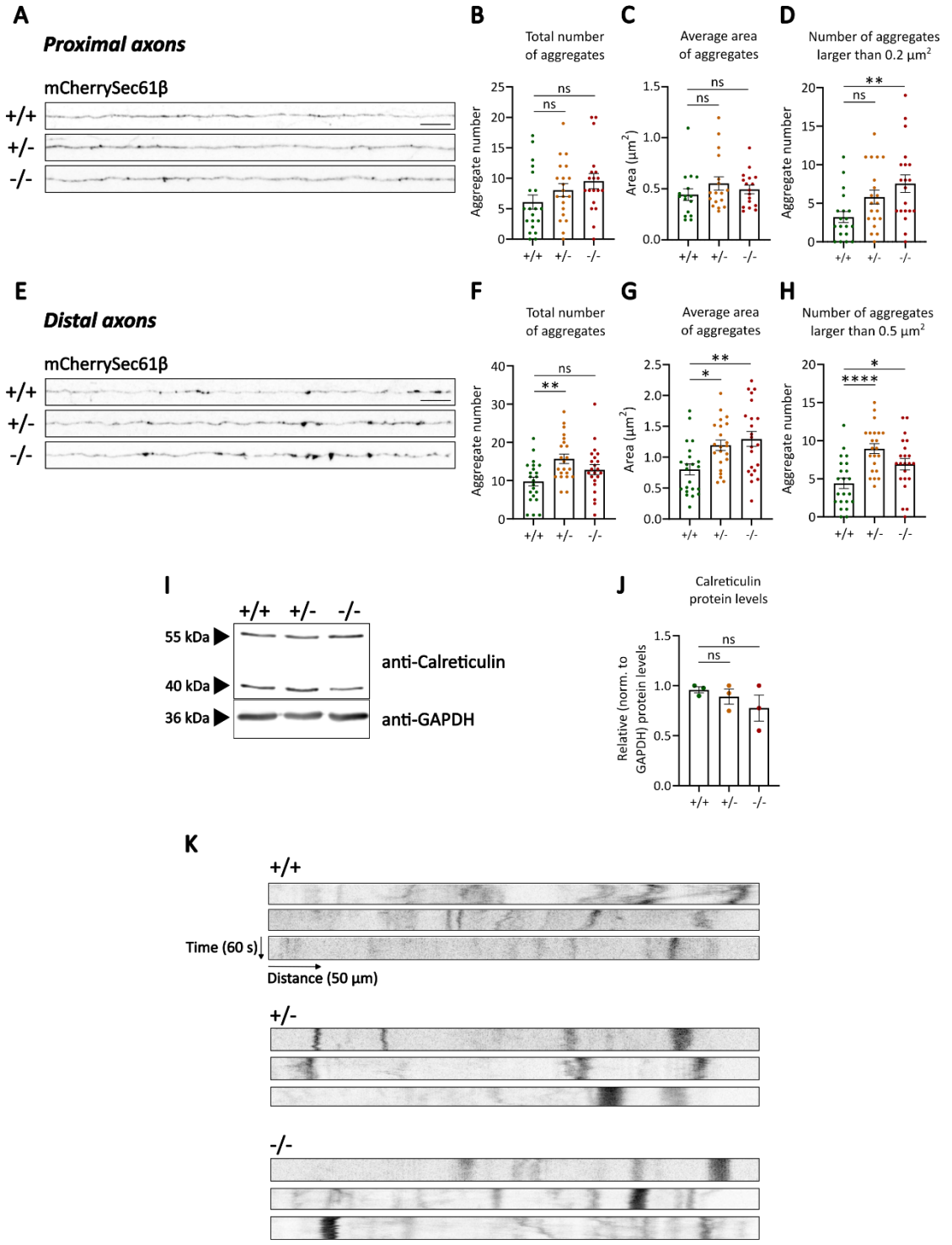

Figure 15. Analysis of axonal ER morphology upon spastin depletion.

(A) Distribution of the ER in representative proximal axon regions of DIV8 primary mouse cortical neurons derived from +/+, spastin +/- and -/- mice. Neurons were co-transfected with EGFP and mCherrySec61β. Straightened distal axons from reconstructed Z-stack images obtained with confocal laser scanning microscopy are shown. Scale bar: 10 µm. (B) Quantifications of the total number of ER aggregates in proximal axon regions. n=20 proximal axons per condition. Kruskal-Wallis test p-value +/+ vs. +/- 0.5191; +/+ vs. -/- 0.1047; +/- vs. -/- >0.9999. (C) Quantifications of

average ER aggregate area in proximal axon regions. n=20 proximal axons per condition. Kruskal-Wallis test p-value +/+ vs. +/- 0.7519; +/+ vs. -/- 0.9973; +/- vs. -/- >0.9999. (D) Quantifications of the number of aggregates larger than 0.2 µm^2 in proximal axon regions. n=20 proximal axons per condition. Kruskal-Wallis test p-value +/+ vs. +/- 0.0951; +/+ vs. -/- 0.0058; +/- vs. -/- >0.9999.
(E) Distribution of the ER in representative distal axon regions of DIV8 primary mouse cortical neurons derived from +/+, spastin +/-, and -/- mice. Neurons were co-transfected with EGFP and mCherrySec61β. Straightened distal axons from reconstructed Z-stack images obtained with confocal laser scanning microscopy are shown. Axon terminals are seen on the right edge of the images. Scale bar: 10 µm. (F) Quantifications of the total number of ER aggregates in distal axon regions. n=22 distal axons per condition. Ordinary one-way ANOVA p-value +/+ vs. +/- 0.0033; +/+ vs. -/- 0.2231; +/- vs. -/- 0.2831. (G) Quantifications of average ER aggregate area in distal axon regions. n=22 distal axons per condition. Ordinary one-way ANOVA p-value +/+ vs. +/- 0.0212; +/+ vs. -/- 0.0025; +/- vs. -/- 0.8517. (H) Quantifications of the number of aggregates larger than 0.5 µm^2 in distal axon regions. n=22 distal axons per condition. Ordinary one-way ANOVA p-value +/+ vs. +/- <0.0001; +/+ vs. -/- 0.0395, +/- vs. -/- 0.1188.
(I) Representative Western blot membrane of immunolabeled endogenous calreticulin in whole brain lysates of 12-week-old +/+, spastin +/-, and -/- mice. GAPDH endogenous levels were used as a loading control. (J) Quantifications of calreticulin protein expression levels normalized to GAPDH protein levels. n=3 whole brain lysates per condition. Brown-Forsythe and Welch ANOVA tests p-value +/+ vs. +/- 0.8515; +/+ vs. -/- 0.6455; +/- vs. -/- 0.8712.
Error bars represent mean ± SEM.
(K) Representative kymographs obtained from straightened 50 µm distal axon regions of DIV6-7 +/+, spastin +/-, and -/- primary cortical neurons (total time of acquisition 60 seconds).

3.5 Axonal ER aggregates induced by spastin depletion show higher levels of ER stress

ER continuity along axons is crucial for proper ER and ultimately neuronal function, as the ER is responsible for Ca^{2+} homeostasis and lipid synthesis, but also protein translation and folding. In this study, spastin reduction and depletion were shown to lead to the formation of mCherrySec61β aggregates in axons of primary mouse cortical neurons. In order to study the functionality of the ER upon spastin depletion within ER aggregates, an antibody against GRP78 was employed. GRP78 is an ER-associated protein involved in numerous processes, including membrane protein translocation, protein folding, and regulation of Ca^{2+} homeostasis, and is generally used as an ER stress sensor (M. Wang et al., 2009). To investigate whether ER aggregate formation within spastin-depleted axons corresponds to a decrease in the general function of the organelle, mCherrySec61β and EGFP were co-expressed

in +/+, spastin +/-, and -/- cortical neurons, and endogenous GRP78 was detected (Figure 16A). Signal intensity of GRP78 in mCherrySec61β-positive compartments in distal axons of DIV8 cortical neurons was measured. The analysis revealed that GRP78 levels in these compartments are significantly increased in spastin +/- and -/- compared to +/+ distal axons (Figure 16B). Increased levels of GRP78 within ER aggregates indicate that the depletion of spastin leads to higher ER stress in axons. The analysis of GRP78 protein expression levels in the whole brain revealed no differences between +/+, +/-, and -/- adult mice (Figure 16C, D), indicating that the observed increase is likely confined to the axonal compartment. Volume-wise, this compartment represents a small fraction of the total neuronal cell body, explaining why an increase in axonal GRP78 levels upon spastin depletion is diluted on a total brain protein level.

Taken together, these results indicate that reduced expression levels of spastin, as present in numerous HSP cases, interfere with the normal distribution and homeostasis of the ER in distal axons of mammalian cortical neurons.

3.6 Distal axonal ER aggregates induced by spastin depletion are in close proximity to MT alterations

Studies have shown alterations in the MT network upon spastin loss in primary mouse hippocampal neurons and in mutant spastin *Drosophila melanogaster* larvae (Lopes et al., 2020; Sherwood et al., 2004). The interaction between the ER and MTs has been shown to have a central role in axonal ER movement and formation (Terasaki et al., 1986; Vajente et al., 2019). In order to investigate where ER aggregates are positioned relatively to such MT abnormalities, mCherrySec61β and EGFP were co-expressed in +/+, spastin +/-, and -/- cortical neurons, and endogenous alpha-tubulin was detected. ER aggregates are present in very close proximity to disorganized microtubule structures (Figure 17).

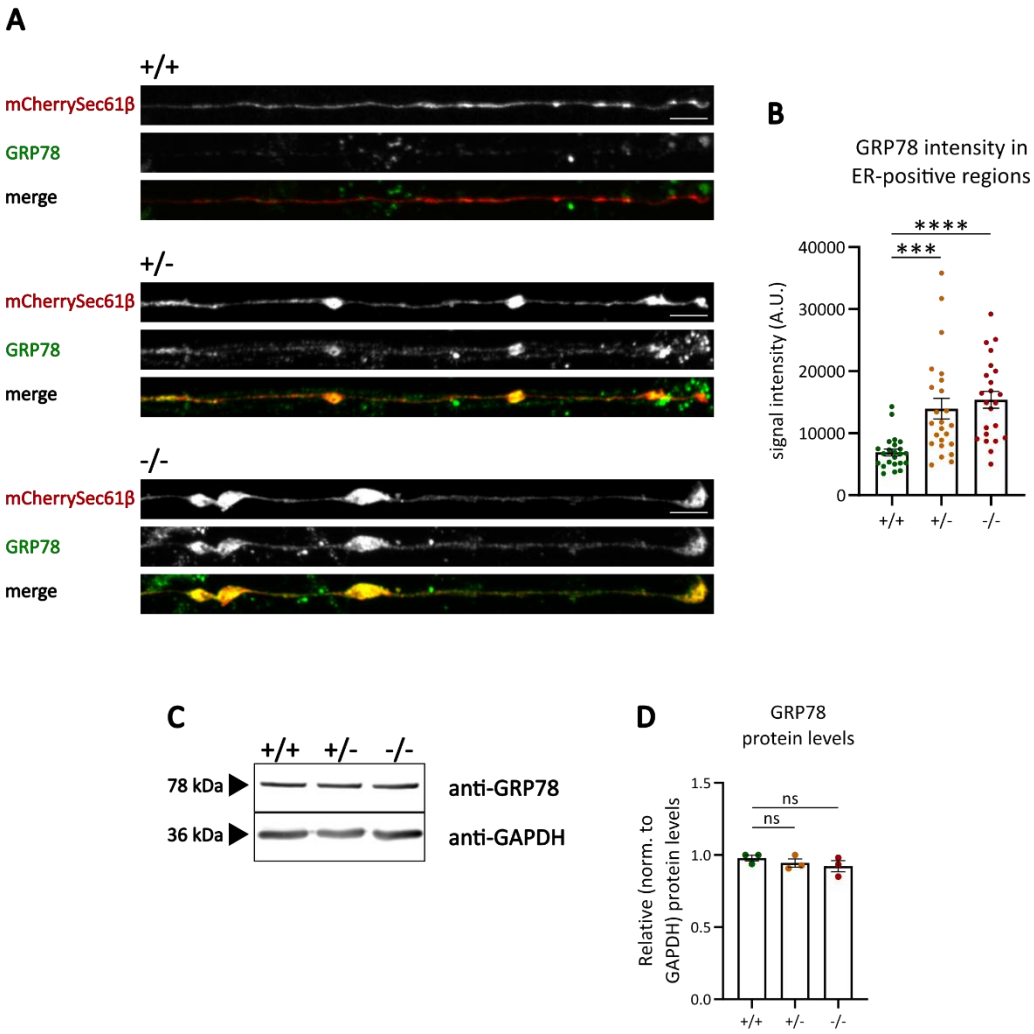

Figure 16. Analysis of endogenous GRP78 signal intensity in ER-positive compartments.

(A) Representative images of endogenous GRP78 in distal axons of DIV8 primary mouse cortical neurons derived from +/+, spastin +/-, and -/- mice. Neurons were co-transfected with EGFP and mCherrySec61β and endogenous GRP78 was detected. Straightened distal axons from reconstructed Z-stack images obtained with confocal laser scanning microscopy are shown. Axon terminals are seen on the right edge of the images. Scale bar: 5 µm. (B) Quantifications of the average signal intensity of GRP78 in mCherrySec61β-positive regions in distal axons. n=24 distal axons. Kruskal-Wallis test p-value +/+ vs. +/- 0.0003; +/+ vs. -/- <0.0001; +/- vs. -/- 0.9148.

(C) Representative Western blot membrane of immunolabeled endogenous GRP78 in whole brain lysates of 12-week-old +/+, spastin +/-, and -/- mice. GAPDH endogenous levels were used as a loading control. (D) Quantifications of GRP78 protein expression levels normalized to GAPDH protein levels. n=3 whole brain lysates per condition. Ordinary one-way ANOVA p-value +/+ vs. +/- 0.8317; +/+ vs. -/- 0.5426; +/- vs. -/- 0.9442.

Error bars represent mean ± SEM.

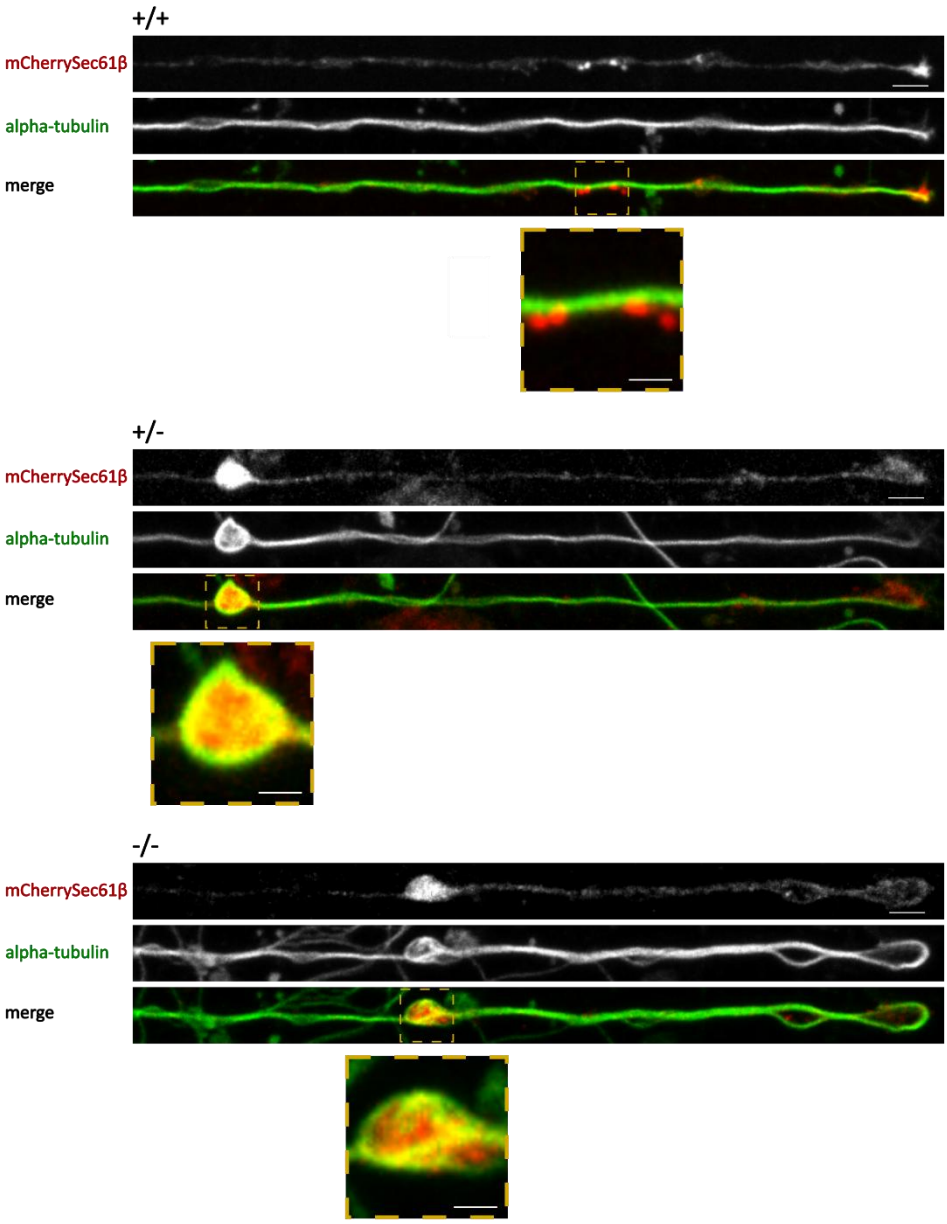

Figure 17. Analysis of ER and MT morphology upon spastin depletion.
Representative images of distal axon regions of DIV8 primary cortical neurons derived from +/+, spastin +/-, and -/- mice. Neurons were co-transfected with EGFP and mCherrySec61β on DIV6, fixed on DIV8 and endogenous alpha-tubulin was detected. Straightened distal axons from reconstructed Z-stack images obtained with confocal laser scanning microscopy are shown. Axon terminals are seen on the right edge of the images. Zoom-ins of ER aggregates in close proximity to MT alterations (yellow dashed boxes) are shown. Scale bar distal axon regions: 5 µm. Scale bar zoom-ins: 2 µm.

3.7 Spastin-mediated MT severing is necessary for distal axonal ER distribution and homeostasis

Human spastin has two main isoforms, known as M1 and M87 (M1 and M85 in mice), presenting two distinct start codons (Claudiani et al., 2005). While the M87 isoform is ubiquitously expressed, M1 spastin is expressed mainly in the brain and spinal cord (Solowska et al., 2008). Also, while M1 is usually perinuclear and presents a punctate pattern, M87 is usually present throughout the cytosol (Sakoe et al., 2021). Evidence suggests that the M1 isoform might be more important for the interaction with organelles and lipid droplets (Papadopoulos et al., 2015; Park et al., 2010), while M87-spastin is more involved in MT severing (Yu et al., 2008).

In order to determine whether proper ER morphology is dependent on spastin-mediated MT severing, expression of a spastin mutant plasmid, referred to as EGFP-M85 K388R, was employed. The K388R plasmid encodes the M85 isoform of the spastin protein containing a point mutation in the AAA ATPase domain of spastin. K388R is still able to bind but not to sever MTs. mCherrySec61β and either EGFP or EGFP-M85 K388R were co-expressed in primary cortical neurons and ER aggregate number and average area in both proximal and distal axons were measured. While MT-severing disruption led to no difference in aggregate formation in proximal axons (Figure 18A-C), neurons expressing the spastin mutant show an increase in both axonal mCherrySec61β aggregate number and size in distal axons (Figure 18D-F), indicating that the MT-severing activity of spastin is crucial for proper axonal ER distribution. However, there might still be other functions of spastin that are also necessary for proper ER regulation, given that the expression of the MT severing-deficient mutant does not lead to the same increase in large aggregate formation in proximal axons as was observed upon spastin loss.

To investigate whether the MT-severing activity of spastin is also important for proper ER stress homeostasis, either EGFP or EGFP-M85 K388R and mCherrySec61β were co-expressed in primary cortical neurons, and endogenous GRP78 was detected (Figure 18G). The average signal intensity of GRP78 in

mCherrySec61β-positive regions was measured. Quantifications show a substantial increase in GRP78 intensity in mCherrySec61β-positive regions, indicating that disrupting the MT-severing activity of spastin is sufficient to induce higher ER stress in distal axons (Figure 18H).

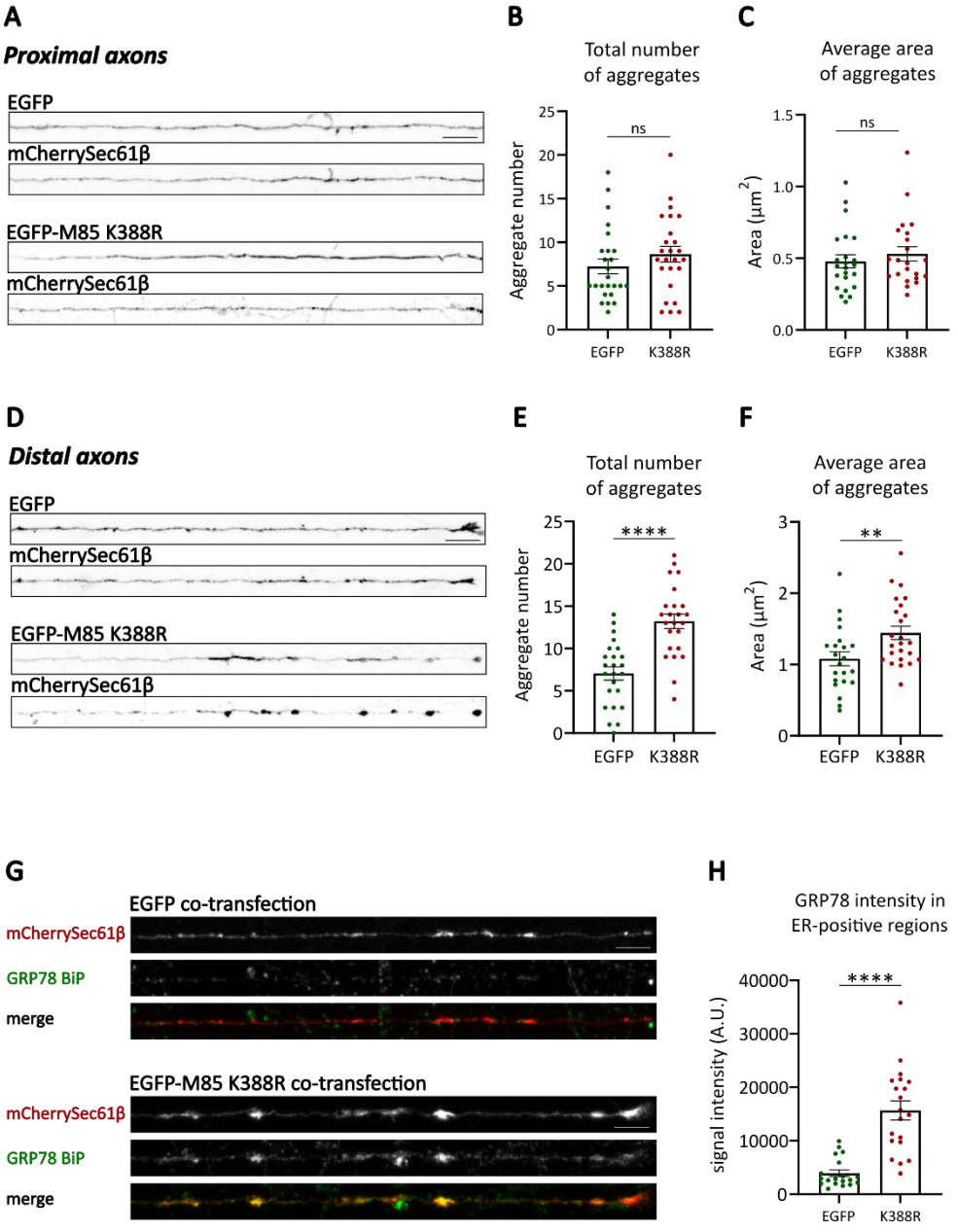

Figure 18. Analysis of ER homeostasis upon spastin-mediated MT severing disruption.
(A) Distribution of the ER in representative proximal axon regions of DIV8 primary mouse cortical neurons co-transfected with mCherrySec61β and either EGFP or EGFP-M85 K388R. Straightened proximal axons from reconstructed Z-stack images obtained with confocal laser scanning microscopy are shown. Scale bar: 10 µm. (B) Quantifications of the total number of ER aggregates in proximal axon regions. n=25 proximal axons per condition. Mann-Whitney test p-value 0.2196. (C)

Quantifications of the average area of ER aggregates in proximal axon regions. n=25 proximal axons per condition p-value 0.4405.
(D) Distribution of the ER in representative distal axon regions of DIV8 primary mouse cortical neurons co-transfected with mCherrySec61β and either EGFP or EGFP-M85 K388R. Straightened distal axons from reconstructed Z-stack images obtained with confocal laser scanning microscopy are shown. Axon terminals are seen on the right edge of the images. Scale bar: 10 µm. (E) Quantifications of the total number of ER aggregates in distal axon regions. n=24 distal axons per condition. Unpaired t-test p-value <0.0001. (F) Quantifications of the average area of ER aggregates in distal axon regions. n=24 distal axons per condition. Unpaired t-test p-value 0.01.
(G) Representative images of endogenous GRP78 immunolabeling in distal axons of DIV8 primary mouse cortical neurons co-transfected with mCherrySec61β and either EGFP or EGFP-M85 K388R. Straightened distal axons from reconstructed Z-stack images obtained with confocal laser scanning microscopy are shown. Axon terminals are seen on the right edge of the images. Scale bar: 5 µm. (H) Quantifications of the average signal intensity of GRP78 in mCherrySec61β-positive regions in distal axons. n=20 distal axons. Mann-Whitney test p-value <0.0001.
Error bars represent mean ± SEM.

3.8 Tubulin polyglutamylation is necessary for proper distal axon ER distribution and homeostasis

MTs are highly dynamic structures, and undergo numerous different post-translational modifications, including detyrosination, acetylation, and polyglutamylation. Glutamylation is the addition of single or chained glutamates to tubulin (Janke & Kneussel, 2010) and the binding affinity of spastin to MTs has been shown to linearly increase with the addition of glutamates to the tubulin C-terminal tails, while MT severing non-linearly decreases (Valenstein & Roll-Mecak, 2016). High levels of glutamylation have been linked to neurodegeneration (Magiera et al., 2018), and studies have shown that upon spastin absence, polyglutamylation levels are increased (Lopes et al., 2020). Among different tubulin isotypes expressed in the brain, tubulin alpha4a contains the longest polyglutamyl side chains (Redeker et al., 1998).

A tuba4aΔpolyGlu mouse line, carrying C-terminal tubulin-alpha4a point mutations that disrupt the polyglutamylation of this isotype, was previously established (Figure 19) (Hausrat et al., 2022). As polyglutamylation directly influences spastin-MT binding affinity and severing activity, axonal ER morphology in primary cortical distal axons derived from tuba4aΔpolyGlu mice was evaluated. The analysis of axonal ER aggregate number and average area in these mice revealed no significant difference between +/+ and tuba4aΔpolyGlu knock-in (referred to as p/p) samples in proximal axon regions (Figure 20A-C), while there is a significant difference in both total aggregate number and area in distal axons (Figure 20D-F). The quantification of GRP78 levels in ER-positive compartments in these neurons revealed that these aggregates also present higher levels of GRP78, indicating higher axonal ER stress (Figure 20G-H).

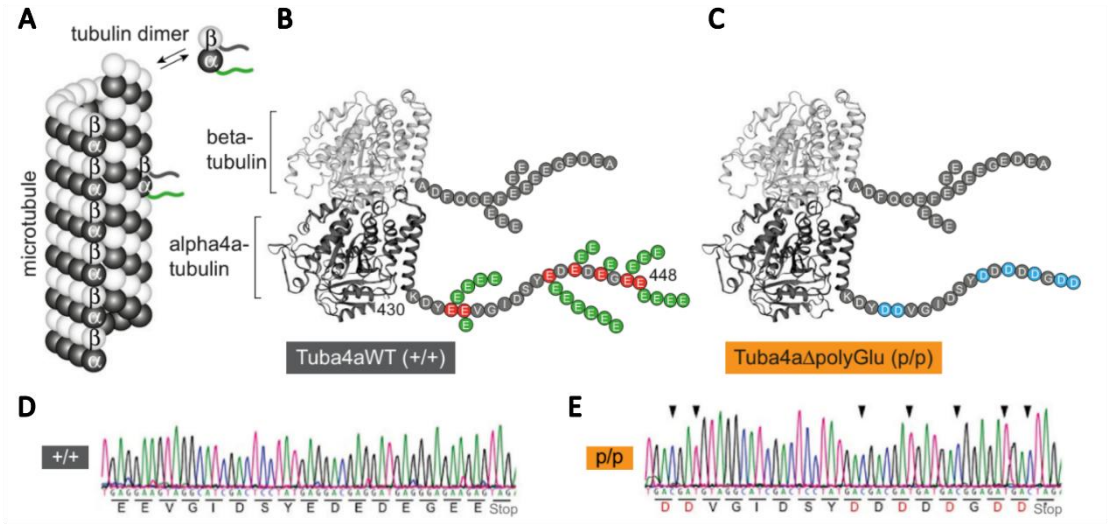

Figure 19. Schematic representation of Tuba4a point mutations in the tuba4aΔpolyGlu knock-in mouse line.

(A) MTs are formed by αβ-tubulin heterodimers. α-tubulin C-terminal tails are subject to post-translational modifications (green). (B) Glutamate (green circles) is added to specific glutamate residues (red circles) of the C-terminal tails of α-tubulin. (C) Tuba4aΔpolyGlu knock-in mice (p/p) harbour point mutations which result in aspartate substitution (blue circles) of glutamate residues. (D, E) DNA sequencing of +/+ and p/p mice. Amino acid substitutions are indicated in red. (Hausrat et al., 2022)

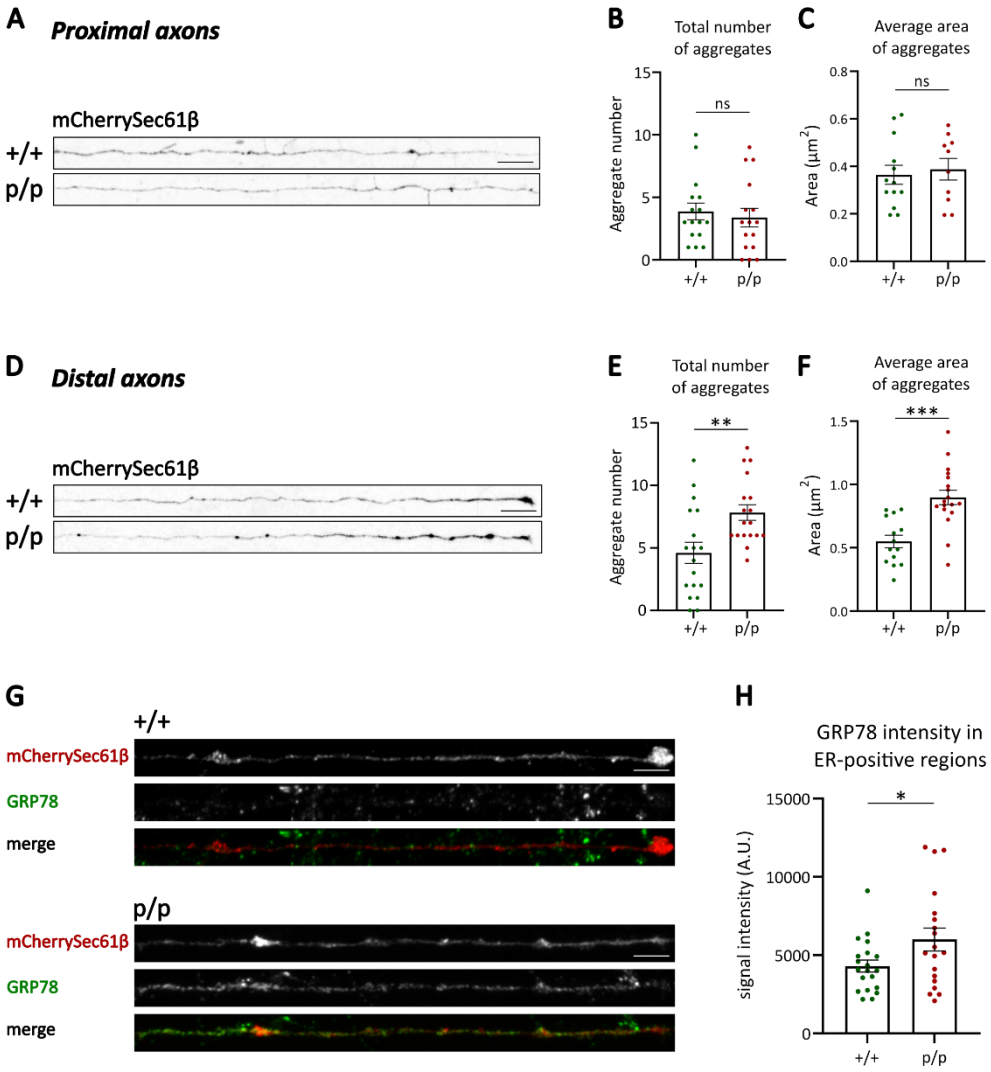

Figure 20. Analysis of ER distribution and stress in tuba4aΔpolyGlu knock-in neurons.

(A) Distribution of the ER in representative proximal axon regions of DIV12-13 primary mouse cortical neurons derived from +/+ and tuba4aDpolyGlu mice (p/p). Neurons were co-transfected with EGFP and mCherrySec61β. Straightened distal axons from reconstructed Z-stack images obtained with confocal laser scanning microscopy are shown. Scale bar: 10 µm. (B) Quantifications of the total number of ER aggregates in proximal axon regions. n=16 proximal axons per condition; Mann-Whitney test p-value 0.4582. (C) Quantifications of the average area of ER aggregates in proximal axon regions. Unpaired t-test p-value 0.7020.

(D) Distribution of the ER in representative distal axon regions of DIV12-13 primary mouse cortical neurons derived from +/+ and tuba4aDpolyGlu mice (p/p). Neurons were co-transfected with EGFP and mCherrySec61β. Straightened distal axons from reconstructed Z-stack images obtained with confocal laser scanning microscopy are shown. Axon terminals are seen on the right edge of the images. Scale bar: 10 µm. (E) Quantifications of the total number of ER aggregates in distal axon regions. n=18 distal axons per condition. Unpaired t-test p-value 0.0043 (F) Quantifications of average area of ER aggregates in distal axon regions. n=18 axons per condition. Unpaired t-test p-value 0.0001.

(G) Representative images of endogenous GRP78 immunolabeling in distal axons of DIV12-13 primary mouse cortical neurons derived from +/+ and tuba4aDpolyGlu (p/p) mice. Neurons were co-

transfected with EGFP and mCherrySec61β and endogenous GRP78 was detected. Straightened distal axons from reconstructed Z-stack images obtained with confocal laser scanning microscopy are shown. Axon terminals are seen on the right edge of the images. Scale bar: 5 µm. (H) Quantifications of the average signal intensity of GRP78 in mCherrySec61β-positive regions in distal axons. n=20 distal axons. Unpaired t-test with Welch's correction p-value +/+ vs. p/p 0.0471.
Error bars represent mean ± SEM.

3.9 Spastin co-expression with mCherrySec61β in primary cortical neurons leads to extensive cell death, even in the background of spastin depletion

In order to assess the effect of M1 and M85 expression on axonal ER, mCherrySec61β and plasmids encoding either the spastin M1 isoform or the M85 isoform were co-expressed in DIV6 primary cortical neurons. On DIV8, neurons were fixed and analysed. In both cases, the overexpression of spastin led to extensive cell death, not allowing for the evaluation of the effects of enhanced M1 and M85 spastin expression on axonal ER distribution (upper panels of Figures 21 and 22). However, it was still possible to observe the distinct patterns of subcellular localization of the different spastin isoforms in these neurons, with M1 presenting a perinuclear punctate pattern and M85 being present throughout the cytosol. Furthermore, mCherrySec61β and M1 or M85 spastin were co-expressed in DIV6 spastin +/- and -/- primary cortical neurons to investigate whether the reintroduction of spastin is sufficient to rescue axonal ER defects observed upon spastin depletion. In both these cases, a similar cell death extent was observed compared to spastin overexpression in +/+ neurons (lower panels of Figures 21 and 22). These results suggest that overexpression of spastin in primary cortical neurons leads to a toxic increase in MT severing, to an extent that cannot be sustained by primary cortical neurons, even in the background of endogenous spastin depletion.

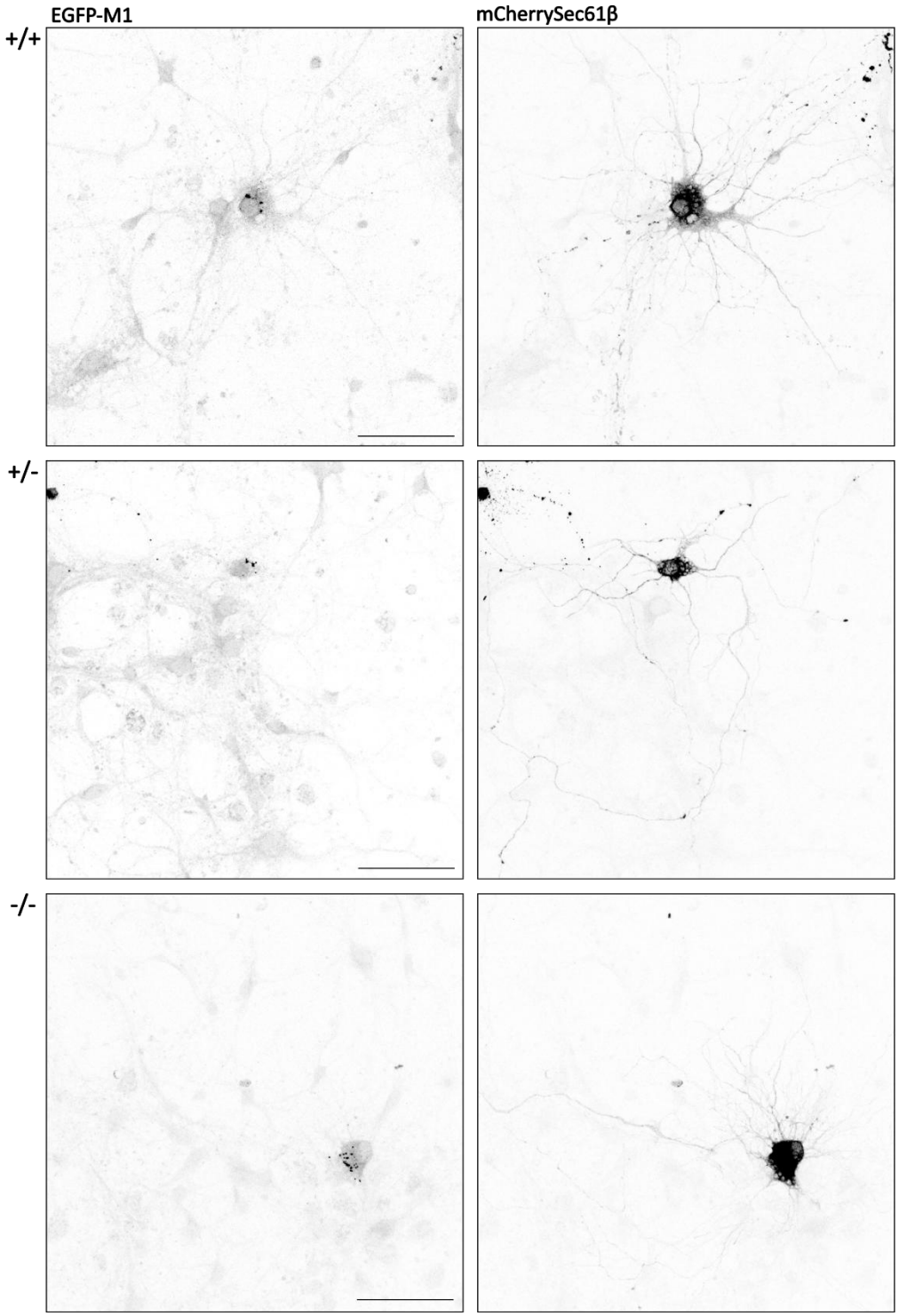

Figure 21. Analysis of M1 spastin overexpression on primary cortical neurons.

Representative images of DIV8 primary mouse cortical neurons derived from +/+, spastin +/- and -/- mice and co-transfected with EGFP-M1 and mCherrySec61β. Neurons were reconstructed from Z-stack images obtained with confocal laser scanning microscopy. Scale bar: 50 µm.

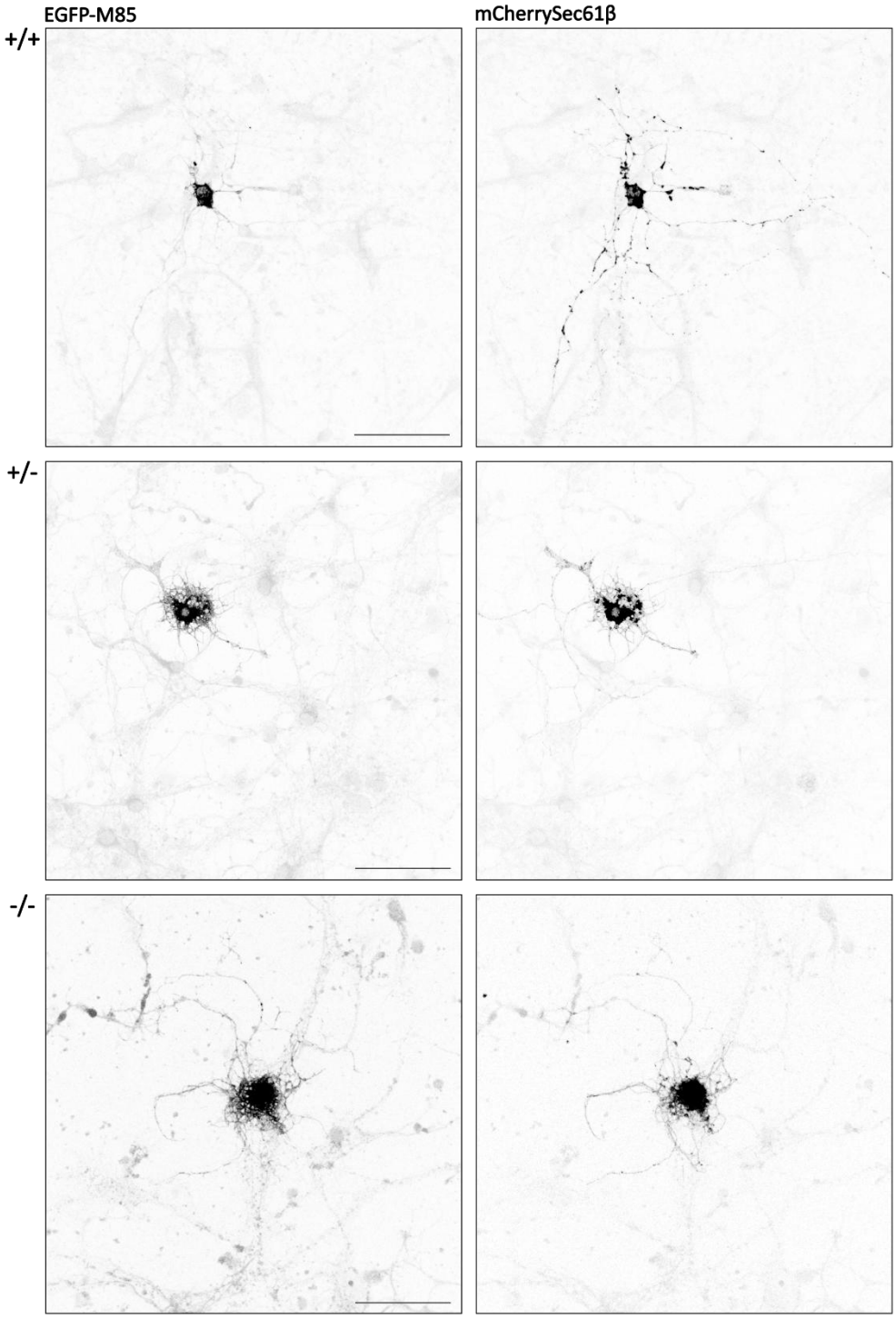

Figure 22. Analysis of M85 spastin overexpression on primary cortical neurons.
Representative images of DIV8 primary mouse cortical neurons derived from +/+, spastin +/- and -/- mice and co-transfected with EGFP-M85 and mCherrySec61β. Neurons were reconstructed from Z-stack images obtained with confocal laser scanning microscopy. Scale bar: 50 µm.

3.10 Compound N- and C-terminal M1 spastin mutations lead to proximal axonal ER distribution defects

In this study, the number of large ER aggregates (larger than 0.2 μm^2) was found to be increased in proximal axon regions upon spastin loss. However, this increase is not present when expressing the MT-severing deficient spastin mutant EGFP-M85 K388R, nor when polyglutamylation levels are reduced, resulting in reduced spastin binding to MTs. However, in both these cases, the number of ER aggregates is increased in distal axons, in a similar way to when spastin is depleted. These results suggest that while the MT-severing activity of spastin is necessary for proper axonal ER distribution, spastin must be involved in other processes affecting axonal ER. Spastin was shown to interact with ER-shaping proteins, specifically with REEP1 (Park et al., 2010), atlastin-1 (Sanderson et al., 2006) and with reticulon-1 (Mannan et al., 2006). These studies have shown how the interaction with reticulon-1 and atlastin-1 is abrogated upon the expression of plasmids encoding M1 spastin mutants lacking residues 1-300 (Mannan et al., 2006) and 1-80 (Sanderson et al., 2006), respectively. Patients with compound P97T N-terminal and R431X C-terminal spastin point mutations present an earlier onset form of the disease compared to HSP caused by spastin C-terminal mutations alone (McCorquodale et al., 2011). Conversely, patients with compound S44L N-terminal and P361L C-terminal spastin point mutations present a more severe form of the disease (Chinnery et al., 2004; Svenson et al., 2004).

The P97 and P361 spastin residues are conserved among numerous mammalian species, highlighting the importance of these residues in its function (Figure 23). The P97T point mutation was introduced in M1 and M85 spastin plasmids, both alone and in combination with the P361L point mutation, to investigate whether these compound mutations lead to similar axonal ER defects compared to spastin loss. This would suggest that, in addition to spastin-mediated MT severing, the interaction between spastin and reticulon-1 is crucial for proper axonal ER regulation.

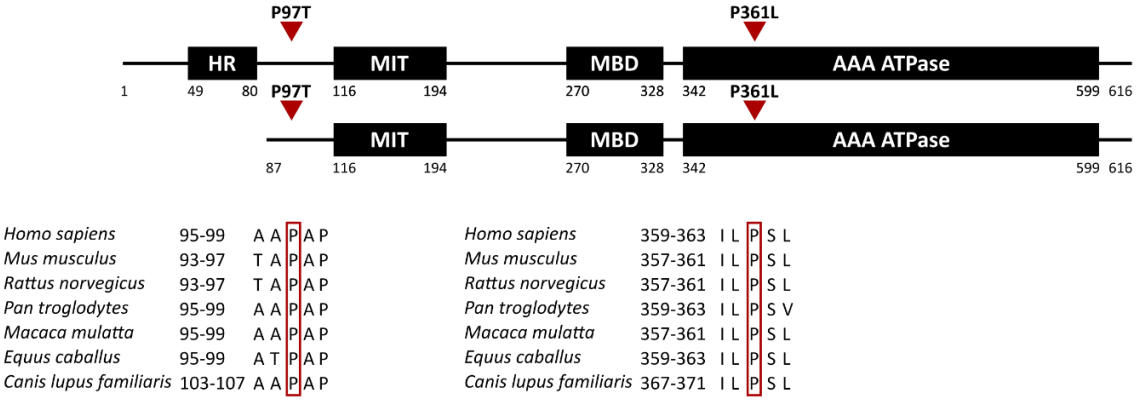

Figure 23. Spastin P97 and P361 residue conservation among some mammalian species.

The two main isoforms of human spastin, M1 and M87, and their domains (HR: hydrophobic region; MIT: MT interacting and endosome trafficking domain; MBD: MT binding domain; AAA ATPase: MT severing domain). Red arrows indicate the introduced point mutations. Below, conservation of the residues of interest in six other mammalian species is shown.

In line, mCherrySec61β and either EGFP, EGFP-M1 P97T, EGFP-M1 P361L, EGFP M1 P97T P361L, EGFP-M85 P97T, EGFP-M85 P361L or EGFP-M85 P97T P361L were co-expressed in DIV6 primary cortical neurons. Neurons were fixed on DIV8 and analysed. In a similar manner as primary cortical neurons co-expressing mCherrySec61β and either EGFP-M1 or EGFP-M85, samples containing primary cortical neurons co-expressing mCherrySec61β and either EGFP-M1 P97T or EGFP-M85 P97T showed extensive cell death (Figure 24). These results are consistent with a toxic increase in spastin-mediated MT severing, as this process is not affected in the plasmids presenting only the P97T mutation.

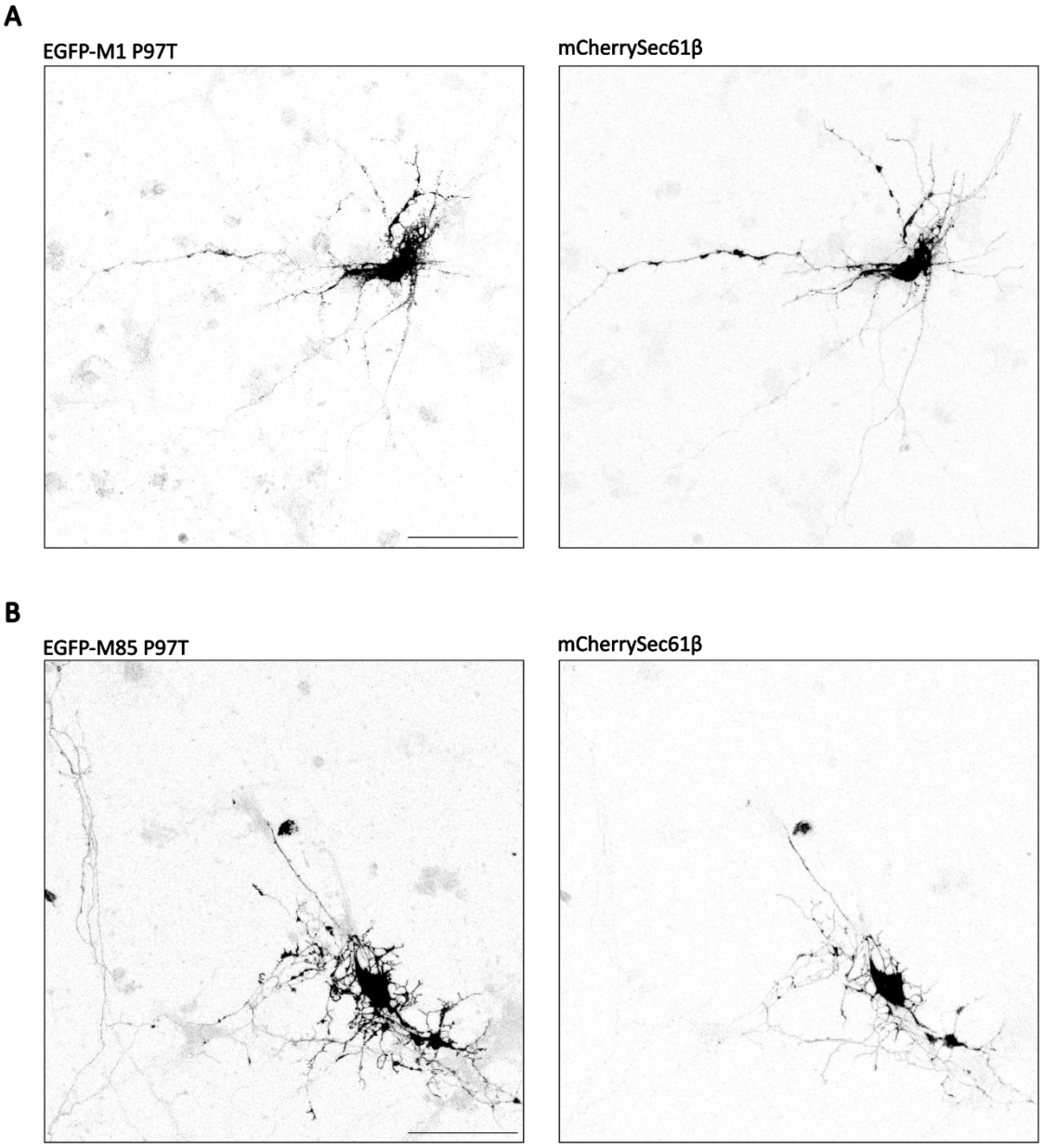

Figure 24. Analysis of M1 and M85 P97T overexpression on primary mouse cortical neurons. DIV8 primary mouse cortical transfected with mCherrySec61β and either EGFP-M1 P97T or EGFP-M85 P97T and mCherrySec61β. Neurons were reconstructed from Z-stack images obtained with confocal laser scanning microscopy. Scale bar: 50 µm.

Primary cortical neurons co-expressing mCherrySec61β and either P361L or P97T P361L spastin mutants were viable. The quantification of the total number of aggregates and average aggregate area in proximal and distal axon regions revealed that both M1 and M85 harbouring only the P361L mutation did not lead to an increase in proximal axon ER aggregate formation, while distal axons showed a

significant increase in ER aggregate number. Similarly, M85 P97T P361L overexpression results in a significant increase in distal axon ER aggregate number. M1 P97T P361L point mutations showed the most severe phenotype, as they lead to a significant increase in ER aggregate number also in proximal axonal regions, and a significant increase in both axonal ER aggregate number and average aggregate area in distal axon regions (Figure 25). Furthermore, endogenous GRP78 was detected in neurons co-expressing mCherrySec61β and spastin mutants to evaluate the level of ER stress within distal ER aggregates (Figure 26A). Quantification of GRP78 levels in ER-positive compartments revealed that there are higher levels of ER stress upon expression of all spastin mutants (Figure 26B). These results suggest that M1 spastin participates in ER distribution and homeostasis through both its N- and C-terminal domains.

In this study, spastin depletion was found to affect distal axon morphology, ER distribution and homeostasis. Moreover, spastin loss results in ER aggregate formation already in proximal axons, suggesting a more dramatic disruption of axonal ER compared to spastin reduction. Albeit spastin-mediated MT-severing and tubulin polyglutamylation are necessary for proper axonal ER distribution and homeostasis, their disruption or reduction results in less severe axonal ER aggregate formation compared to spastin loss. These results suggest that other spastin domains might also be involved in axonal ER distribution. Indeed, expression of an M1 mutant harbouring both an N- and C-terminal mutation leads to higher ER aggregate formation in proximal axons, similarly to spastin loss. These results suggest a role for M1 spastin in axonal ER distribution through both its N-terminal domain, important for interaction with ER-shaping proteins, and the C-terminal domain, crucial for MT severing.

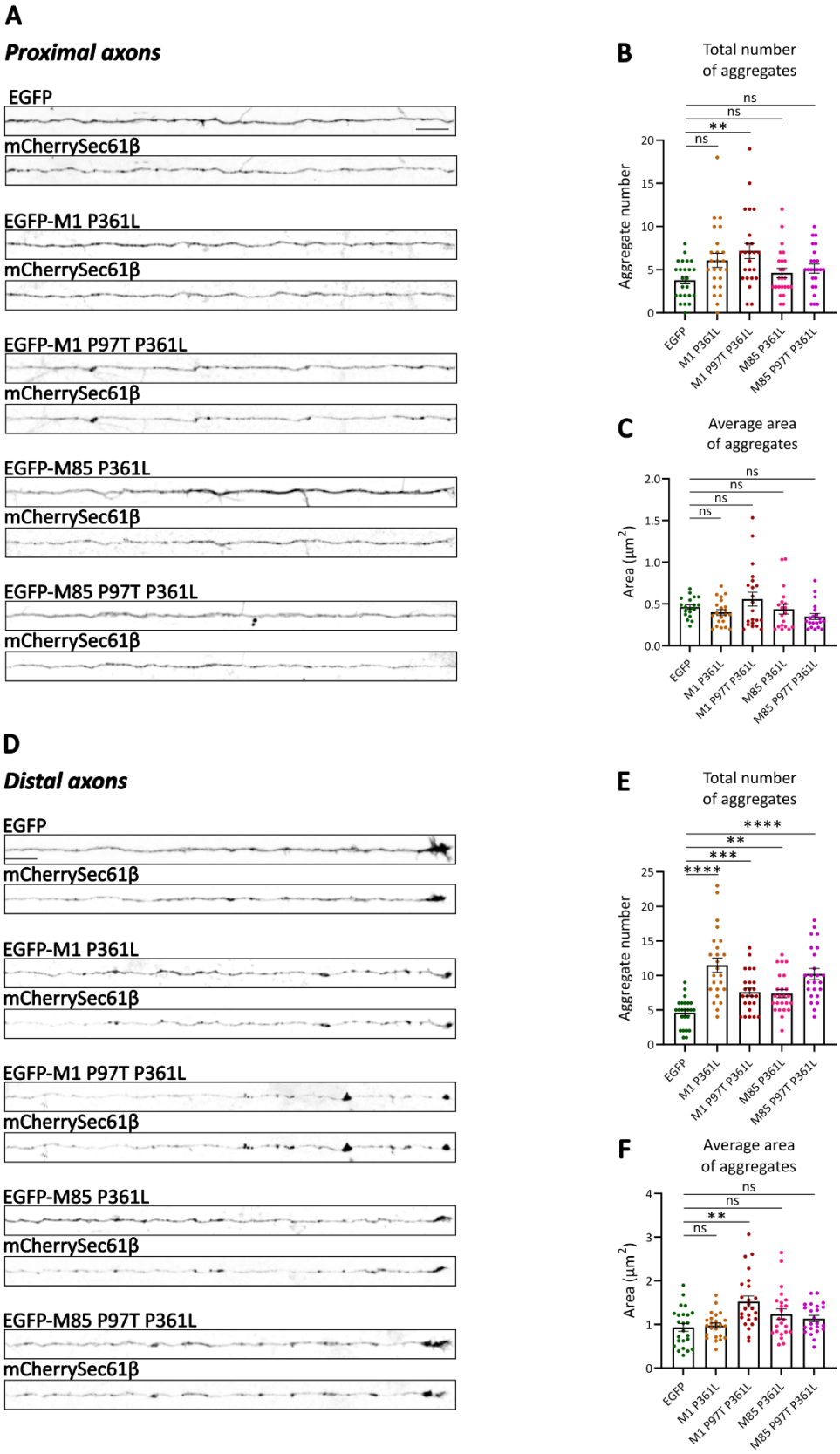

Figure 25. Analysis of M1 and M85 compound mutants on axonal ER distribution.
(A) Distribution of the ER in representative proximal axon regions of DIV8 primary mouse cortical neurons co-transfected with mCherrySec61β and either EGFP, EGFP-M1 P361L, EGFP-M1 P97T

P361L, EGFP-M85 P361L, or EGFP-M85 P97T P361L. Straightened proximal axons from reconstructed Z-stack images obtained with confocal laser scanning microscopy are shown. Scale bar: 10 µm. (B) Quantifications of the total number of ER aggregates in proximal axon regions. n=24 proximal axons per condition. Kruskal-Wallis test p-value EGFP vs. M1 P361L 0.1020; EGFP vs. M1 P97T P361L 0.0064; EGFP vs. M85 P361L >0.9999; EGFP vs. M85 P97T P361L 0.4120. (C) Quantifications of the average area of ER aggregates in proximal axon regions. n=24 proximal axons per condition. Kruskal-Wallis test p-value EGFP vs. M1 P361L 0.6677; EGFP vs. M1 P97T P361L >0.9999; EGFP vs. M85 P361L 0.7431; EGFP vs. M85 P97T P361L 0.0624.
(D) Distribution of the ER in representative distal axon regions of DIV8 primary mouse cortical neurons co-transfected with mCherrySec61β and either EGFP, EGFP-M1 P361L, EGFP-M1 P97T P361L, EGFP-M85 P361L, or EGFP-M85 P97T P361L. Straightened distal axons from reconstructed Z-stack images obtained with confocal laser scanning microscopy are shown. Axon terminals are seen on the right edge of the images. Scale bar: 10 µm. (E) Quantifications of the total number of ER aggregates in distal axon regions. n=24 distal axons per condition. Brown-Forsythe and Welch ANOVA tests p-value EGFP vs. M1 P361L <0.0001; EGFP vs. M1 P97T P361L 0.0008; EGFP vs. M85 P361L 0.0017; EGFP vs. M85 P97T P361L <0.0001. (F) Quantifications of the average area of ER aggregates in distal axon regions. n=24 distal axons per condition. Kruskal-Wallis test p-value EGFP vs. M1 P361L >0.9999; EGFP vs. M1 P97T P361L 0.0011; EGFP vs. M85 P361L 0.2666; EGFP vs. M85 P97T P361L 0.4280.
Error bars represent mean ± SEM.

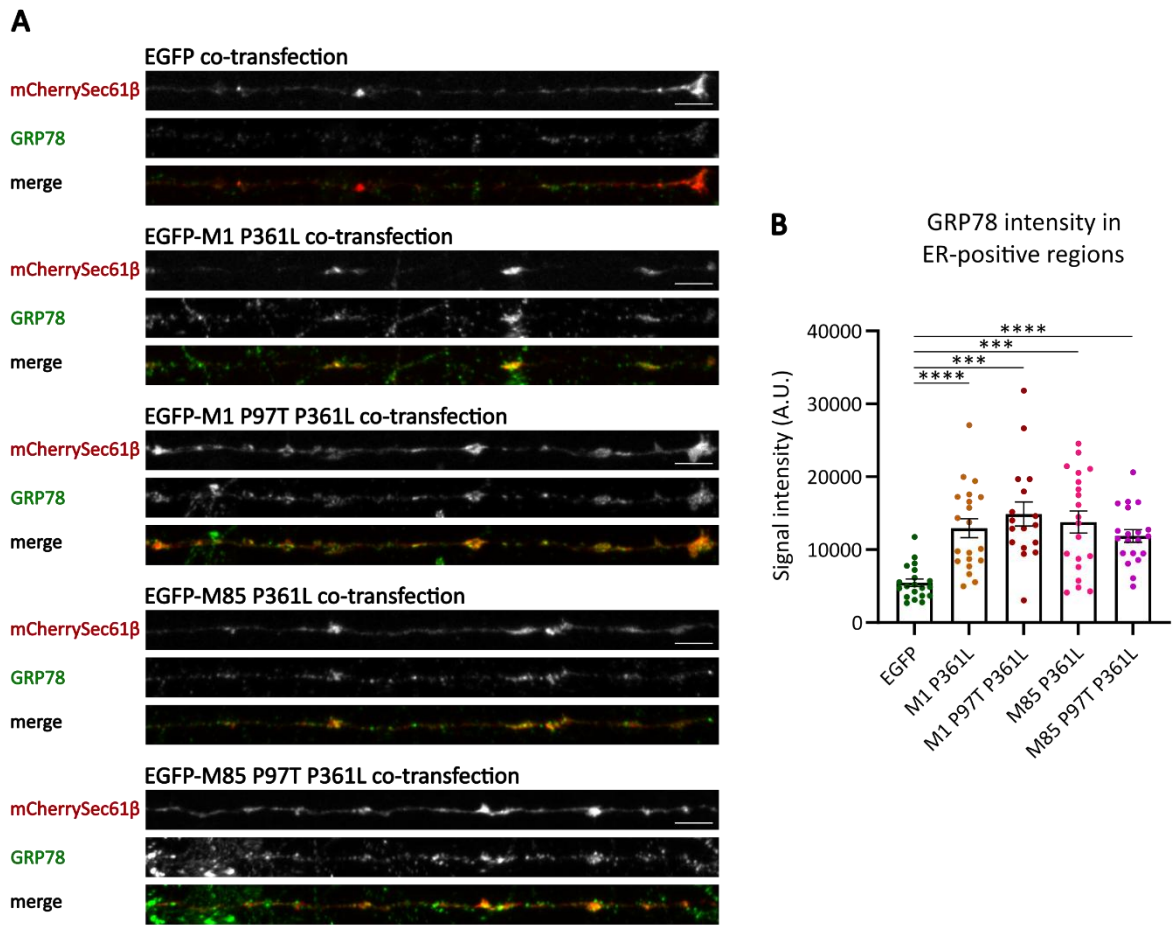

Figure 26. Analysis of ER homeostasis upon M1 and M85 compound mutant expression.
(A) Representative images of endogenous GRP78 immunolabeling in distal axons of DIV8 primary mouse cortical neurons co-transfected with mCherrySec61β and either EGFP, EGFP-M1 P361L, EGFP-M1 P97T P361L, EGFP-M85 P361L or EGFP-M85 P97T P361L. Straightened distal axons from reconstructed Z-stack images obtained with confocal laser scanning microscopy are shown. Axon terminals are seen on the right edge of the images. Scale bar: 5 µm. (B) Quantifications of the average signal intensity of GRP78 in mCherrySec61β-positive regions in distal axons. n=20 distal axons per condition. Brown-Forsythe and Welch ANOVA tests p-value EGFP vs. M1 P361L <0.0001; EGFP vs. M1 P97T P361L 0.0001; EGFP vs. M85 P361L 0.0001; EGFP vs. M85 P97T P361L <0.0001.
Error bars represent mean ± SEM.

4. Discussion

4.1 Spastin loss affects distal axon morphology

HSPs are a group of neurodegenerative disorders mainly characterized by the dying-back degeneration of corticospinal axons. Corticospinal neurons typically originate in the cerebral cortex, and their function is to deliver motor information to the spinal cord, responsible for the innervation of muscles and voluntary movement control. Corticospinal axon degeneration in HSP leads to disruptions in skeletal muscle innervation and deficits in movement of the lower limbs (Blackstone, 2018). Roughly 40% of all AD-HSP cases are due to mutations in the *SPAST* gene. Spastin has been linked to axonal outgrowth in rat hippocampal neurons (Ji et al., 2018; Yu et al., 2008), together with growth cone motility in the zebrafish embryo (Butler et al., 2010; Wood et al., 2006). Spastin loss has been found to lead to the formation of axonal swellings, structures frequently observed in the context of HSP, which are thought to be sites of abnormal organelle and protein accumulation preceding axonal dying-back degeneration (Fassier et al., 2012; Tarrade et al., 2006).

To examine axonal morphology upon spastin depletion in primary cortical neurons, primary cortical neurons derived from +/+, spastin +/-, and -/- mice were used. Total axon length at DIV8 was found not to be affected.

Although spastin reduction has been found to lead to a decrease in total axonal length in hippocampal neurons, studies have also shown no difference in primary mouse cortical neurons (Fassier et al., 2012). Therefore, it is possible that spastin reduction or loss leads to different effects depending on the culture system.

Although spastin depletion did not affect total axon length in primary mouse cortical neurons, frequent axonal swellings were observed in distal axons, and distal axon area was found to be significantly increased in spastin-depleted neurons. This

result is consistent with previous reports (Fassier et al., 2012). Further studies at different timepoints will be crucial to follow the development of the swellings and examine whether cortical axons show a reduction in total length upon spastin depletion at later time points or not at all. Furthermore, it would be interesting to examine the composition of axonal swellings in cross-sections of spastin-depleted mouse spinal cords by electron microscopy. This would provide insights into organelle organization and accumulation within these swellings.

4.2 Spastin affects axonal ER distribution and stress

ER defects have been reported in corticospinal axons of double mutant atlastin-1/REEP1 mouse model of HSP (P.-P. Zhu et al., 2022) and following the expression of a reticulon-1 mutant in *S. cerevisiae* (De Craene et al., 2006). Atlastin-1, REEP1, and reticulon-1 have a hydrophobic region in their amino acidic sequence, which inserts itself in the ER membrane and performs hydrophobic wedging to induce ER membrane curvature. M1 spastin interacts with these proteins and presents a similar hydrophobic region, suggesting that it may play a role in ER morphology in a similar manner to its interacting partners. Studies have shown that at 6 months of age, before the onset of motor impairments, axon numbers and perimeter are decreased in spinal cord cross-sections derived from the lumbar region of SPG4 mouse models (Piermarini et al., 2022).

In this study, lumbar region cross-sections of spinal cords of 7-month-old +/+, spastin +/- and -/- mice were evaluated with electron microscopy to evaluate whether spastin depletion also affects ER morphology. Average ER area, perimeter, and density within axons are significantly reduced in the spinal cords of spastin +/- and -/- mice. As this phenotype is already present before the onset of the first motor symptoms, which typically happens between 8 and 14 months of age (Lopes et al., 2020), these ER defects are likely causative for the development of HSPs. It would be interesting to analyse the same ER parameters at the onset of motor symptoms and then again at 14 months of age, to observe changes in corticospinal axonal ER

and correlate them with axonal degeneration and with the development and evolution of the disease.

Furthermore, spastin has been found to be involved in the regulation of contacts between the ER and mitochondria and ER and endosomes, and is thought to mediate the crosstalk between the ER and MTs (Raby et al., 2024; Reid et al., 2005). It would be interesting to examine lumbar region cross-sections to evaluate whether there are any differences in ER-organelle contact formation upon spastin depletion. Specifically, it would be interesting to evaluate whether contacts between ER and MTs are still present and whether MTs in proximity to ER structures are morphologically affected. Furthermore, the limitation of analysing spinal cord cross-sections with conventional electron microscopy is the fact that it only allows the collection of two-dimensional information about cellular structures. Evaluating the 3D structure of the ER in the lumbar region of spinal cords using other techniques, such as Focused Ion Beam Scanning Electron Microscopy (FIB-SEM), would be decisive in determining parameters such as total axonal ER volume, curvature, and spatial distribution, but also in providing more information on ER contacts with other organelles.

The reduction in axonal ER area, perimeter, and density upon spastin depletion in spinal cord lumbar regions suggests a role for spastin in axonal ER distribution and regulation. To date, tools to analyse endogenous ER in axons using light microscopy are lacking, with the majority of studies resorting to the overexpression of ER markers. In this study, overexpression of a plasmid encoding Sec61β, a member of the ER translocon complex, was used as a tool to investigate axonal ER morphology in primary cortical neurons derived from +/+, spastin +/-, and -/- mice. When examining 150 µm-long axonal regions, ER distribution and aggregate formation were found to be altered upon spastin depletion. Specifically, spastin loss is sufficient to induce the formation of large Sec61β aggregates in proximal axon regions, and the situation gradually worsens moving along the axon. In distal axon regions, a 50% reduction in spastin levels is already sufficient to induce the formation of large aggregates. To verify whether the increase in formation of large

ER aggregates upon spastin depletion is due to higher total ER levels, the expression of calreticulin, an established ER marker, was assessed in total brain lysates. Calreticulin levels were found not to be altered upon spastin depletion. This indicates that the formation of large ER aggregates upon spastin loss is not ascribable to an upregulation in ER levels but rather to a dramatic change in axonal ER distribution. Although it was not possible to measure endogenous axonal ER levels in mCherrySec61β-expressing neurons, differences in axonal ER distribution patterns could be clearly observed. While mCherrySec61β distribution in +/+ axons is homogeneous, high levels of discontinuity can be observed in spastin-depleted axons, where aggregates are characterized by high ER signal intensity, and the regions present between aggregates often present lower signal levels. Axonal ER homogeneity and continuity are crucial to maintain axonal homeostasis and function. Reticulon-1 and REEPA/B loss was shown to lead to higher discontinuity in ER signal and partial ER loss from distal motor axons in *Drosophila melanogaster* (Yalçın et al., 2017). Spastin loss could lead to similar effects on axonal ER on mammalian neurons.

While there have been other reports on axonal ER discontinuity caused by HSP-related mutations, this is the first study to report the formation of large axonal ER aggregates upon spastin depletion. The formation of these aggregates could be due to different reasons. ER sheets are structures typical of the rough ER; they are flat and large, and are important for protein synthesis and folding. Although axonal ER is mainly smooth and composed of narrow interconnected tubules and irregularly spaced cisternae, there is also a small fraction of ER sheets (Shibata et al., 2006). Mutations or loss of reticulons, REEP1, atlastin-1 and spastin lead to ER sheet expansion and alteration of ER sheet to tubule ratio (O'Sullivan et al., 2012; Vajente et al., 2019; Voeltz et al., 2006; Yalçın et al., 2017; P.-P. Zhu et al., 2003). The formation of Sec61β aggregates upon spastin depletion could be explained by an abnormal increase in axonal ER sheet formation.

In addition, the expression of plasmid DNA is strictly dependent on ER function. Sec61β could be aggregating upon spastin depletion because of folding defects due

to axonal ER dysfunction. It is possible that such ER aggregates are not present on an endogenous level and that spastin loss actually induces a total decrease in axonal ER structures. Further studies making use of super-resolution microscopy would be crucial to more precisely analyse axonal ER structures, evaluate ER sheet/tubule ratio, and ER association to bending proteins upon spastin depletion. Also, the development of tools to study endogenous ER in cultured neurons is of the utmost importance to shed light on the effects of spastin depletion on endogenous axonal ER morphology, continuity, and aggregation.

Moreover, axonal swellings are thought to be sites of organelle accumulation, as disorganized MTs were found in axonal swellings upon spastin loss (Fassier et al., 2012) and retrograde axonal transport from axonal swellings was shown to be impaired upon spastin mutation (Tarrade et al., 2006). These results indicate that accumulated structures are not being properly trafficked and cleared from distal axons. ER aggregates could therefore be accumulating within axonal swellings without being properly cleared due to defects in axonal retrograde transport.

Finally, MT alterations have been found both in primary mouse hippocampal neurons and in *Drosophila melanogaster* larvae (Lopes et al., 2020; Sherwood et al., 2004). Spastin loss was also found to lead to impairments in MT disassembly in primary cortical neurons (Fassier et al., 2012). The ER and MTs are known to interact, and such interaction is crucial for proper tubular ER morphology and dynamics (Joensuu et al., 2014; Terasaki et al., 1986; Vajente et al., 2019). Sec61β aggregate formation could be due to the interaction of the ER with defective MTs, leading to tubular ER abnormalities. To evaluate the localization of Sec61β aggregates relative to MT abnormalities, endogenous alpha-tubulin was detected in +/+, spastin +/-, and-/- primary cortical neurons expressing mCherrySec61β. ER aggregates were found to be in close proximity to bundled MT structures. Further studies are needed to determine the relationship between the two organelles in this context. It would be interesting to analyse axonal ER dynamics upon spastin depletion, as these have been found to depend on ER-MT interactions (Farías et al., 2019). Further studies will be crucial in determining whether ER abnormalities are

caused by the interaction with altered MTs or whether they occur independently of MTs.

Alterations in ER distribution and an increase in aggregation within axons suggest functional impairments in these compartments. In order to study ER homeostasis, endogenous GRP78 levels within ER aggregates were assessed with light microscopy. GRP78 is a member of the Heat Shock Protein 70 family and is activated during the unfolded protein response within the ER, but also in the presence of other ER stressors, such as Ca^{2+} storage disturbances (Lee, 1987). When analysing GRP78 protein levels in distal axon Sec61β compartments, these were significantly increased upon spastin depletion. These results indicate that axonal ER aggregates are subject to higher levels of stress. Further studies are needed to elucidate whether spastin depletion leads to impairments in axonal ER function. To this end, Ca^{2+} levels in axonal ER upon spastin depletion could be examined via the expression of a Ca^{2+} sensor to study Ca^{2+} levels in distal axons. A decrease in store-operated Ca^{2+} entry and disruptions in Ca^{2+} homeostasis were found in SPG4-HSP iPSC-derived neurons (Rizo et al., 2022), suggesting a link between ER abnormalities and improper Ca^{2+} storage. Total axonal Ca^{2+} levels upon spastin depletion should be evaluated following thapsigargin treatment. Thapsigargin is an inhibitor of the Ca^{2+}-ATPase SERCA pump, responsible for Ca^{2+} transport from the cytosol to the ER. Treatment with thapsigargin raises levels of intracellular free Ca^{2+} (Jones & Sharpe, 1994). These studies would allow the evaluation of the effects of spastin on distal axonal capacity for Ca^{2+} storage.

4.3 Spastin-mediated MT severing is necessary for distal axonal ER distribution and stress

Spastin is a hexameric protein that forms a central loop and mediates MT-severing through its AAA ATPase domain. This domain binds to the C-terminal region of the tubulin tail and mediates ATP hydrolysis (Solowska & Baas, 2015). Thanks to the energy supplied by this process, the tubulin tail is pulled through the central pore

and tubulin subunits are cleaved. Studies have shown that mutations in the AAA ATPase region disrupt its severing activity but do not affect spastin binding to MTs (White et al., 2007). A substantial number of cases of SPG4-HSP are caused by mutations localized within the AAA cassette (Ferese et al., 2023).

To evaluate whether defects in ER distribution within axons upon spastin depletion are due to disrupted spastin-mediated MT severing, a plasmid encoding the MT severing-deficient K388R spastin mutant was overexpressed in primary mouse cortical neurons. The expression of K388R spastin leads to an increase in ER aggregate formation in distal axons without affecting proximal axons. Moreover, GRP78 protein levels were significantly increased in distal axonal ER-positive compartments. These results indicate that spastin-mediated MT severing is necessary for proper distal axonal ER distribution and homeostasis. However, total spastin loss leads to large ER aggregate formation already in proximal axons, indicating that it is likely that other spastin domains are also involved in axonal ER distribution and stress.

MT-severing enzymes present partially overlapping functions. Fidgetin was found to preferentially sever unstable MTs, whereas spastin and katanin mostly sever the stable fraction (Leo et al., 2015; Riano et al., 2009; Sudo & Baas, 2010). It would be interesting to label endogenous katanin and fidgetin to examine their levels and distribution in primary mouse cortical axons upon K388R spastin expression to investigate whether these are upregulated or redistributed upon spastin-mediated MT severing disruption.

4.4 Tubulin polyglutamylation regulates distal axonal ER distribution and stress

Spastin binding and severing of MTs is regulated by different factors, including post-translational modifications of tubulin, the main component of MTs. The addition of glutamate chains to the C-terminal tails of tubulin, known as polyglutamylation, was shown to directly impact spastin binding and severing of MTs. Specifically, an

increase in polyglutamylation leads to a linear increase in spastin binding affinity and concurrently to a non-linear decrease in spastin-mediated MT severing (Lacroix et al., 2010; Valenstein & Roll-Mecak, 2016). Tubulin alpha4a was previously shown to be the tubulin isotype with the longest glutamate side chains present in the brain (Redeker et al., 1998). Knock-in tuba4aΔpolyGlu (p/p) mice carrying point mutations that lead to the disruption of the polyglutamylation of this tubulin isotype were used to investigate whether a dramatic reduction in both spastin binding to and consequent severing of MTs leads to similar axonal defects to those observed upon spastin loss. There is an increase in distal axonal ER aggregate formation in p/p-derived primary cortical neurons, and GRP78 protein levels are also increased within the aggregates. These results indicate that tubulin polyglutamylation is important for proper axonal ER distribution and homeostasis, but its reduction leads to less severe axonal ER defects compared to spastin loss. The lower severity of ER defects in p/p-derived neurons is consistent with the fact that p/p mice do not present any motor defects (Hausrat et al., 2022). This indicates that in these mice there must be some compensatory mechanism which is activated in response to a reduction in tubulin polyglutamylation to restore normal levels of MT severing, perhaps through the upregulation of MT-severing enzymes katanin or fidgetin. Previous studies have shown that polyglutamylation levels are increased upon spastin absence (Lopes et al., 2020), and high polyglutamylation levels have been associated with impaired motor transport and neurodegeneration (Magiera et al., 2018). It would be useful to employ super-resolution microscopy techniques to analyse axonal tubulin post-translational modification patterns together with spastin, atlastin-1, REEP1 and reticulon-1/2 axonal localization. It would be interesting to examine whether these proteins are homogeneously distributed throughout axons or if they are present within specific tubulin microdomains. Performing these studies in +/+ and spastin-depleted neurons would provide further insight into the regulation of spastin-mediated MT-severing by tubulin post-translational modifications and the influence of the loss of spastin-mediated MT severing on ER-bending protein localization.

Furthermore, the addition of glutamate to C-terminal chains of tubulin is orchestrated by tubulin tyrosine ligase-like (TTLL) glutamylases. The removal of glutamate is instead mediated by cytoplasmic carboxypeptidase (CCP) deglutamylases (Janke & Bulinski, 2011). Examining ER morphology upon precise modulation of polyglutamylation levels, for example through the up- or down-regulation of TTLLs and CCPs, would shed light on the exact influence of spastin-mediated MT binding and severing on axonal ER distribution and homeostasis. Tweaking polyglutamylation levels also upon spastin depletion would be useful to determine whether inducing lower levels of polyglutamylation in spastin-depleted cortical neurons is sufficient to restore distal axonal ER defects.

Moreover, it would be useful to crossbreed the tuba4aΔpolyGlu and spastin-depleted mice to study the compound effect of polyglutamylation reduction and spastin depletion. First, it would be interesting to analyse whether there are any behavioural or motor defects in these mice. Further, analysing ER morphology in spinal cord lumbar regions of tuba4aΔpolyGlu/spastin-depleted mice could provide further insight into the relationship between MT severing and axonal ER. Moreover, analysing katanin and fidgetin localization and levels in neurons derived from these mice could provide insight into mechanisms of MT binding and severing upon spastin loss.

4.5 Spastin overexpression leads to extensive cortical neuron death

Spastin is mainly present in two isoforms, known as M1 and M87 in humans and M1 and M85 in rodents. M1 is longer and presents an N-terminal hydrophobic region through which spastin interacts with ER-shaping proteins and likely inserts itself in the ER bilayer to mediate the ER-MT crosstalk and regulate ER formation (Park et al., 2010). M1 and M87 spastin share an MT interacting and endosome trafficking (MIT) domain, an MT-binding domain (MTBD), and the AAA ATPase domain required for MT severing. In order to evaluate the effect of spastin overexpression on axonal ER, plasmids encoding the two main isoforms of spastin in mice, M1 and M85, were

overexpressed in primary mouse cortical neurons. M1 overexpression leads to ER collapse in HeLa cells (Lumb et al., 2012), alterations in lipid droplet morphology (Papadopoulos et al., 2015), and in MT stability (Plaud et al., 2018). M87 overexpression has been found to alter MT polymerization necessary for proper presynaptic cargo dynamics in iPSC-derived neurons (Aiken & Holzbaur, 2024).
In this study, the expression of M1 or M85 together with Sec61β in primary mouse cortical neurons led to extensive cell death. This effect is likely due to excessive MT-severing activity, leading to neuronal dysfunction. Even M1 and M85 reintroduction upon the background of endogenous spastin depletion resulted in extensive cell death. Due to these limitations, the effects of an excess of spastin activity on axonal ER morphology could not be studied. Tightly controlled overexpression leading to much lower expression of the spastin isoforms, for example through the use of a weaker promoter, will be crucial in gaining insights into the role of different spastin isoforms on axonal ER regulation and in determining whether spastin reintroduction can rescue ER defects caused by spastin loss.

4.6 M1 spastin is involved in axonal ER distribution and homeostasis both through its N- and C-terminal domains

In this study, MT severing mediated by spastin was found to be necessary for distal axonal ER distribution and homeostasis. However, axonal ER was found to be more dramatically affected upon spastin loss, suggesting multiple roles of spastin in axonal ER distribution and homeostasis. Spastin interacts with ER-shaping proteins reticulon-1, atlastin-1, and REEP1 with its N-terminal domain (Mannan et al., 2006; Park et al., 2010). These proteins are inserted within the ER lipid bilayer, and studies suggest that M1 spastin participates in a complex with them to mediate the crosstalk between ER and MTs and regulate ER formation and localization (Denton et al., 2016). Patients presenting both N- and C-terminal spastin mutations were shown to develop early-onset symptoms of HSP (McCorquodale et al., 2011). It is likely that spastin exerts its function on axonal ER morphology through both its N-

and C-terminal domains. The combination of a P97T mutation (N-terminal) and a R431X (C-terminal) mutation was found in patients presenting early-onset HSP (McCorquodale et al., 2011). Also, S44L and P361L compound mutations lead to a severe form of infantile HSP (Chinnery et al., 2004). In this study, P97T and P361L point mutations were introduced in plasmids encoding M1 and M85 spastin isoforms. The plasmids were co-expressed with Sec61β in primary mouse cortical neurons to investigate whether the expression of spastin compound mutants produces similar effects on the axonal ER as spastin loss. Overexpression of spastin mutants presenting only the N-terminal point mutation was found to lead to extensive cell death. This is likely due to the fact that in these mutants, MT severing is not affected, and therefore their overexpression leads to similar effects to M1 and M85 spastin overexpression. Expression of all the other mutants leads to an increase in ER aggregate formation in distal axons and an increase in GRP78 levels, with the exception of M1 P97T P361L, which leads to an increase in ER aggregate formation already in proximal axons. This phenotype closely aligns with that observed upon spastin loss. These results suggest that the N-terminal region of M1 spastin, likely through its interaction with reticulon-1, is involved in axonal ER morphology regulation, in addition to the C-terminal region involved in MT severing (Mannan et al., 2006). Both the reduction in disease-onset age and an increase in its severity upon compound N- and C-terminal spastin mutations could indicate that these compound mutations exacerbate HSP symptoms through the combined loss of spastin interaction with reticulon-1 and of MT severing activity. In order to shed light on the role of different spastin isoforms on axonal ER regulation, the use of isoform-specific knock-out models will be pivotal.

Furthermore, it would be interesting to explore the interaction between reticulon-1 and spastin upon expression of M1 P97T P361L, to determine whether this is indeed disrupted or whether some other mechanism is involved. Also, it would be useful to examine reticulon-1, atlastin-1, and REEP1 axonal localization upon expression of the compound mutants. This would provide information on how the compound

P97T P361L point mutation affects spastin interactions with ER-bending proteins and its role in axonal ER regulation.

Furthermore, it would be interesting to study the interaction of spastin with other ER-bending proteins as well. Plasmids encoding M1 and M85 spastin with S44L P361L mutations could be useful to determine whether the rare infantile HSP caused by these mutations is also linked to enhanced axonal ER defects. Spastin interaction with atlastin-1 was found to be disrupted upon deletion of the first 80 amino acids in M1 spastin (Sanderson et al., 2006). Studying the interaction between M1 spastin harbouring the S44L point mutation and atlastin-1 could provide insights into the influence of this interaction on axonal ER regulation.

Moreover, it would be interesting to study the effect of a reduction in ER-bending protein levels on spastin localization and function to precisely depict the effects of their interaction with spastin on axonal ER.

In conclusion, spastin was found to affect corticospinal axonal ER morphology. Its loss was also found to result in distal axonal swelling formation and defects in proximal and distal axonal ER morphology and homeostasis in primary mouse cortical neurons. Spastin likely has multiple roles in axonal ER distribution and homeostasis, which it exerts through its N-terminal hydrophobic domain, required for the interaction with ER-shaping proteins, and its C-terminal domain, necessary for its MT-severing activity. Indeed, MT-severing disruption and tubulin polyglutamylation reduction resulted in distal axonal ER defects, similarly to spastin reduction, while the expression of a compound M1 N- and C-terminal spastin mutant led to similar ER abnormalities compared to spastin loss. These data suggest that M1 spastin may be more important than M87 in axonal ER distribution and homeostasis and may be more involved in the development of HSPs.

Further studies are needed to determine the contributions of each isoform to axonal ER regulation, the effects on axonal ER of SPG4-HSP mutations and to depict the

function of the interaction between spastin and ER-shaping proteins in health and disease. These efforts will be pivotal in gaining insight into the pathogenesis of HSP and developing therapies to ameliorate or treat HSP symptoms. Furthermore, these studies will shed light on mechanisms of axonal ER maintenance, possibly leading to new insights into the pathogenesis of numerous other diseases characterized by axonopathy, such as neurodegenerative disorders and spinal cord injury.

References

Aiken, J., & Holzbaur, E. L. F. (2024). Spastin locally amplifies microtubule dynamics to pattern the axon for presynaptic cargo delivery. *Current Biology*, *34*(8), 1687-1704.e8. https://doi.org/10.1016/j.cub.2024.03.010

Alberts, B., Johnson, A., Lewis, J., Morgan, D., Raff, M., Roberts, K., & Walter, P. (2002). *Molecular Biology of the Cell*.

Appenzeller-Herzog, C., & Hauri, H.-P. (2006). The ER-Golgi intermediate compartment (ERGIC): in search of its identity and function. *Journal of Cell Science*, *119*(11), 2173–2183. https://doi.org/10.1242/jcs.03019

Baas, P. W., Deitch, J. S., Black, M. M., & Banker, G. A. (1988). Polarity orientation of microtubules in hippocampal neurons: uniformity in the axon and nonuniformity in the dendrite. *Proceedings of the National Academy of Sciences*, *85*(21), 8335–8339. https://doi.org/10.1073/pnas.85.21.8335

Bear, M. F., Connors, B. W., & Paradiso, M. A. (2016). *Neuroscience: Exploring the Brain*.

Beetz, C., Koch, N., Khundadze, M., Zimmer, G., Nietzsche, S., Hertel, N., Huebner, A.-K., Mumtaz, R., Schweizer, M., Dirren, E., Karle, K. N., Irintchev, A., Alvarez, V., Redies, C., Westermann, M., Kurth, I., Deufel, T., Kessels, M. M., Qualmann, B., & Hübner, C. A. (2013). A spastic paraplegia mouse model reveals REEP1-dependent ER shaping. *Journal of Clinical Investigation*, *123*(10), 4273–4282. https://doi.org/10.1172/JCI65665

Bican, O., Minagar, A., & Pruitt, A. A. (2013). The Spinal Cord. *Neurologic Clinics*, *31*(1), 1–18. https://doi.org/10.1016/j.ncl.2012.09.009

Blackstone, C. (2012). Cellular Pathways of Hereditary Spastic Paraplegia. *Annual Review of Neuroscience*, *35*(1), 25–47. https://doi.org/10.1146/annurev-neuro-062111-150400

Blackstone, C. (2018). Hereditary spastic paraplegia. In *Handbook of Clinical Neurology* (pp. 633–652). https://doi.org/10.1016/B978-0-444-64076-5.00041-7

Brill, M. S., Kleele, T., Ruschkies, L., Wang, M., Marahori, N. A., Reuter, M. S., Hausrat, T. J., Weigand, E., Fisher, M., Ahles, A., Engelhardt, S., Bishop, D. L., Kneussel, M., & Misgeld, T. (2016). Branch-Specific Microtubule Destabilization Mediates Axon Branch Loss during Neuromuscular Synapse Elimination. *Neuron*, *92*(4), 845–856. https://doi.org/10.1016/j.neuron.2016.09.049

Butler, R., Wood, J. D., Landers, J. A., & Cunliffe, V. T. (2010). Genetic and chemical modulation of spastin-dependent axon outgrowth in zebrafish embryos indicates a role for impaired microtubule dynamics in hereditary spastic paraplegia. *Disease Models & Mechanisms*, *3*(11–12), 743–751. https://doi.org/10.1242/dmm.004002

Chen, F., Yan, B., Ren, J., Lyu, R., Wu, Y., Guo, Y., Li, D., Zhang, H., & Hu, J. (2021). FIT2 organizes lipid droplet biogenesis with ER tubule-forming proteins and septins. *Journal of Cell Biology*, *220*(5). https://doi.org/10.1083/jcb.201907183

Chinnery, P. F., Keers, S. M., Holden, M. J., Ramesh, V., & Dalton, A. (2004). Infantile hereditary spastic paraparesis due to codominant mutations in the spastin gene. *Neurology*, *63*(4), 710–712. https://doi.org/10.1212/01.WNL.0000135346.63675.3E

Claudiani, P., Riano, E., Errico, A., Andolfi, G., & Rugarli, E. (2005). Spastin subcellular localization is regulated through usage of different translation start sites and active export from the nucleus. *Experimental Cell Research*, *309*(2), 358–369. https://doi.org/10.1016/j.yexcr.2005.06.009

Connell, J. W., Lindon, C., Luzio, J. P., & Reid, E. (2009). Spastin Couples Microtubule Severing to Membrane Traffic in Completion of Cytokinesis and Secretion. *Traffic*, *10*(1), 42–56. https://doi.org/10.1111/j.1600-0854.2008.00847.x

De Craene, J.-O., Coleman, J., Estrada de Martin, P., Pypaert, M., Anderson, S., Yates, J. R., Ferro-Novick, S., & Novick, P. (2006). Rtn1p Is Involved in

Structuring the Cortical Endoplasmic Reticulum. *Molecular Biology of the Cell*, *17*(7), 3009–3020. https://doi.org/10.1091/mbc.e06-01-0080

Denton, K. R., Lei, L., Grenier, J., Rodionov, V., Blackstone, C., & Li, X.-J. (2014). Loss of Spastin Function Results in Disease-Specific Axonal Defects in Human Pluripotent Stem Cell-Based Models of Hereditary Spastic Paraplegia. *Stem Cells*, *32*(2), 414–423. https://doi.org/10.1002/stem.1569

Denton, K. R., Xu, C., Shah, H., & Li, X.-J. (2016). Modeling axonal defects in hereditary spastic paraplegia with human pluripotent stem cells. *Frontiers in Biology*, *11*(5), 339–354. https://doi.org/10.1007/s11515-016-1416-0

Eddé, B., Rossier, J., Le Caer, J.-P., Desbruyères, E., Gros, F., & Denoulet, P. (1990). Posttranslational Glutamylation of α-tubulin. *Science*, *247*(4938), 83–85. https://doi.org/10.1126/science.1967194

Espadas, J., Pendin, D., Bocanegra, R., Escalada, A., Misticoni, G., Trevisan, T., Velasco del Olmo, A., Montagna, A., Bova, S., Ibarra, B., Kuzmin, P. I., Bashkirov, P. V., Shnyrova, A. V., Frolov, V. A., & Daga, A. (2019). Dynamic constriction and fission of endoplasmic reticulum membranes by reticulon. *Nature Communications*, *10*(1), 5327. https://doi.org/10.1038/s41467-019-13327-7

Farías, G. G., Fréal, A., Tortosa, E., Stucchi, R., Pan, X., Portegies, S., Will, L., Altelaar, M., & Hoogenraad, C. C. (2019). Feedback-Driven Mechanisms between Microtubules and the Endoplasmic Reticulum Instruct Neuronal Polarity. *Neuron*, *102*(1), 184-201.e8. https://doi.org/10.1016/j.neuron.2019.01.030

Fassier, C., Hutt, J. A., Scholpp, S., Lumsden, A., Giros, B., Nothias, F., Schneider-Maunoury, S., Houart, C., & Hazan, J. (2010). Zebrafish atlastin controls motility and spinal motor axon architecture via inhibition of the BMP pathway. *Nature Neuroscience*, *13*(11), 1380–1387. https://doi.org/10.1038/nn.2662

Fassier, C., Tarrade, A., Peris, L., Courageot, S., Mailly, P., Dalard, C., Delga, S., Roblot, N., Lefevre, J., Job, D., Hazan, J., Curmi, P. A., & Melki, J. (2012). Microtubule-targeting drugs rescue axonal swellings in cortical neurons from

spastin knock-out mice. *Disease Models & Mechanisms*. https://doi.org/10.1242/dmm.008946

Ferese, R., Scala, S., Suppa, A., Campopiano, R., Asci, F., Zampogna, A., Chiaravalloti, M. A., Griguoli, A., Storto, M., Pardo, A. Di, Giardina, E., Zampatti, S., Fornai, F., Novelli, G., Fanelli, M., Zecca, C., Logroscino, G., Centonze, D., & Gambardella, S. (2023). Cohort analysis of novel SPAST variants in SPG4 patients and implementation of in vitro and in vivo studies to identify the pathogenic mechanism caused by splicing mutations. *Frontiers in Neurology*, *14*. https://doi.org/10.3389/fneur.2023.1296924

Ferreirinha, F., Quattrini, A., Pirozzi, M., Valsecchi, V., Dina, G., Broccoli, V., Auricchio, A., Piemonte, F., Tozzi, G., Gaeta, L., Casari, G., Ballabio, A., & Rugarli, E. I. (2004). Axonal degeneration in paraplegin-deficient mice is associated with abnormal mitochondria and impairment of axonal transport. *Journal of Clinical Investigation*, *113*(2), 231–242. https://doi.org/10.1172/JCI20138

Fonknechten, N. (2000). Spectrum of SPG4 mutations in autosomal dominant spastic paraplegia. *Human Molecular Genetics*, *9*(4), 637–644. https://doi.org/10.1093/hmg/9.4.637

Ghribi, O., Herman, M. M., Pramoonjago, P., & Savory, J. (2003). MPP+ induces the Endoplasmic Reticulum Stress Response in Rabbit Brain Involving Activation of the ATF-6 and NF-κB Signaling Pathways. *Journal of Neuropathology & Experimental Neurology*, *62*(11), 1144–1153. https://doi.org/10.1093/jnen/62.11.1144

Grigoriev, I., Gouveia, S. M., van der Vaart, B., Demmers, J., Smyth, J. T., Honnappa, S., Splinter, D., Steinmetz, M. O., Putney, J. W., Hoogenraad, C. C., & Akhmanova, A. (2008). STIM1 Is a MT-Plus-End-Tracking Protein Involved in Remodeling of the ER. *Current Biology*, *18*(3), 177–182. https://doi.org/10.1016/j.cub.2007.12.050

Harding, A. E. (1983). Classification of the Hereditary Ataxias and Paraplegias. *The Lancet*, *321*(8334), 1151–1155. https://doi.org/10.1016/S0140-6736(83)92879-9

Harding, H. P., Zhang, Y., & Ron, D. (1999). Protein translation and folding are coupled by an endoplasmic-reticulum-resident kinase. *Nature*, *397*(6716), 271–274. https://doi.org/10.1038/16729

Hausrat, T. J., Janiesch, P. C., Breiden, P., Lutz, D., Hoffmeister-Ullerich, S., Hermans-Borgmeyer, I., Failla, A. V., & Kneussel, M. (2022). Disruption of tubulin-alpha4a polyglutamylation prevents aggregation of hyper-phosphorylated tau and microglia activation in mice. *Nature Communications*, *13*(1), 4192. https://doi.org/10.1038/s41467-022-31776-5

Hentati, A., Pericak-Vance, M. A., Lennon, F., Wasserman, B., Hentati, F., Juneja, T., Angrist, M. H., Hung, W.-Y., Boustany, R.-M., Bohlega, S., Iqbal, Z., Huether, C. H., Hamida, M. Ben, & Siddique, T. (1994). Linkage of a locus for autosomal dominant familial spastic paraplegia to chromosome 2p markers. *Human Molecular Genetics*, *3*(10), 1867–1871. https://doi.org/10.1093/hmg/3.10.1867

Hetz, C., & Saxena, S. (2017). ER stress and the unfolded protein response in neurodegeneration. *Nature Reviews Neurology*, *13*(8), 477–491. https://doi.org/10.1038/nrneurol.2017.99

Hirokawa, N., & Takemura, R. (2005). Molecular motors and mechanisms of directional transport in neurons. *Nature Reviews Neuroscience*, *6*(3), 201–214. https://doi.org/10.1038/nrn1624

Hohmann, T., & Dehghani, F. (2019). The Cytoskeleton-A Complex Interacting Meshwork. *Cells*, *8*(4). https://doi.org/10.3390/cells8040362

Hoozemans, J. J. M., van Haastert, E. S., Nijholt, D. A. T., Rozemuller, A. J. M., & Scheper, W. (2012). Activation of the Unfolded Protein Response Is an Early Event in Alzheimer's and Parkinson's Disease. *Neurodegenerative Diseases*, *10*(1–4), 212–215. https://doi.org/10.1159/000334536

Hu, J., Shibata, Y., Zhu, P.-P., Voss, C., Rismanchi, N., Prinz, W. A., Rapoport, T. A., & Blackstone, C. (2009). A Class of Dynamin-like GTPases Involved in the Generation of the Tubular ER Network. *Cell*, *138*(3), 549–561. https://doi.org/10.1016/j.cell.2009.05.025

Janke, C., & Bulinski, J. C. (2011). Post-translational regulation of the microtubule cytoskeleton: mechanisms and functions. *Nature Reviews Molecular Cell Biology*, *12*(12), 773–786. https://doi.org/10.1038/nrm3227

Janke, C., & Kneussel, M. (2010). Tubulin post-translational modifications: encoding functions on the neuronal microtubule cytoskeleton. *Trends in Neurosciences*, *33*(8), 362–372. https://doi.org/10.1016/j.tins.2010.05.001

Ji, Z., Zhang, G., Chen, L., Li, J., Yang, Y., Cha, C., Zhang, J., Lin, H., & Guo, G. (2018). Spastin Interacts with CRMP 5 to Promote Neurite Outgrowth by Controlling the Microtubule Dynamics. *Developmental Neurobiology*, *78*(12), 1191–1205. https://doi.org/10.1002/dneu.22640

Joensuu, M., Belevich, I., Rämö, O., Nevzorov, I., Vihinen, H., Puhka, M., Witkos, T. M., Lowe, M., Vartiainen, M. K., & Jokitalo, E. (2014). ER sheet persistence is coupled to myosin 1c–regulated dynamic actin filament arrays. *Molecular Biology of the Cell*, *25*(7), 1111–1126. https://doi.org/10.1091/mbc.e13-12-0712

Jones, K. T., & Sharpe, G. R. (1994). Thapsigargin Raises Intracellular Free Calcium Levels in Human Keratinocytes and Inhibits the Coordinated Expression of Differentiation Markers. *Experimental Cell Research*, *210*(1), 71–76. https://doi.org/10.1006/excr.1994.1011

Kasher, P. R., De Vos, K. J., Wharton, S. B., Manser, C., Bennett, E. J., Bingley, M., Wood, J. D., Milner, R., McDermott, C. J., Miller, C. C. J., Shaw, P. J., & Grierson, A. J. (2009). Direct evidence for axonal transport defects in a novel mouse model of mutant spastin-induced hereditary spastic paraplegia (HSP) and human HSP patients. *Journal of Neurochemistry*, *110*(1), 34–44. https://doi.org/10.1111/j.1471-4159.2009.06104.x

Klemm, R. W., Norton, J. P., Cole, R. A., Li, C. S., Park, S. H., Crane, M. M., Li, L., Jin, D., Boye-Doe, A., Liu, T. Y., Shibata, Y., Lu, H., Rapoport, T. A., Farese, R. V., Blackstone, C., Guo, Y., & Mak, H. Y. (2013). A Conserved Role for Atlastin GTPases in Regulating Lipid Droplet Size. *Cell Reports*, *3*(5), 1465–1475. https://doi.org/10.1016/j.celrep.2013.04.015

Kuo, Y.-W., & Howard, J. (2021). Cutting, Amplifying, and Aligning Microtubules with Severing Enzymes. *Trends in Cell Biology*, *31*(1), 50–61. https://doi.org/10.1016/j.tcb.2020.10.004

La Rovere, R. M. L., Roest, G., Bultynck, G., & Parys, J. B. (2016). Intracellular Ca 2+ signaling and Ca 2+ microdomains in the control of cell survival, apoptosis and autophagy. *Cell Calcium*, *60*(2), 74–87. https://doi.org/10.1016/j.ceca.2016.04.005

Lacroix, B., van Dijk, J., Gold, N. D., Guizetti, J., Aldrian-Herrada, G., Rogowski, K., Gerlich, D. W., & Janke, C. (2010). Tubulin polyglutamylation stimulates spastin-mediated microtubule severing. *Journal of Cell Biology*, *189*(6), 945–954. https://doi.org/10.1083/jcb.201001024

Lee, A. S. (1987). Coordinated regulation of a set of genes by glucose and calcium ionophores in mammalian cells. *Trends in Biochemical Sciences*, *12*, 20–23. https://doi.org/10.1016/0968-0004(87)90011-9

Leo, L., Yu, W., D'Rozario, M., Waddell, E. A., Marenda, D. R., Baird, M. A., Davidson, M. W., Zhou, B., Wu, B., Baker, L., Sharp, D. J., & Baas, P. W. (2015). Vertebrate Fidgetin Restrains Axonal Growth by Severing Labile Domains of Microtubules. *Cell Reports*, *12*(11), 1723–1730. https://doi.org/10.1016/j.celrep.2015.08.017

Li, J., Ni, M., Lee, B., Barron, E., Hinton, D. R., & Lee, A. S. (2008). The unfolded protein response regulator GRP78/BiP is required for endoplasmic reticulum integrity and stress-induced autophagy in mammalian cells. *Cell Death & Differentiation*, *15*(9), 1460–1471. https://doi.org/10.1038/cdd.2008.81

Li, M., Baumeister, P., Roy, B., Phan, T., Foti, D., Luo, S., & Lee, A. S. (2000). ATF6 as a Transcription Activator of the Endoplasmic Reticulum Stress Element:

Thapsigargin Stress-Induced Changes and Synergistic Interactions with NF-Y and YY1. *Molecular and Cellular Biology*, *20*(14), 5096–5106. https://doi.org/10.1128/MCB.20.14.5096-5106.2000

Lim, Y., Cho, I., Schoel, L. J., Cho, G., & Golden, J. A. (2015). Hereditary spastic paraplegia-linked REEP1 modulates endoplasmic reticulum/mitochondria contacts. *Annals of Neurology*, *78*(5), 679–696. https://doi.org/10.1002/ana.24488

Lopes, A. T., Hausrat, T. J., Heisler, F. F., Gromova, K. V., Lombino, F. L., Fischer, T., Ruschkies, L., Breiden, P., Thies, E., Hermans-Borgmeyer, I., Schweizer, M., Schwarz, J. R., Lohr, C., & Kneussel, M. (2020). Spastin depletion increases tubulin polyglutamylation and impairs kinesin-mediated neuronal transport, leading to working and associative memory deficits. *PLOS Biology*, *18*(8), e3000820. https://doi.org/10.1371/journal.pbio.3000820

Lorrain, M. (1898). Contribuition a l'étude de la paraplégie spasmodique familiale. . *Steinheil Paris*.

Lumb, J. H., Connell, J. W., Allison, R., & Reid, E. (2012). The AAA ATPase spastin links microtubule severing to membrane modelling. *Biochimica et Biophysica Acta (BBA) - Molecular Cell Research*, *1823*(1), 192–197. https://doi.org/10.1016/j.bbamcr.2011.08.010

Luo, S., Mao, C., Lee, B., & Lee, A. S. (2006). GRP78/BiP Is Required for Cell Proliferation and Protecting the Inner Cell Mass from Apoptosis during Early Mouse Embryonic Development. *Molecular and Cellular Biology*, *26*(15), 5688–5697. https://doi.org/10.1128/MCB.00779-06

Magiera, M. M., Bodakuntla, S., Žiak, J., Lacomme, S., Marques Sousa, P., Leboucher, S., Hausrat, T. J., Bosc, C., Andrieux, A., Kneussel, M., Landry, M., Calas, A., Balastik, M., & Janke, C. (2018). Excessive tubulin polyglutamylation causes neurodegeneration and perturbs neuronal transport. *The EMBO Journal*, *37*(23). https://doi.org/10.15252/embj.2018100440

Mancuso, G., & Rugarli, E. I. (2008). A cryptic promoter in the first exon of the SPG4gene directs the synthesis of the 60-kDa spastin isoform. *BMC Biology*, *6*(1), 31. https://doi.org/10.1186/1741-7007-6-31

Mannan, A. U., Boehm, J., Sauter, S. M., Rauber, A., Byrne, P. C., Neesen, J., & Engel, W. (2006). Spastin, the most commonly mutated protein in hereditary spastic paraplegia interacts with Reticulon 1 an endoplasmic reticulum protein. *Neurogenetics*, *7*(2), 93–103. https://doi.org/10.1007/s10048-006-0034-4

Martinez, A. J., & Friede, R. L. (1970). Accumulation of axoplasmic organelles in swollen nerve fibers. *Brain Research*, *19*(2), 183–198. https://doi.org/10.1016/0006-8993(70)90433-6

McCorquodale, D. S., Ozomaro, U., Huang, J., Montenegro, G., Kushman, A., Citrigno, L., Price, J., Speziani, F., Pericak-Vance, M. A., & Züchner, S. (2011). Mutation screening of spastin, atlastin, and REEP1 in hereditary spastic paraplegia. *Clinical Genetics*, *79*(6), 523–530. https://doi.org/10.1111/j.1399-0004.2010.01501.x

McDaid, J., Mustaly-Kalimi, S., & Stutzmann, G. E. (2020). Ca2+ Dyshomeostasis Disrupts Neuronal and Synaptic Function in Alzheimer's Disease. *Cells*, *9*(12). https://doi.org/10.3390/cells9122655

McMahon, H. T., & Boucrot, E. (2015). Membrane curvature at a glance. *Journal of Cell Science*, *128*(6), 1065–1070. https://doi.org/10.1242/jcs.114454

Meyyazhagan, A., & Orlacchio, A. (2022). Hereditary Spastic Paraplegia: An Update. *International Journal of Molecular Sciences*, *23*(3). https://doi.org/10.3390/ijms23031697

Montenegro, G., Rebelo, A. P., Connell, J., Allison, R., Babalini, C., D'Aloia, M., Montieri, P., Schüle, R., Ishiura, H., Price, J., Strickland, A., Gonzalez, M. A., Baumbach-Reardon, L., Deconinck, T., Huang, J., Bernardi, G., Vance, J. M., Rogers, M. T., Tsuji, S., … Züchner, S. (2012). Mutations in the ER-shaping protein reticulon 2 cause the axon-degenerative disorder hereditary spastic

paraplegia type 12. *Journal of Clinical Investigation*, *122*(2), 538–544. https://doi.org/10.1172/JCI60560

Nielsen, J. E., Johnsen, B., Koefoed, P., Scheuer, K. H., Grønbech-Jensen, M., Law, I., Krabbe, K., Nørremølle, A., Eiberg, H., Søndergård, H., Dam, M., Rehfeld, J. F., Krarup, C., Paulson, O. B., Hasholt, L., & Sørensen, S. A. (2004). Hereditary spastic paraplegia with cerebellar ataxia: a complex phenotype associated with a new *SPG4* gene mutation. *European Journal of Neurology*, *11*(12), 817–824. https://doi.org/10.1111/j.1468-1331.2004.00888.x

Nunnari, J., & Suomalainen, A. (2012). Mitochondria: In Sickness and in Health. *Cell*, *148*(6), 1145–1159. https://doi.org/10.1016/j.cell.2012.02.035

Orlacchio, A., Kawarai, T., Totaro, A., Errico, A., St George-Hyslop, P. H., Rugarli, E. I., & Bernardi, G. (2004). Hereditary Spastic Paraplegia. *Archives of Neurology*, *61*(6), 849. https://doi.org/10.1001/archneur.61.6.849

Orso, G. (2005). Disease-related phenotypes in a Drosophila model of hereditary spastic paraplegia are ameliorated by treatment with vinblastine. *Journal of Clinical Investigation*, *115*(11), 3026–3034. https://doi.org/10.1172/JCI24694

Orso, G., Pendin, D., Liu, S., Tosetto, J., Moss, T. J., Faust, J. E., Micaroni, M., Egorova, A., Martinuzzi, A., McNew, J. A., & Daga, A. (2009). Homotypic fusion of ER membranes requires the dynamin-like GTPase Atlastin. *Nature*, *460*(7258), 978–983. https://doi.org/10.1038/nature08280

O'Sullivan, N. C., Jahn, T. R., Reid, E., & O'Kane, C. J. (2012). Reticulon-like-1, the Drosophila orthologue of the Hereditary Spastic Paraplegia gene reticulon 2, is required for organization of endoplasmic reticulum and of distal motor axons. *Human Molecular Genetics*, *21*(15), 3356–3365. https://doi.org/10.1093/hmg/dds167

Ovsepian, S. V., O'Leary, V. B., & Martinez, S. (2023). Selective vulnerability of motor neuron types and functional groups to degeneration in amyotrophic lateral sclerosis: review of the neurobiological mechanisms and functional correlates. *Brain Structure and Function*, *229*(1), 1–14. https://doi.org/10.1007/s00429-023-02728-6

Öztürk, Z., O'Kane, C. J., & Pérez-Moreno, J. J. (2020). Axonal Endoplasmic Reticulum Dynamics and Its Roles in Neurodegeneration. *Frontiers in Neuroscience*, *14*. https://doi.org/10.3389/fnins.2020.00048

Paillard, M., Tubbs, E., Thiebaut, P.-A., Gomez, L., Fauconnier, J., Crola Da Silva, C., Teixeira, G., Mewton, N., Belaidi, E., Durand, A., Abrial, M., Lacampagne, A., Rieusset, J., & Ovize, M. (2013). Depressing Mitochondria-Reticulum Interactions Protects Cardiomyocytes From Lethal Hypoxia-Reoxygenation Injury. *Circulation*, *128*(14), 1555–1565. https://doi.org/10.1161/CIRCULATIONAHA.113.001225

Pantakani, D. V. K., Swapna, L. S., Srinivasan, N., & Mannan, A. U. (2008). Spastin oligomerizes into a hexamer and the mutant spastin (E442Q) redistribute the wild-type spastin into filamentous microtubule. *Journal of Neurochemistry*, *106*(2), 613–624. https://doi.org/10.1111/j.1471-4159.2008.05414.x

Papadopoulos, C., Orso, G., Mancuso, G., Herholz, M., Gumeni, S., Tadepalle, N., Jüngst, C., Tzschichholz, A., Schauss, A., Höning, S., Trifunovic, A., Daga, A., & Rugarli, E. I. (2015). Spastin Binds to Lipid Droplets and Affects Lipid Metabolism. *PLOS Genetics*, *11*(4), e1005149. https://doi.org/10.1371/journal.pgen.1005149

Park, S. H., Zhu, P.-P., Parker, R. L., & Blackstone, C. (2010). Hereditary spastic paraplegia proteins REEP1, spastin, and atlastin-1 coordinate microtubule interactions with the tubular ER network. *Journal of Clinical Investigation*, *120*(4), 1097–1110. https://doi.org/10.1172/JCI40979

Peris, L., Wagenbach, M., Lafanechère, L., Brocard, J., Moore, A. T., Kozielski, F., Job, D., Wordeman, L., & Andrieux, A. (2009). Motor-dependent microtubule disassembly driven by tubulin tyrosination. *Journal of Cell Biology*, *185*(7), 1159–1166. https://doi.org/10.1083/jcb.200902142

Piermarini, E., Akarsu, S., Connors, T., Kneussel, M., Lane, M. A., Morfini, G., Karabay, A., Baas, P. W., & Qiang, L. (2022). Modeling gain-of-function and loss-of-function components of *SPAST* -based hereditary spastic paraplegia

using transgenic mice. *Human Molecular Genetics*, *31*(11), 1844–1859. https://doi.org/10.1093/hmg/ddab367

Plaud, C., Joshi, V., Kajevu, N., Poüs, C., Curmi, P. A., & Burgo, A. (2018). Functional differences of short and long isoforms of spastin harboring missense mutation. *Disease Models & Mechanisms*, *11*(9). https://doi.org/10.1242/dmm.033704

Puri, R., Cheng, X.-T., Lin, M.-Y., Huang, N., & Sheng, Z.-H. (2019). Mul1 restrains Parkin-mediated mitophagy in mature neurons by maintaining ER-mitochondrial contacts. *Nature Communications*, *10*(1), 3645. https://doi.org/10.1038/s41467-019-11636-5

Qiang, L., Piermarini, E., Muralidharan, H., Yu, W., Leo, L., Hennessy, L. E., Fernandes, S., Connors, T., Yates, P. L., Swift, M., Zholudeva, L. V, Lane, M. A., Morfini, G., Alexander, G. M., Heiman-Patterson, T. D., & Baas, P. W. (2019). Hereditary spastic paraplegia: gain-of-function mechanisms revealed by new transgenic mouse. *Human Molecular Genetics*, *28*(7), 1136–1152. https://doi.org/10.1093/hmg/ddy419

Raby, A., Missiroli, S., Sanatine, P., Langui, D., Pansiot, J., Beaude, N., Vezzana, L., Saleh, R., Marinello, M., Laforge, M., Pinton, P., Buj-Bello, A., & Burgo, A. (2024). Spastin regulates ER-mitochondrial contact sites and mitochondrial homeostasis. *IScience*, *27*(9), 110683. https://doi.org/10.1016/j.isci.2024.110683

Rapoport, T. A. (2007). Protein translocation across the eukaryotic endoplasmic reticulum and bacterial plasma membranes. *Nature*, *450*(7170), 663–669. https://doi.org/10.1038/nature06384

Redeker, V., Rossier, J., & Frankfurter, A. (1998). Posttranslational Modifications of the C-Terminus of α-Tubulin in Adult Rat Brain: α4 Is Glutamylated at Two Residues. *Biochemistry*, *37*(42), 14838–14844. https://doi.org/10.1021/bi981335k

Reed, N. A., Cai, D., Blasius, T. L., Jih, G. T., Meyhofer, E., Gaertig, J., & Verhey, K. J. (2006). Microtubule Acetylation Promotes Kinesin-1 Binding and Transport.

Current Biology, *16*(21), 2166–2172. https://doi.org/10.1016/j.cub.2006.09.014

Reid, E., Connell, J., Edwards, T. L., Duley, S., Brown, S. E., & Sanderson, C. M. (2005). The hereditary spastic paraplegia protein spastin interacts with the ESCRT-III complex-associated endosomal protein CHMP1B. *Human Molecular Genetics*, *14*(1), 19–38. https://doi.org/10.1093/hmg/ddi003

Renvoisé, B., Malone, B., Falgairolle, M., Munasinghe, J., Stadler, J., Sibilla, C., Park, S. H., & Blackstone, C. (2016). Reep1 null mice reveal a converging role for hereditary spastic paraplegia proteins in lipid droplet regulation. *Human Molecular Genetics*, ddw315. https://doi.org/10.1093/hmg/ddw315

Riano, E., Martignoni, M., Mancuso, G., Cartelli, D., Crippa, F., Toldo, I., Siciliano, G., Di Bella, D., Taroni, F., Bassi, M. T., Cappelletti, G., & Rugarli, E. I. (2009). Pleiotropic effects of spastin on neurite growth depending on expression levels. *Journal of Neurochemistry*, *108*(5), 1277–1288. https://doi.org/10.1111/j.1471-4159.2009.05875.x

Rizo, T., Gebhardt, L., Riedlberger, J., Eberhardt, E., Fester, L., Alansary, D., Winkler, J., Turan, S., Arnold, P., Niemeyer, B. A., Fischer, M. J. M., & Winner, B. (2022). Store-operated calcium entry is reduced in spastin-linked hereditary spastic paraplegia. *Brain*, *145*(9), 3131–3146. https://doi.org/10.1093/brain/awac122

Rogowski, K., van Dijk, J., Magiera, M. M., Bosc, C., Deloulme, J.-C., Bosson, A., Peris, L., Gold, N. D., Lacroix, B., Grau, M. B., Bec, N., Larroque, C., Desagher, S., Holzer, M., Andrieux, A., Moutin, M.-J., & Janke, C. (2010). A Family of Protein-Deglutamylating Enzymes Associated with Neurodegeneration. *Cell*, *143*(4), 564–578. https://doi.org/10.1016/j.cell.2010.10.014

Ruggiano, A., Foresti, O., & Carvalho, P. (2014). ER-associated degradation: Protein quality control and beyond. *Journal of Cell Biology*, *204*(6), 869–879. https://doi.org/10.1083/jcb.201312042

Saheki, Y., & De Camilli, P. (2017). Endoplasmic Reticulum–Plasma Membrane Contact Sites. *Annual Review of Biochemistry*, *86*(1), 659–684. https://doi.org/10.1146/annurev-biochem-061516-044932

Sakoe, K., Shioda, N., & Matsuura, T. (2021). A newly identified NES sequence present in spastin regulates its subcellular localization and microtubule severing activity. *Biochimica et Biophysica Acta (BBA) - Molecular Cell Research*, *1868*(1), 118862. https://doi.org/10.1016/j.bbamcr.2020.118862

Sanderson, C. M., Connell, J. W., Edwards, T. L., Bright, N. A., Duley, S., Thompson, A., Luzio, J. P., & Reid, E. (2006). Spastin and atlastin, two proteins mutated in autosomal-dominant hereditary spastic paraplegia, are binding partners. *Human Molecular Genetics*, *15*(2), 307–318. https://doi.org/10.1093/hmg/ddi447

Saxena, S., & Caroni, P. (2007). Mechanisms of axon degeneration: From development to disease. *Progress in Neurobiology*, *83*(3), 174–191. https://doi.org/10.1016/j.pneurobio.2007.07.007

Schindelin, J., Arganda-Carreras, I., Frise, E., Kaynig, V., Longair, M., Pietzsch, T., Preibisch, S., Rueden, C., Saalfeld, S., Schmid, B., Tinevez, J.-Y., White, D. J., Hartenstein, V., Eliceiri, K., Tomancak, P., & Cardona, A. (2012). Fiji: an open-source platform for biological-image analysis. *Nature Methods*, *9*(7), 676–682. https://doi.org/10.1038/nmeth.2019

Schwarz, D. S., & Blower, M. D. (2016). The endoplasmic reticulum: structure, function and response to cellular signaling. *Cellular and Molecular Life Sciences*, *73*(1), 79–94. https://doi.org/10.1007/s00018-015-2052-6

Seeligmüller, A. (1876). Sklerose der Seitenstränge des Rückenmarks bei vier Kindern derselben Familie. *Dtsch Med Wschr*.

Seiser, R. M., & Nicchitta, C. V. (2000). The Fate of Membrane-bound Ribosomes Following the Termination of Protein Synthesis. *Journal of Biological Chemistry*, *275*(43), 33820–33827. https://doi.org/10.1074/jbc.M004462200

Sharoar, M. G., Shi, Q., Ge, Y., He, W., Hu, X., Perry, G., Zhu, X., & Yan, R. (2016). Dysfunctional tubular endoplasmic reticulum constitutes a pathological

feature of Alzheimer's disease. *Molecular Psychiatry*, *21*(9), 1263–1271. https://doi.org/10.1038/mp.2015.181

Sharp, D. J., & Ross, J. L. (2012). Microtubule-severing enzymes at the cutting edge. *Journal of Cell Science*. https://doi.org/10.1242/jcs.101139

Sherwood, N. T., Sun, Q., Xue, M., Zhang, B., & Zinn, K. (2004). Drosophila Spastin Regulates Synaptic Microtubule Networks and Is Required for Normal Motor Function. *PLoS Biology*, *2*(12), e429. https://doi.org/10.1371/journal.pbio.0020429

Shibata, Y., Voeltz, G. K., & Rapoport, T. A. (2006). Rough Sheets and Smooth Tubules. *Cell*, *126*(3), 435–439. https://doi.org/10.1016/j.cell.2006.07.019

Shribman, S., Reid, E., Crosby, A. H., Houlden, H., & Warner, T. T. (2019). Hereditary spastic paraplegia: from diagnosis to emerging therapeutic approaches. *The Lancet Neurology*, *18*(12), 1136–1146. https://doi.org/10.1016/S1474-4422(19)30235-2

Sleigh, J. N., Mech, A. M., & Schiavo, G. (2020). Developmental demands contribute to early neuromuscular degeneration in CMT2D mice. *Cell Death & Disease*, *11*(7), 564. https://doi.org/10.1038/s41419-020-02798-y

Smith, M., Gay, L., & Babst, M. (2024). ER–plasma membrane contact sites deliver ER lipids and proteins for rapid cell surface expansion. *Journal of Cell Biology*, *223*(12). https://doi.org/10.1083/jcb.202308137

Solowska, J. M., & Baas, P. W. (2015). Hereditary spastic paraplegia SPG4: what is known and not known about the disease. *Brain*, *138*(9), 2471–2484. https://doi.org/10.1093/brain/awv178

Solowska, J. M., Morfini, G., Falnikar, A., Himes, B. T., Brady, S. T., Huang, D., & Baas, P. W. (2008). Quantitative and Functional Analyses of Spastin in the Nervous System: Implications for Hereditary Spastic Paraplegia. *The Journal of Neuroscience*, *28*(9), 2147–2157. https://doi.org/10.1523/JNEUROSCI.3159-07.2008

Solowska, J. M., Rao, A. N., & Baas, P. W. (2017). Truncating mutations of SPAST associated with hereditary spastic paraplegia indicate greater accumulation

and toxicity of the M1 isoform of spastin. *Molecular Biology of the Cell*, *28*(13), 1728–1737. https://doi.org/10.1091/mbc.e17-01-0047

Steenbergen, R., Nanowski, T. S., Beigneux, A., Kulinski, A., Young, S. G., & Vance, J. E. (2005). Disruption of the Phosphatidylserine Decarboxylase Gene in Mice Causes Embryonic Lethality and Mitochondrial Defects. *Journal of Biological Chemistry*, *280*(48), 40032–40040. https://doi.org/10.1074/jbc.M506510200

Stokin, G. B., Lillo, C., Falzone, T. L., Brusch, R. G., Rockenstein, E., Mount, S. L., Raman, R., Davies, P., Masliah, E., Williams, D. S., & Goldstein, L. S. B. (2005). Axonopathy and Transport Deficits Early in the Pathogenesis of Alzheimer's Disease. *Science*, *307*(5713), 1282–1288. https://doi.org/10.1126/science.1105681

Strümpell, A. (1893). Über die hereditäre spastische Spinalparalyse. *Deutsche Zeitschrift Für Nervenheilkunde*, *4*(3–4), 173–188. https://doi.org/10.1007/BF01665286

Sudo, H., & Baas, P. W. (2010). Acetylation of Microtubules Influences Their Sensitivity to Severing by Katanin in Neurons and Fibroblasts. *The Journal of Neuroscience*, *30*(21), 7215–7226. https://doi.org/10.1523/JNEUROSCI.0048-10.2010

Svenson, I. K., Kloos, M. T., Gaskell, P. C., Nance, M. A., Garbern, J. Y., Hisanaga, S., Pericak-Vance, M. A., Ashley-Koch, A. E., & Marchuk, D. A. (2004). Intragenic modifiers of hereditary spastic paraplegia due to spastin gene mutations. *Neurogenetics*, *5*(3), 157–164. https://doi.org/10.1007/s10048-004-0186-z

Tarrade, A., Fassier, C., Courageot, S., Charvin, D., Vitte, J., Peris, L., Thorel, A., Mouisel, E., Fonknechten, N., Roblot, N., Seilhean, D., Diérich, A., Hauw, J. J., & Melki, J. (2006). A mutation of spastin is responsible for swellings and impairment of transport in a region of axon characterized by changes in microtubule composition. *Human Molecular Genetics*, *15*(24), 3544–3558. https://doi.org/10.1093/hmg/ddl431

Tenedini, F., Yin, C., Huang, J., Dhiman, N., Soba, P., & Parrish, J. Z. (2024). *Axon length-dependent synapse loss is mediated by neuronal cytokine-induced glial phagocytosis*. https://doi.org/10.1101/2024.06.09.598122

Terasaki, M., Chen, L. B., & Fujiwara, K. (1986). Microtubules and the endoplasmic reticulum are highly interdependent structures. *The Journal of Cell Biology*, *103*(4), 1557–1568. https://doi.org/10.1083/jcb.103.4.1557

Trotta, N., Orso, G., Rossetto, M. G., Daga, A., & Broadie, K. (2004). The Hereditary Spastic Paraplegia Gene, spastin, Regulates Microtubule Stability to Modulate Synaptic Structure and Function. *Current Biology*, *14*(13), 1135–1147. https://doi.org/10.1016/j.cub.2004.06.058

Vajente, N., Norante, R., Redolfi, N., Daga, A., Pizzo, P., & Pendin, D. (2019). Microtubules Stabilization by Mutant Spastin Affects ER Morphology and Ca2+ Handling. *Frontiers in Physiology*, *10*. https://doi.org/10.3389/fphys.2019.01544

Valadas, J. S., Esposito, G., Vandekerkhove, D., Miskiewicz, K., Deaulmerie, L., Raitano, S., Seibler, P., Klein, C., & Verstreken, P. (2018). ER Lipid Defects in Neuropeptidergic Neurons Impair Sleep Patterns in Parkinson's Disease. *Neuron*, *98*(6), 1155-1169.e6. https://doi.org/10.1016/j.neuron.2018.05.022

Valenstein, M. L., & Roll-Mecak, A. (2016). Graded Control of Microtubule Severing by Tubulin Glutamylation. *Cell*, *164*(5), 911–921. https://doi.org/10.1016/j.cell.2016.01.019

Voeltz, G. K., Prinz, W. A., Shibata, Y., Rist, J. M., & Rapoport, T. A. (2006). A Class of Membrane Proteins Shaping the Tubular Endoplasmic Reticulum. *Cell*, *124*(3), 573–586. https://doi.org/10.1016/j.cell.2005.11.047

Wang, J. T., Medress, Z. A., & Barres, B. A. (2012). Axon degeneration: Molecular mechanisms of a self-destruction pathway. *Journal of Cell Biology*, *196*(1), 7–18. https://doi.org/10.1083/jcb.201108111

Wang, M., Wey, S., Zhang, Y., Ye, R., & Lee, A. S. (2009). Role of the unfolded protein response regulator GRP78/BiP in development, cancer, and

neurological disorders. *Antioxidants & Redox Signaling*, *11*(9), 2307–2316. https://doi.org/10.1089/ars.2009.2485

Waterman-Storer, C. M., & Salmon, E. D. (1998). Endoplasmic reticulum membrane tubules are distributed by microtubules in living cells using three distinct mechanisms. *Current Biology*, *8*(14), 798–807. https://doi.org/10.1016/S0960-9822(98)70321-5

White, S. R., Evans, K. J., Lary, J., Cole, J. L., & Lauring, B. (2007). Recognition of C-terminal amino acids in tubulin by pore loops in Spastin is important for microtubule severing. *The Journal of Cell Biology*, *176*(7), 995–1005. https://doi.org/10.1083/jcb.200610072

Wood, J. D., Landers, J. A., Bingley, M., McDermott, C. J., Thomas-McArthur, V., Gleadall, L. J., Shaw, P. J., & Cunliffe, V. T. (2006). The microtubule-severing protein Spastin is essential for axon outgrowth in the zebrafish embryo. *Human Molecular Genetics*, *15*(18), 2763–2771. https://doi.org/10.1093/hmg/ddl212

Wu, H., Carvalho, P., & Voeltz, G. K. (2018). Here, there, and everywhere: The importance of ER membrane contact sites. *Science (New York, N.Y.)*, *361*(6401). https://doi.org/10.1126/science.aan5835

Wu, J., & Kaufman, R. J. (2006). From acute ER stress to physiological roles of the Unfolded Protein Response. *Cell Death & Differentiation*, *13*(3), 374–384. https://doi.org/10.1038/sj.cdd.4401840

Yalçın, B., Zhao, L., Stofanko, M., O'Sullivan, N. C., Kang, Z. H., Roost, A., Thomas, M. R., Zaessinger, S., Blard, O., Patto, A. L., Sohail, A., Baena, V., Terasaki, M., & O'Kane, C. J. (2017). Modeling of axonal endoplasmic reticulum network by spastic paraplegia proteins. *ELife*, *6*. https://doi.org/10.7554/eLife.23882

Yu, W., Qiang, L., Solowska, J. M., Karabay, A., Korulu, S., & Baas, P. W. (2008). The Microtubule-severing Proteins Spastin and Katanin Participate Differently in the Formation of Axonal Branches. *Molecular Biology of the Cell*, *19*(4), 1485–1498. https://doi.org/10.1091/mbc.e07-09-0878

Zhu, P.-P., Denton, K. R., Pierson, T. M., Li, X.-J., & Blackstone, C. (2014). Pharmacologic rescue of axon growth defects in a human iPSC model of hereditary spastic paraplegia SPG3A. *Human Molecular Genetics*, *23*(21), 5638–5648. https://doi.org/10.1093/hmg/ddu280

Zhu, P.-P., Hung, H.-F., Batchenkova, N., Nixon-Abell, J., Henderson, J., Zheng, P., Renvoisé, B., Pang, S., Xu, C. S., Saalfeld, S., Funke, J., Xie, Y., Svara, F., Hess, H. F., & Blackstone, C. (2022). Transverse endoplasmic reticulum expansion in hereditary spastic paraplegia corticospinal axons. *Human Molecular Genetics*, *31*(16), 2779–2795. https://doi.org/10.1093/hmg/ddac072

Zhu, P.-P., Patterson, A., Lavoie, B., Stadler, J., Shoeb, M., Patel, R., & Blackstone, C. (2003). Cellular Localization, Oligomerization, and Membrane Association of the Hereditary Spastic Paraplegia 3A (SPG3A) Protein Atlastin. *Journal of Biological Chemistry*, *278*(49), 49063–49071. https://doi.org/10.1074/jbc.M306702200

Zhu, X., Tan, X., Wang, J., Dai, L., Li, J., Guan, X., Wang, Z., Zhang, M., Hu, J., Bai, Y., & Guo, H. (2023). Disruption of Intracellular Calcium Homeostasis Leads to ERLIN2-Linked Hereditary Spastic Paraplegia in Patient-Derived Stem Cell Models. *Human Mutation*, *2023*, 1–14. https://doi.org/10.1155/2023/4834423

Zlamalova, E., Rodger, C., Greco, F., Cheers, S. R., Kleniuk, J., Nadadhur, A. G., Kadlecova, Z., & Reid, E. (2024). Atlastin-1 regulates endosomal tubulation and lysosomal proteolysis in human cortical neurons. *Neurobiology of Disease*, *199*, 106556. https://doi.org/10.1016/j.nbd.2024.106556

Acknowledgements

Embarking on a PhD, I knew the path would be challenging, but I hadn't anticipated just how unpredictable it would be. Fortunately, I was surrounded by extraordinary people whose support, encouragement, and presence helped me navigate this journey. I am deeply grateful to each of them.

First, I would like to thank Prof. Dr. Matthias Kneussel for welcoming me into his research group and giving me the chance to pursue this path. I also sincerely thank Prof. Dr. Christian Lohr for agreeing to be my supervisor at the University of Hamburg and for taking the time to evaluate my doctoral thesis.
A special thanks goes to my daily supervisor, Dr. Torben Hausrat, for his supervision and guidance throughout my doctoral studies, for his support during the course of my research project, and for the insights he shared when I sought his advice.
I wish to thank Dr. Michaela Schweizer and the Electron Microscopy Core Facility team at the ZMNH for their work in electron microscopy sample preparation and imaging.

To all my colleagues at the Institute of Molecular Neurogenetics at the ZMNH – thank you for the engaging scientific discussions, the collaboration, and the great times we shared.
Special thanks to:

- Dr. Marcel Klein, my beautiful dandelion, for being such a ray of sunshine, for indulging me in horoscope reading, and for making every day brighter.
- Dr. Jennifer Radwitz, for hosting amazing art sessions, for unmatched milk-foaming skills, and for her grounded approach to life.
- Dominik Böck, for being such a visionary in both modelling and photography, and for always being so easy to talk to.
- Dr. Kira Brune, for her enthusiasm in coming up with new ideas and for never being afraid to be the amazingly glorious diva that she is.

- Dr. Guido Hermey, for being a great listener, for his kindness, thoughtful advice, and perspective.
- Christoph Janiesch and Yvonne Pechmann, for their incredible technical support and for being the backbone of my research efforts.
    - Christoph, for making me laugh and always speaking his mind, often offering a new perspective.
    - Yvonne, for our great conversations, her empathy, inspiring outlook on life, and for doing everything with a smile.
- Dr. Frank Heisler, for his support during my project and for always being available to discuss new directions.

Thank you to:

- Oriana, for our beautiful and stimulating conversations about pretty much everything, for being my absolute favourite singer, and for always moving me with her music.
- Francesco, for cooking the best dinners, for his huge heart, and for being the most entertaining frontman I have ever seen.

To my family: thank you to my parents, for always making me feel loved and supported, for passing on their passion for science, and for being people I deeply admire. Thank you to my sister, for always being there for me and believing in me - her opinions and words of advice are the most precious to me.

And finally, thank you to Andrea, for his constant love and support throughout the years, for being my favourite person to talk to, and for making me feel at home, wherever we are.